# Investigation of the Effect of Water Quality on Formation Damage using Porous Discs

*M.W.R. de Jonge*

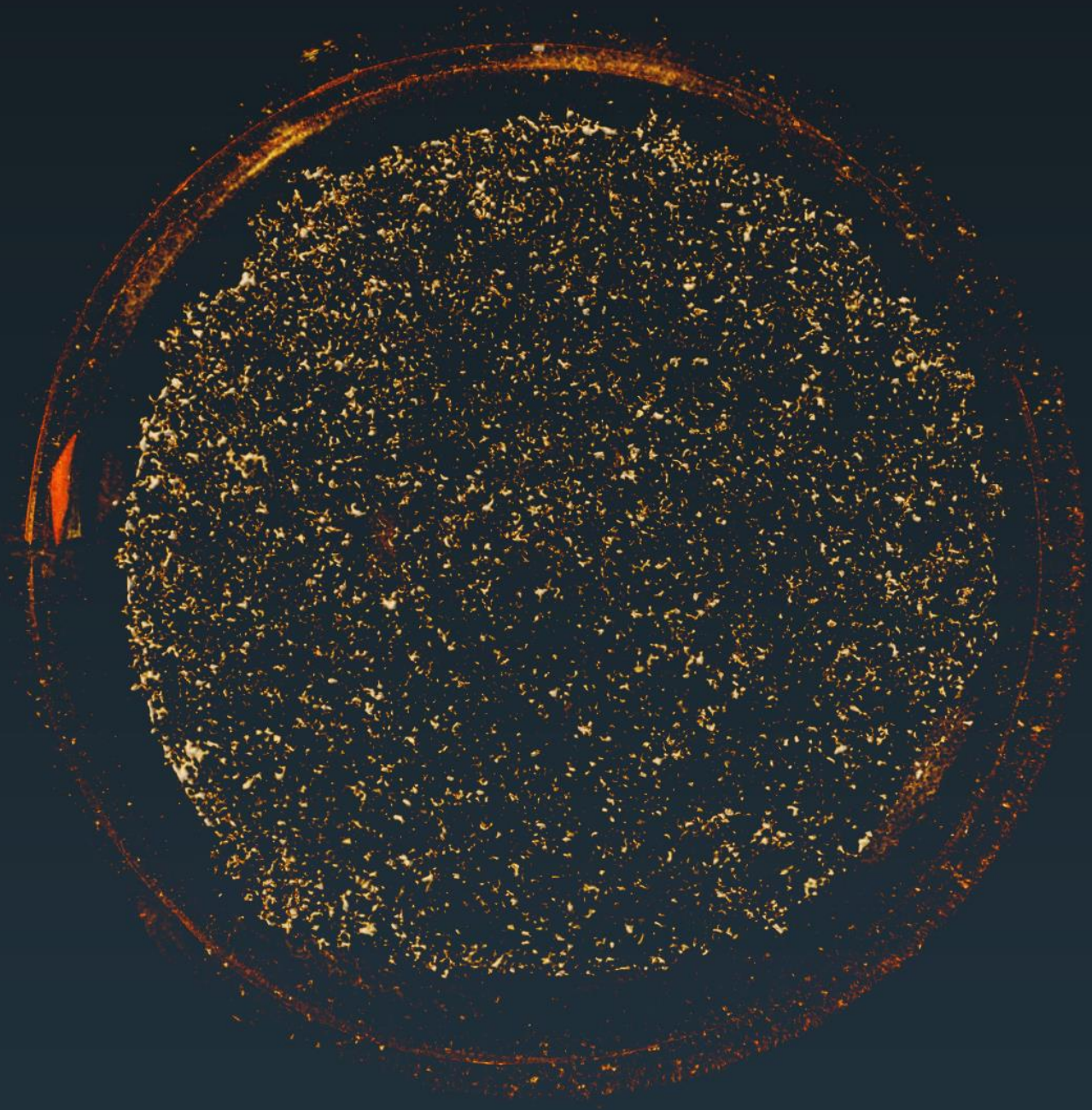

TU Delft

# Investigation of the Effect of Water Quality on Formation Damage using Porous Discs

By

M.W.R. de Jonge

in partial fulfilment of the requirements for the degree of

**Master of Science**
in Applied Earth Sciences

at the Delft University of Technology,
to be defended publicly on Thursday, June 18, 2020, at 14:00 AM.

| | | |
|---|---|---|
| Supervisor: | Prof. Dr. Ir. P.J. Zitha, | Delft University of Technology |
| Thesis committee: | Dr. D. V. Voskov, | Delft University of Technology |
| | Dr. J. Gebert, | Delft University of Technology |
| | Dr. M.S. Welling, | Shell Global Solutions B.V. |

*This thesis is confidential and cannot be made public until June 18, 2020.*

An electronic version of this thesis is available at http://repository.tudelft.nl/.

# Abstract

Water injection is widely used in the petroleum industry for the increase of hydrocarbon recovery or disposal of wastewater. Water production and injection are the primary mechanisms in Geothermal Energy. Both include injecting water into a porous formation under matrix injection conditions. While maintaining water injection is vital in these branches in the industry, so is the occurrence of formation damage (FD) due to suspended contaminants or brine incompatibility. Suspended particles in injection water are retained or deposited due to the creation of an External Filter Cake (EFC) or Internal Filter Cake (IFC) impairing the permeability. Consequently, FD results in Water Injectivity Decline (WID). In most cases, the negative impact on injectivity translates into operational and economic targets not being met. WID, as a result of FD, is highly connected to the Water Quality (WQ) of the injection water.

A new approach to water quality (WQ) testing is proposed which suffices as a bridging application of membrane filtration and core flooding. To establish a foundation for this method, tests are conducted by performing particle-laden suspension injection experiments with porous outcrop sandstone 8 mm thin discs utilizing the 'Con-vergence Hydra'. An experimental study is conducted investigating the effect of water quality (WQ) on formation damage, using dilute (20-100 mg/l) Baracarb2 ($CaCO_3$) particle suspension as a model contaminant. Baracarb2 is tested for particle size distribution, mineral content and stability within synthetic brine (resembling Seawater). Subsequently, suspension flow experiments are conducted on porous thin discs (Bentheimer & Berea sandstone) as well as membrane filters (MF0.45µm). As performing suspension injection test with porous thin disc test utilising the Hydra has not been done before, reproducibility of the experiments is tested. The reproducibility of performing experiments utilising the Hydra is high, with very little difference between the experimental outcomes.

Varying WQ within each different porous media type illustrates remarkably similar trends. Moreover, it is demonstrated that by performing a similarity curve collapse, a master curve is obtained for each porous medium type which scales with suspension concentration for Baracarb2. The damage mechanisms explaining this master curve all demonstrate a linear permeability impairment in the early part of the experiments. Subsequently, a linear impedance trend is observed where it is assumed that cake filtration is dominant. The latter is demonstrated by calculating the Modified fouling Index (MFI), which shows a linear dependency with suspension concentration. SEM imaging and Micro-CT scan images substantiate the damage mechanisms hypothesized from the pressure and rate data.

The Con-vergence Hydra utilising porous thin discs has great potential for on-site testing which allows fast and reliable results on permeability impairment, i.e. formation damage. Subsequently, monitoring of the water quality can be done by performing MFI analysis during cake filtration.

**Keywords:** Water quality; Formation damage; Con-vergence Hydra; Baracarb2; Calcium carbonate; Porous sandstone disc; MFI

# Acknowledgement

I like to take this opportunity to thank my supervisors Marco Welling, Shikha Rathi and mentor Katie Humphry for continuous support and involvement in the project during my Assessed Internship at Shell. Special thanks to Marco for all the frequent meetings, brainstorm sessions, discussions, guidance and encouragement during the project as well as my personal development. I want to thank Prof. Dr. Pacelli Zitha for the support and supervision during my thesis, and I'm grateful for the inputs, expertise and guidance.

I want to thank my Denis Voskov and Julia Gebert for accepting to be part of my final thesis committee.

I have had the opportunity of working alongside specialists in the laboratory at STCA. I want to thank Fons Marcelis, Ab Coorn, Niels Brussee and Sebastiaan Pieterse for the extensive technical support and experienced consult on performing experiments in the lab. Without them, I wouldn't have successfully carried out my experimental study. I want to thank Carl van Rijn and Robert van Schalm for the support and effort of helping me with lab equipment.

I am fortunate to gain experience in working with a diverse team within Shell, which is on the forefront of research in waterflooding technology. I would like to thank Ron Bouwmeester, Frank van der Heyden and Geurt Deinum for all the contribution and views around the experimental results.

I want to thank my friends and family for their support and care. Last but not least, I also want to thank my girlfriend for having the patience for always hearing my deeply technical stories about water quality and the effect on formation damage.

*M.W.R. Jonge*
*Rotterdam, June 2020*

# Nomenclature

| | | |
|---|---|---|
| $A$ | Cross-sectional Area | [$m^2$] |
| $A_{eff}$ | Effective Cross-sectional Area | [$mm^2$] |
| $A_m$ | Cross-sectional Area of the porous medium | [$m^2$] |
| $\alpha_{av}$ | Specific Cake resistance | [m/kg] |
| $A_{TD}$ | Cross-sectional Area Thin disc | [$mm^2$] |
| $c$ | Suspension concentration | [mg/l] |
| $D_{eff}$ | Effective Diameter | [mm] |
| $D_{TD}$ | Diameter Thin Disc | [mm] |
| $J$ | Impedance | [-] |
| $k$ | Permeability | [$m^2$] |
| $k_i$ | Initial permeability | [$m^2$] |
| $L$ | Length | [m] |
| $L_m$ | Length porous medium | [m] |
| $L_{TD}$ | Length Thin Disc | [mm] |
| $\varphi$ | Porosity | [%] |
| $\varphi_{eff}$ | Effective Porosity | [%] |
| $dP$ | Pressure drop | [bar] or [$10^5$ Pa] |
| $dP_{0,cor}$ | Pressure drop correction | [bar] or [$10^5$ Pa] |
| $dP_0$ | Pressure drop at time/volume = 0 | [bar] or [$10^5$ Pa] |
| $dP_{max}$ | Maximum Pressure drop | [bar] or [$10^5$ Pa] |
| $\Delta P_c$ | Pressure drop over the cake | [Pa] |
| $\Delta P_m$ | Pressure drop over porous medium | [Pa] |
| $\Delta P_t$ | Pressure drop over porous medium and cake | [Pa] |
| $pH$ | Hydrogen Potential | [-] |
| $Q$ | Flowrate | [l/hr] or [$m^3$/s] |
| $Q_0$ | Initial Flowrate | [l/hr] or [$m^3$/s] |
| $Rc$ | Resistivity cake | [1/m] |
| $R_m$ | Resistivity medium | [1/m] |
| $\rho_{br}$ | Brine density | [$g/cm^3$] |
| $\rho_b$ | Bulk density | [$g/cm^3$] |
| $\rho_g$ | Grain density | [$g/cm^3$] |
| $\rho_c$ | Cake (Particle) density | [$g/cm^3$] |
| $t$ | Time | [s] |
| $V$ | Volume | [L] |
| $V_b$ | Bulk volume | [ml] |
| $V_{BC}$ | Volume flowed at Boundary Condition (CR to CP shift) | [L] |
| $V_d$ | Dead Volume | [L] |
| $V_g$ | Grain volume | [ml] |
| $V_{inj}$ | Total volume injected | [ml] |
| $V_p$ | Pore Volume | [ml] |
| $V_s$ | Suspension Volume | [L] |
| $V_t$ | Total Volume | [L] |
| $\mu_b$ | Viscosity Brine | [Pa.s] |
| $\mu_s$ | Viscosity Suspension | [Pa.s] |

# Abbreviations

| | |
|---|---|
| BER18 | Berea sandstone block 18 |
| BH11 | Bentheimer sandstone block 11 |
| CP | Constant pressure |
| CR | Constant rate |
| CT | Computed Tomography |
| DBF | Deep Bed Filtration |
| DOE | Department of Energy (U.S.) |
| EFC | External Filter Cake |
| FD | Formation Damage |
| FSB | Filtered Synthetic Brine |
| GSD | Grain Size Distribution |
| GWPC | Ground Water Protection Council |
| IFC | Internal Filter Cake |
| IOGP | International Association of Oil & Gas Producers |
| IOR | Improved Oil Recovery |
| LOT | Laser Obscuration Time |
| MCE | Mixed Cellulose Esther |
| MF | Membrane Filters |
| MF0.45 | MCE Membrane filters of pore size 0.45 $\mu$m |
| MICP | Mercury Injection Capillary Pressure |
| ODE | Ordinary Differential Equation |
| PC | Polycarbonate |
| PSD | Particle Size Distribution |
| PTD | Porous Thin Disc |
| PTSD | Pore-Throat size Distribution |
| PUB | Post-Ultrasonic Bath |
| PV | Pore Volume |
| PWRI | Produced Water Re-Injection |
| SCAL | Special Core Analysis |
| SEM | Scanning Electron Microscopy |
| STCA | Shell Technology Centre Amsterdam |
| TSS | Total Suspended Solids |
| USDW | Underground Sources of Drinking Water |
| WID | Water Injectivity Decline |
| WQ | Water Quality |
| XRD | X-Ray Diffraction |

# Contents

# 1 Introduction

Subsurface water injection is widely used in the petroleum industry for the increase of hydrocarbon production. This includes injecting water into a porous formation under matrix injection conditions. The most common types of water injection take place in the form of freshwater injection, seawater injection or produced water re-injection (PWRI). Water injection is done for either pressure maintenance, Improved Oil Recovery (IOR), or simply to dispose of treated production wastewater[1]. The latter is a common practice because vast amounts of formation water usually accompany the production of oil or gas. *Figure 1.1* illustrates a schematic picture of a waterflooding process.

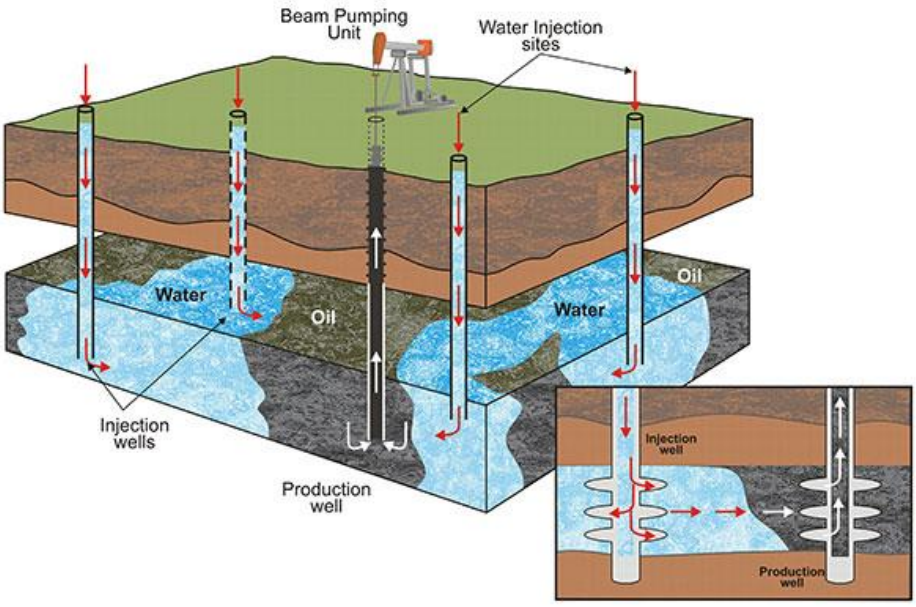


Figure 1.1: Schematic picture of water injection for improving hydrocarbon recovery.[2]

A produced water report from the Ground Water Protection Council (GWPC) [1] shows that, in the U.S. alone, 21.2 billion barrels (1 barrel ≈ 159 litres) of water is produced each year. *Figure 1.2* shows how this amount of produced water is disposed of in the U.S. in 2012. Here 84% is re-injected into the subsurface. The International Association of Oil & Gas Producers (IOGP) show in the environmental performance indicators report [2] that for every tonne (1000 kg) of hydrocarbon produced in 2018, 0.6 tonnes of produced water was re-injected into the subsurface. That means that for the estimated global oil and gas production in 2018 of 2,131 million tonnes [2], about 1,279 million tonnes of produced water is re-injected.

[1] More information on water injection for increasing recovery of oil and gas: https://www.rigzone.com/training/insight.asp?insight_id=341&c_id=

[2] Picture taken from: https://plant-engineering.tistory.com/267

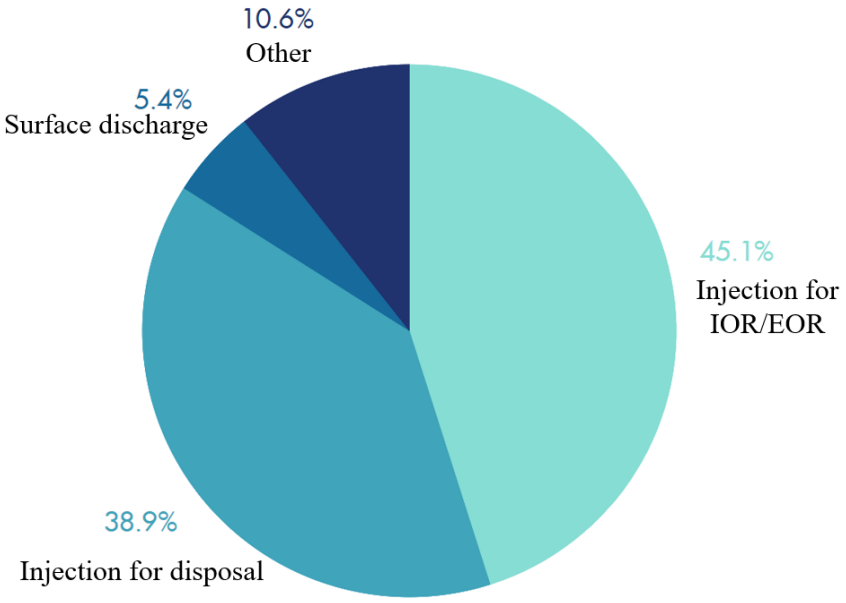


Figure 1.2: Management practices of produced water by percentage in the U.S. (2012) [1]

Water production and injection is the primary mechanism in Geothermal Energy. In the geothermal application, water is injected into the subsurface, where the injected water gains energy by being heated by the subsurface formation. The heated water produced, and the energy is extracted, which can be used for heating houses or electricity generation[3]. A continuous injection scheme is crucial for this application to work. Geothermal is still a small contributor to the global energy mix. However, according to recent plans of the Dutch government, the contribution of geothermal energy is expected to rise from 0.5% today to 23% of the Dutch total heat production in 2050 [3]. This means water injection projects are expected to increase in the near future.

While maintaining water injection is key in various branches in the industry [4], [5], so is the occurrence of formation damage due to its sensitivity to suspended contaminants or brine incompatibility. Consequently, formation damage results in Water Injectivity Decline (WID), fracture growth or even in out of zone injection, which in many cases induces undesirable operational and economic consequences. The term formation damage refers to the impairment of the permeability of a porous medium in the near-wellbore region [6]. It tends to be a great challenge to predict when and how much formation damage can be expected due to many factors involved. The amount of formation damage occurring while injecting water relates to water quality, water-rock compatibility and injection conditions [7].

Ideally, water is injected over a project life span with limited formation damage. Water Quality (WQ) is a term often used in literature to quantify injection water by the severity of formation damage induced [8], [9]. In other words, WQ is high if it causes low formation damage and vice versa. WQ is affected by multiple parameters, including particle invasion, hydrocarbon presence (or invasion in solid form), induced scale deposition, corrosion as well as organic content. Many researchers [6], [8], [10]–[12] suggest that suspended solids in the injection water tend to have the most significant impact on formation damage. Therefore, formation damage mechanisms resulting from particle invasion has been extensively studied. Focusing on total suspended solids (TSS), the particles in suspension can be retained and

[3] More information on geothermal energy can be found at: https://www.irena.org/geothermal

accumulated inside the porous rock forming formation damage in the form of internal filter cake (IFC) and/or at the formation injection face in the form of external filter cake (EFC). These formation damage concepts will be extensively discussed in the next chapter.

Figure 1.3: Wilmington field (California) performance, where loss of injectivity is demonstrated [13].

*Figure 1.3*, for example, discusses the historic Wilmington Field performance to demonstrate in-zone water injection in multi-layered, unconsolidated reservoirs gathering evidence for containment and the absence of fracturing conditions. Waterfloods in California operate under the EPA's class II Underground Injection Control (UIC) regulations to ensure injected water does not induce and/or extend formation fractures that could create a potential conduit connecting the hydrocarbon zone with identified Underground Sources of Drinking Water (USDW) [13]. Clear identification of injectivity loss is presented in a matter of days.

Identification, assessment as well as an understanding of root causes of the impact of water quality on formation damage is vital in including the rate of injectivity decline seen in predicting water injection project performances in the Oil and Gas and Geothermal energy industry. This also allows for optimization when designing facilities.

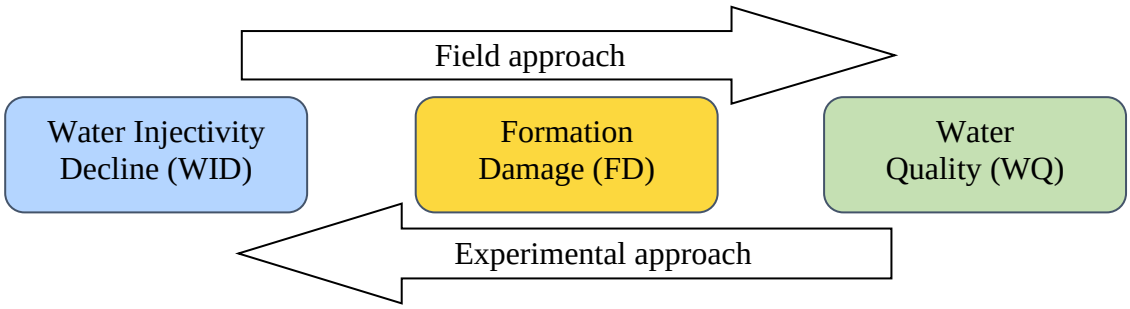

Figure 1.4: A schematic representation of the problem approach.

Considering *Figure 1.4*, the problem can be approached from to angles: a) from the field performance perspective through analyzing field injectivity data or b) from an experimental perspective through laboratory study. The latter approach carries the benefit of allowing more control over the assessed experimental conditions. Typical lab experiments reported in literature investigate the different mechanism through particle-laden core flooding or membrane filter tests.

Water Quality tests are most commonly performed in the form of membrane filtration, where the filtered constituents (i.e. particles, bacterial content, hydrocarbons, just to name a few) are

analyzed and linked to possible WID. Formation damage tests, on the other hand, are usually carried out by performing core flooding experiments. Here injection water is injected in cylindrical sandstone cores where the pressure drop is analyzed by maintaining a constant rate. Instead of analyzing the constituents, the formation damage in time (or with volume) is investigated. Both tests have their benefits and limitations. Some operators have tried to establish a benchmark with onsite core flooding testing equipment (e.g. ASCET) [14], [15]. However, testing time, costs, availability of equipment and simplicity in the test procedure seems to limit the applicability of these onsite testing methods. A cheap, easy to use and online monitoring tool is required.

## 1.1 Research objective & Approach

Membrane filtration is a well-established practice in WQ analysis for injection water. However, as this test method serves as an excellent application for the review of the constituents of the injection water, this application fails when it comes to predicting and understanding the establishment of formation damage seen in the subsurface. This limitation is due to the difficulty in proper water quality sampling, water quality changes over time and the membrane filters not resembling the reservoir rock.

This work seeks to improve the water quality testing method by the introduction of porous thin discs. The benefits of using porous thin discs instead of membrane filters is that porous thin discs resemble the reservoir rock, formation damage forming within or on top of the thin disc is closer to reality as seen in the reservoir porous medium. By using the Con-vergence Hydra, an application is proposed which can be used in the lab or in the field, where inline WQ tests can be performed. The test method with using porous thin discs and the Hydra is fast, cheap and, by following a very accessible experimental procedure, could function as a new standard of monitoring WQ.

The primary research objective of this experimental study is investigating the effect of water quality (WQ) on formation damage, utilising dilute (20-100 mg/l) calcium carbonate particle suspension as a model contaminant. The secondary research objective is to investigate the role of the porous media consisting of either a porous thin disc or a membrane filter. This is done by performing the same suspension flow experiments on porous thin discs and membrane filters, sequentially. From primary and secondary research objectives stated above, the main research question is formulated as follows:

***'What is the effect of water quality on formation damage using porous thin discs?'***

Sub-research objectives are formulated to substantiate and answer the main research question, and states as follows:

- *Particle characterization and suspension stability study in synthetic brine.*
  Baracarb2 ($CaCO_3$) particles are analyzed and tested for stability and reproducible behaviour in synthetic brine. This includes analyzing the dry particles for their mineral composition and characteristics. Furthermore, the particle size distribution and turbidity are tested for different concentration of particles (20-100 mg/l) in synthetic brine of fixed salt composition.

- *Preparing porous discs from two different sandstone cores with a length of 8 mm.*

For constructing the porous thin discs, a core sample is cut in various sections of 8 mm. Experiments are conducted to obtain the permeability and porosity, like synthetic brine flow tests and mercury intrusion tests.

- *Flooding experiments with porous thin discs and membrane filters using the Hydra.*
  Flooding experiments are all done with the Con-vergence Hydra located at Shell Technology Centre Amsterdam (STCA). Porous thin discs and membrane filters are tested on the same suspensions, where all parameters are kept the same, where only the porous media is changed.

- *Post analyses of the porous thin discs.*
  The porous thin discs are analyzed after each experiment for reversible and irreversible damage by performing permeability experiments after an ultrasonic bath cleaning procedure. Some thin discs are imaged using a micro-CT scan and SEM imaging technique to identify the significance and depth of damage.

- *Analyzing data with applying known filtration models.*
  The data is explained by using a numerical filtration model for validating some of the experimental outcomes. Procedures and workflows, as well as analytical models, should demonstrate repeatability and predictability of experimental findings.

## 1.2 Outline

This MSc thesis study is carried out as part of a cooperation between Shell and TU Delft and condenses the results from the experimental investigation measured at the Shell Technology Centre Amsterdam (STCA). This report consists of eight chapters structured as follows; Chapter one gives an overall introduction about the problem and states the research objective and approach. Chapter two comprises a literature review on previously done research and dives into the underlying mechanisms and concepts that cause formation damage. Chapter three states the mathematical approach of the filtration model used to describe the behaviour being observed. Chapter four entails the experimental procedure and experimental setup used for all experiments. The results from the suspension flow experiments are presented in chapter five, followed by a discussion in chapter six. Chapter seven states the conclusions drawn from the experimental study, and chapter eight gives recommendations on further research in this field.

# 2 Theory

Many attempts have been made to model formation damage and predict impairment. Unfortunately, there is not one unifying approach or model which can describe the formation damage observed in fields or experimental studies. There has been some extensive work done in this field of study that helps to understand and predict the mechanisms involved in formation damage due to suspended particles. This chapter contains some of the essential findings and theories developed by researchers.

## 2.1 Literature review

Herzig, 1970 [16] was one of the first to state formation damage mechanisms due to the flow of suspended solids invading a porous medium, also known as deep bed filtration. Barkman & Davidson, 1972 [12] suggested that formation impairment due to suspended solids can occur by four mechanism: wellbore narrowing, invasion, perforation plugging and wellbore fill-up. Barkman & Davidson [12] pursued further developing injection water characterisation parameters defining a measure of water quality ratio defined as the ratio of suspended particles to the permeability of the filter cake. This can be done via membrane filter and core filtration tests. The water quality ratio can be used to calculate the rate of impairment by considering the injectors half-life formula. Abrams, 1977 [17] conducted laboratory flow tests on two different rock samples. One high perm (4-6 d) unconsolidated sand and one low perm (5-50 md) dolomite is used. His work focussed on minimizing formation impairment by altering the drilling mud by altering the particle concentration to stimulate bridging. This resulted in the rule of thumb that bridging of drilling mud particles and external filter cake occurs when the ratio of mean particle size/pore size diameter is above ⅓. Donaldson and Baker, 1977 [18] studied injection of various suspensions (particles of 4, 6 and 7 $\mu$m) into three types of sandstones with different mean pore sizes (10, 15 and 30 $\mu$m). A mathematical model was proposed to describe the mechanical particle transport in a porous medium. It is assumed external filter cake builds for a given optimal particle size. Below the optimal particle size would suggest there is no damage to porosity or permeability, which is contradicted by the work of Vetter and Murtaza [19], [20]. McCune, 1972 [21] represented for the first time on-site core permeability tests on sandstone and carbonate cores. To determine the water quality requirements to prevent formation damage, McCune illustrates what kind of problems could occur when varying salinity, iron content, scale on permeability reduction. Roque et al. [22] gave a more detailed view on the microscopic scale process, identifying that the retention of suspended particles follows four overlapping phases. Distinct phases are particle capturing by deposition/retainment, particle bridging, internal damage and eventually internal damage resulting in an external filter cake. Pang and Sharma emphasized that formation damage is a combination of first internal filter cake formation subsequentially followed after a particular transition time in external formation damage [23], [24]. Khatib [25] proposed a method of analyzing different particles and the creation of an external filter cake in a compression-permeability cell. An empirical relation between cake permeability and cake porosity was set up to be used in predicting injectivity decline for four different types of completions. The resulting computer program was called ‘FORDAM [26]’. Khatib shed some light on the effect of type of particles in solution and the presence of oil. This shows to have a significant impact on the permeability and porosity of the formed cake. Results also show that assuming an incompressible cake is incorrect for with certain solid types. Eylander, 1987 [27] proposed a method for predicting the injectivity decline rate. He observed reversible and irreversible formation damage by clean brine backflushing, where

external filter cake is reversible and internal filtration cake reversible to some extent. A broad literature review by Vetter, 1987 [19] concludes that submicron sizes particles, i.e. particles below 2 microns, are fundamental to include. Vetter et al. did some laboratory study on core floods (Berea sandstone) and tested different parameters as concentration, flow rate and particle charge effects. Important finding was that there is no non-retaining bed from core floods with two cores in series. From three reports for the U.S. Department of Energy (DOE) he concludes that membrane filtration cannot be linked or related to core data. This is argued by that some particles are retained by the filter and not by the sand medium and vice versa.

Yerramilli et al. [28] show the application of using computed tomography (CT) scanning during flow experiments. Hereby, the depth of internal filter cake within cores can be visualized. This serves as a great method for understanding the extent of the penetrated solids and within a porous medium.

More recently, Karazincir et al. (2019) [9] basically attempts to repeat Khatib's work as well as studies single- and two phase FD in Castlegate cores using Silica-Kaolinite (11 or 35 $\mu$m), calcium carbonate ($CaCO_3$, 15 $\mu$m), Barium sulphate ($BaSO_4$, 12 $\mu$m) and iron oxide ($Fe_xO_y$, 3 $\mu$m) plus oil suspension with the objective to identify the optimum water filtration specs prior to injection. The results of Karazanicer et al. are presented in *Figure 2.1*, which illustrate a very common trend.

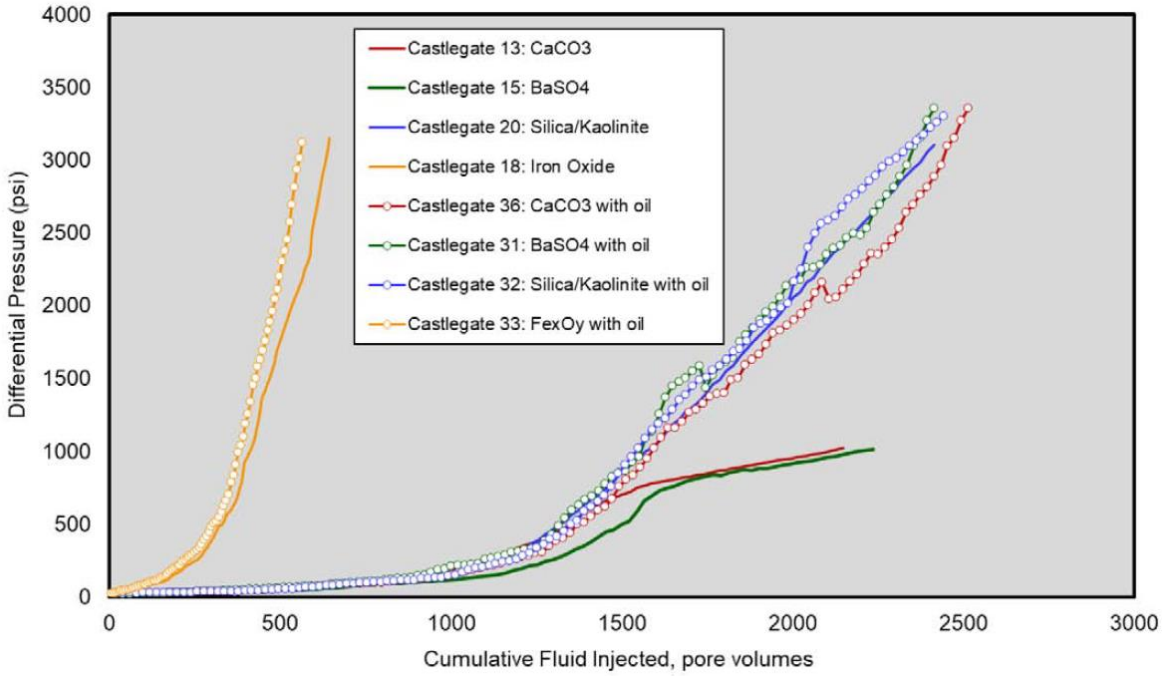


Figure 2.1: Karazincir et al. (2019) [9]: Differential pressure versus cumulative fluid injected for multiple particle suspension floods utilizing Castlegate cores.

## 2.2 Theoretical Background

To capture the impact of water quality on injectivity decline, it is vital to understand the concepts and the underlying mechanisms of particle retainment in porous media. These mechanisms are well documented by Civan [6] and by Herzig [16]. Explanation below all descend from this literature.

### 2.2.1 Formation Damage due to Suspended Particles

The source of the particles plugging the porous media arises from mobilized in-situ formation particles or can be introduced along with the carrying fluid, also known as the invasion of foreign particles. Usually, injection water (seawater or produced water) contains some form of suspended particles. Also, suspended particles are generated in the process of injection, e.g. iron particles, originating from eroded equipment which is in contact with the water. There is also a possibility of particles formed by chemical reactions like scaling precipitations or precipitated ions from the injection water.

As detailed in the previous section, extensive experimental research was carried out in order to assess and understand formation damage due to suspended solids and how water quality could be optimised to predict formation damage. As a result, lots of findings confirm that micron-sized suspended solids are of significant influence on induced WID by formation damage. The establishment of formation damage is traditionally explained by either a single particle and single collector or multiple particles and multiple collectors.

#### 2.2.1.1 Retention sites

A porous sandstone medium is made up out of sand grains, where each sand grain has a surface area which can act as a collector of particles. Focussing on single grains, particles can get retained in several manners [16], [24].

*i.* *Surface sites:* A particle in suspension stops at the surfaces of the grains and stays retained.
*ii.* *Crevice sites:* Particles in suspension gets retained in a convex part formed by two or more grains
*iii.* *Constriction sites:* A particle gets retained at a site because of size exclusion, i.e. that the pore is smaller than the particle.
*iv.* *Cavern sites:* Particles get retained in an area where particles can accumulate and shelter from fluid flow streams.

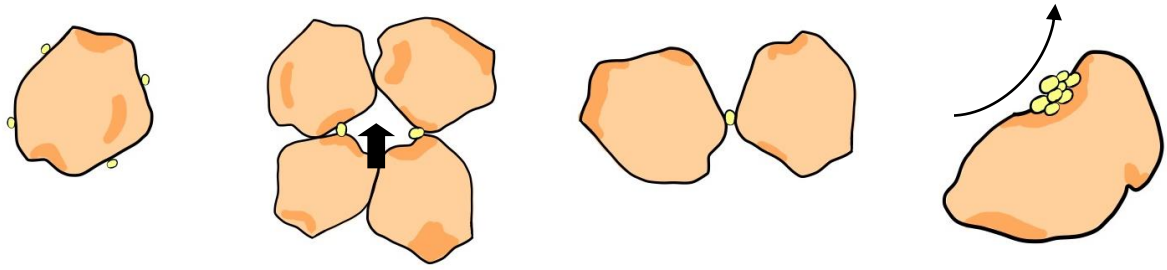


Figure 2.2: Types of particle retention sites: (*i*) Surface sites, (*ii*) Crevice sites, (*iii*) Constriction sites, (*iv*) Cavern sites.

#### 2.2.1.2 Retention forces

Next to retention sites, the following retentions forces play a role in retaining a particle.

*i.* *Axial pressure of the fluid:* The pressure of the fluid generated by fluid flow may push a particle against a wall or constriction, retaining the particle from suspension.
*ii.* *Friction forces:* Due to the rough grain surface and constriction sites created by multiple grains, particles can get retained.
*iii.* *Surface forces:* As the porous medium and fluid may have different electrostatic charge, some form of attraction or repulsion effects can take place.

iv. *Chemical forces:* Forces which act upon the system due to the chemical composition of the brine and porous medium.

#### 2.2.1.3 Capturing mechanisms

Considering a single grain and single particle, some of the dominant capturing mechanisms are given below.

i. *Sedimentation:* In the case of a density difference between fluid and particle, the particle is impacted by gravity and deflects from the flow stream. As a result, the particle meets the porous medium due to sedimentation.
ii. *Inertia:* The sudden changes in the flow direction due to the tortuosity in the porous medium makes particles deflect from the flow stream. This response is generated by inertial forces being more significant than the hydrodynamic forces.
iii. *Direct interception:* Direct interception takes place when a particle crosses path with a grain and stays attached.
iv. *Dispersion:* Two processes give rise to dispersion, which is diffusion and hydrodynamic dispersion. Particle diffusion can take place in the form of Brownian diffusion, occurring with low Peclet number, i.e. small particles below 1 $\mu$m. As a result, the particle may deflect from the flow stream and meet a grain and gets retained. Here particle size is of the influence of the significance of diffusion. Hydrodynamic dispersion effects tend to have more impact with a higher Peclet number.

#### 2.2.1.4 Particle plugging mechanisms

As detailed in the above sections, several possibilities are present for particles to get retained at the surface of a grain. Considering multiple grains and multiple particles, retentions can take place in the form of deposition (or absorption). Another feature of particle retention can take place in the form of plugging. This is explained by size exclusion due to particles (or particle clusters) being too large to pass through a pore throat. Plugging can take place in the form of mono particle plugging, multiple particle plugging or in the form of bridged particle plugging. Retention of particles can also take place in the form of entrainment, which is explained by deposited particles or cluster of particles that re-enters the flow after deposition by erosion.

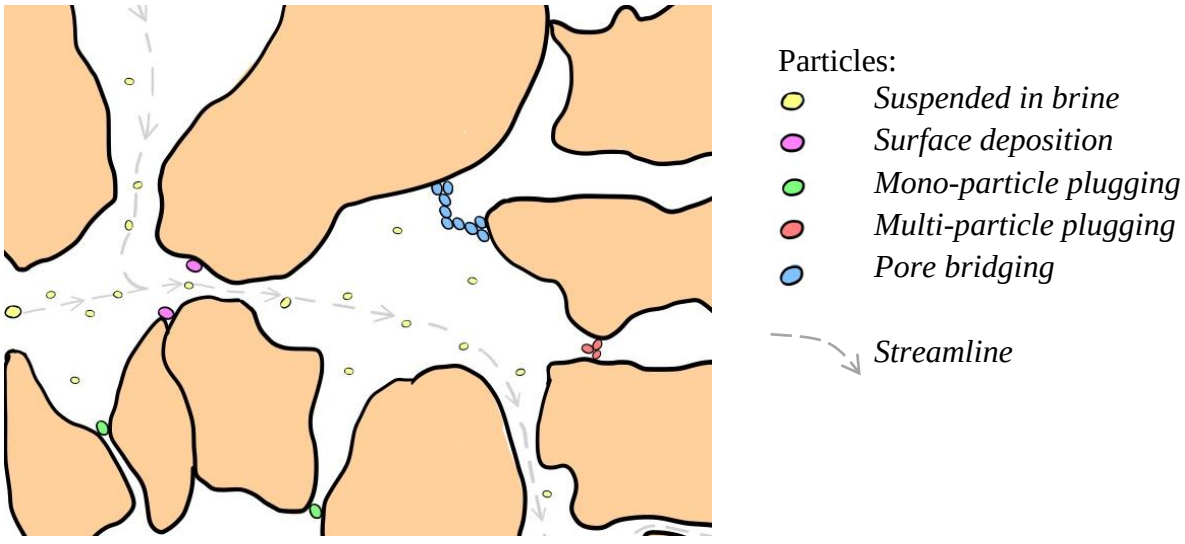


Figure 2.3: Schematic drawing of a porous medium with different types of retention of particles: surface deposition, pore-throat plugging and entrainment.

Viewing the retention of particles within or at the face of a porous medium from a more macro perspective, two main types of filtration are considered: Internal Filter Cake (IFC) and External Filter Cake (EFC). IFC, also known as Deep Bed Filtration (DBF), includes particles entering the porous medium and accumulating internally. Especially small particles can penetrate the medium for large distances compared to large particles. This correlates largely to the pore-throat size of the porous medium. EFC may be the response of IFC accumulating upstream as well as straining, i.e. particles are bigger than the pore throats. EFC is usually referred to as the external accumulation.

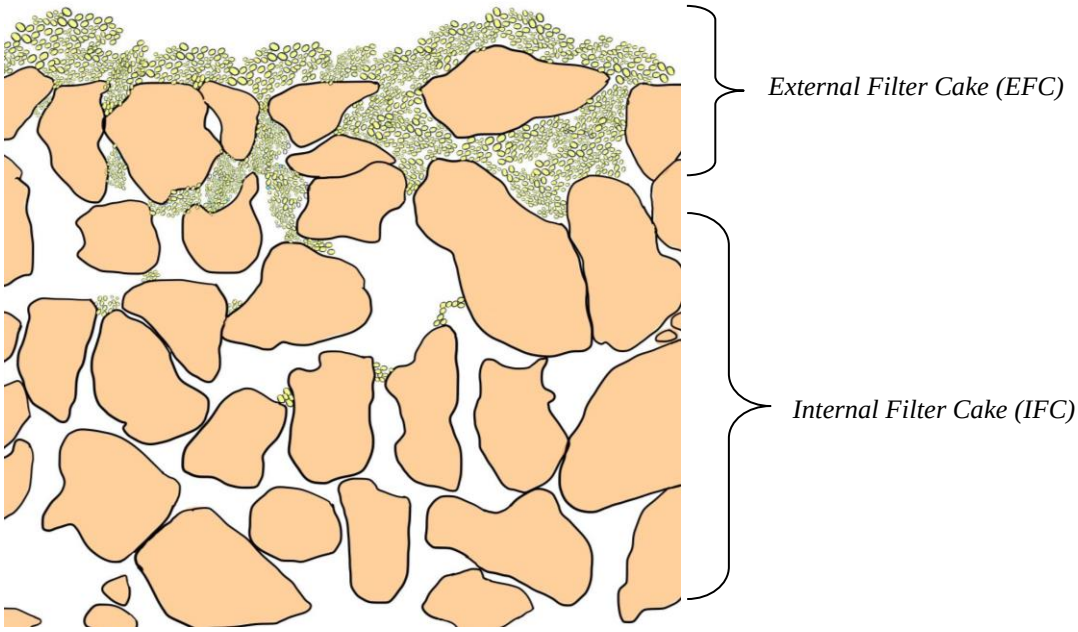


Figure 2.4. Schematic drawing of the porous medium with Internal Filter Cake (IFC) as well as External Filter Cake (EFC).

### 2.2.2 Water Quality

As discussed before, water quality is a term used to measure injection water by the impact it has on the amount of formation damage. The following aspects have an impact on water quality, i.e. inducing formation damage [8];

- Chemical composition
- Dissolved gasses,
- Corrosivity,
- Bacterial content,
- Suspended solids
- Hydrocarbon content

This is quite a list where the variation of each component could interact in a different way on inducing formation damage. In this research, focus lays on total suspended solids (TSS). Therefore, each time the term Water Quality (WQ) is used, it references to the number of suspended particles within the suspension.

# 3 Model Formulation

Membrane filtration is a well-established practice where significant research has been done in understanding cake filtration and membrane fouling in microfiltration. In this report, a dead-end filtration model is used, which is well-described by Greg Foley [29]. In this book, various membrane filtration processes are described in detail, and some excellent MATLAB examples are presented to help explain the concepts. Porous thin disc permeability impairment is slightly different as seen with membrane filtration, due to pore size and available surface area and damage mechanism. Nevertheless, the model for dead-end filtration provides a useful tool in applying the same kind of approach to understanding permeability impairment due to suspended solids.

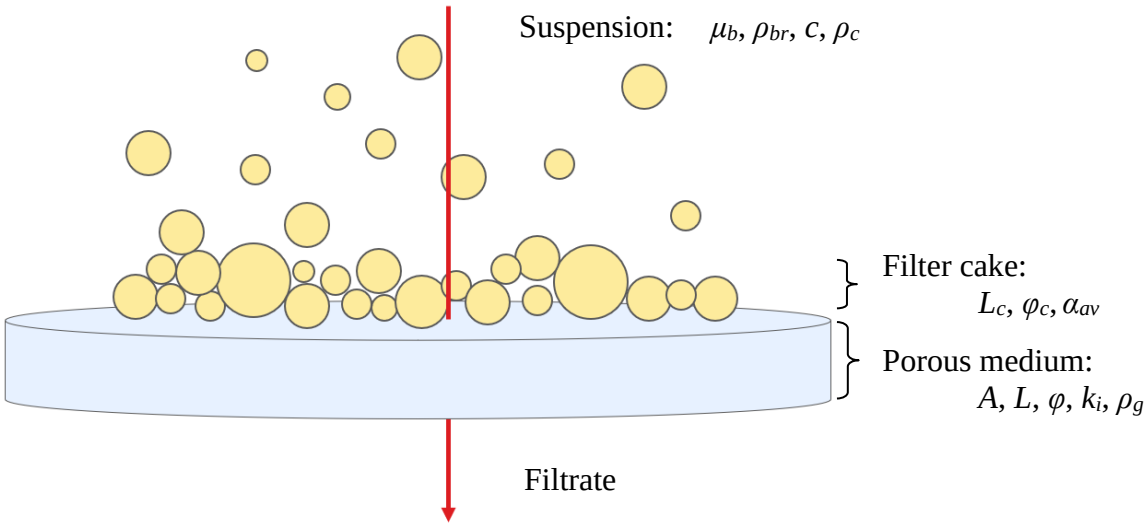


Figure 3.1. Dead-end filtration utilizing a porous medium.[30]

A model porous medium is defined. This porous medium is assumed to be homogenous and is described by a cross-sectional area $A$ and length $L$. The model porous medium is of known composition and characteristics, which are defined by isotropic porosity $\varphi$, initial permeability $k_i$ and porous medium density $\rho_g$. Usually, the porous medium length is very small. Therefore the term resistivity $R_m$ is used, which is equal to length divided by the permeability. The model assumes a single aqueous brine phase characterised by viscosity $\mu_b$ and density $\rho_{br}$. Non-coalescing model particles are introduced, which are specified by concentration $c$ and density $\rho_c$. The filtration process induces a build-up of a filter cake, which has a length $L_c$, porosity $\varphi_c$. Permeability impairment due to suspended particles is captured by introducing a term called specific cake resistance $\alpha_{av}$. The filter cake properties are highly depended on volume $V$ flowed.

In section *3.2*, the governing equations are specified, which are derived from Darcy's Law following the model assumptions stated in section *3.1*.

## 3.1 Model assumptions

For implementing the model, a few basic assumptions are made which are listed as follows:

- Flow is one dimensional and laminar.
- Porous medium and fluid are incompressible.
- Porous medium permeability/resistance is constant over time.
- The medium filter efficiency is 100%, i.e. only EFC is considered.
- Cake formation is instantaneous.
- Brownian particle diffusion is absent.
- The suspension viscosity is concentration-independent.

## 3.2 Governing equations

In this section, the governing equations are formulated, considering the assumptions given in the previous section. Here only the most relevant equations are given. It is important to emphasize that permeability impairs due forming of EFC and that particle penetration in the form of IFC is neglected.

Darcy's law is used for describing one dimensional flow in porous media using a clean (non-damaging fluid), which states that:

$$\frac{Q}{A_m} = \frac{k_i}{\mu_b}\frac{\Delta P_m}{L_m} = \frac{\Delta P_m}{\mu_b R_m} \tag{1}$$

Here $Q$ is the flow rate ($m^3/s$), $A_m$ is the medium cross-sectional area ($m^2$), $k_i$ is the initial permeability ($m^2$ or $10^{-12}$ Darcy), $\mu_b$ is the brine viscosity (Pa.s), $\Delta P_m$ is the pressure drop over the porous medium (Pa), $L_m$ is the length of the medium (m), and $R_m$ is the medium resistance (1/m).

Darcy's law can be expressed in terms of permeability or resistance, where $R_m = L_m / k_m$. With suspended particles damaging the porous medium, the permeability impairs due build-up of a filter cake. As a result, the total pressure drop over the system is described by a pressure drop over medium and pressure drop over formed cake:

$$\Delta P_t = \Delta P_m + \Delta P_c \tag{2}$$

Here $\Delta P_t$ is the total pressure drop over the porous medium and cake (Pa), $\Delta P_m$ is the pressure drop over the porous medium (Pa), and $\Delta P_c$ is the pressure drop over the cake (Pa).

Equation (1) is written in the terms of flux ($q = Q/A$) through the medium as follows:

$$q_m = \frac{\Delta P_m}{\mu_s R_m} \tag{3}$$

Where $q_m$ is the flux through the medium (m/s), $\mu_s$ is the suspension viscosity (Pa.s), and $R_m$ is the medium resistance (1/m).

In the same way, the flux through the cake is expressed as:

$$q_c = \frac{\Delta P_c}{\mu_s R_c} \tag{4}$$

Here $q_c$ is the flux through the cake (m/s), $\mu_s$ is the suspension viscosity (Pa.s), and $R_c$ is the cake resistance (1/m). The resistance generated by the cake $R_c$ is best described in terms of the amount of cake deposited per unit area:

$$R_c = \alpha_{av} \rho_c \varphi_c L_c \tag{5}$$

Where $\alpha_{av}$ is the average specific resistance (m/kg), $\rho_c$ is the density of cake (kg/m$^3$), $\varphi_c$ is the particle volume fraction in the cake (-), and $L_c$ is the length of the cake (m)

*Equation (3)* and *Equation (4)* are substituted in Darcy's Law and with some rearranging the following equation is given:

$$\frac{Q}{A} = \frac{\Delta P}{\mu\left(R_m + R_c\right)} \tag{6}$$

*Equation (6)* illustrates that a total resistance over the system is described by the medium $R_m$ plus the cake resistance $R_c$. As stated in the model assumptions, the permeability or resistance is not changing over time. Therefore *Equation (6)* is rearranged in the form known as the 'General Filtration Equation':

$$\frac{dt}{dV} = \frac{\mu \alpha_{av} c}{\Delta P A^2} V + \frac{\mu R_m}{\Delta P A} \tag{7}$$

*Equation (7)* is written in the form of y = *a*x + *b* in order to solve this equation as an ordinary differential equation (ODE).

## 3.3 Solving the General Filtration Equation

In this work, the filtration of $CaCO_3$ particles is considered, in two operation modes: Constant flow rate and constant pressure drop. Either way, *Equation (7)* is solved for constant rate or constant pressure solution using the ode45 function in MATLAB, which solves first-order differential equation. These solutions are easily obtained by rearranging the general filtration equation.

### 3.3.1 Constant Rate Filtration

Considering the flow rate (*dV/dt*) to be constant, rearrangement of *Equation (7)* provides the following equation:

$$\Delta P = \frac{\mu \alpha_{av} c}{A^2} \frac{dV}{dt} V + \frac{\mu R_m}{A} \frac{dV}{dt} \tag{8}$$

$$\alpha_{av} = \alpha_0 \left(1 + kc \Delta P_c\right)^m \tag{9}$$

*Equation (8)* is written in the form of y = *a*x + *b*, and by taking compressibility from the cake into account, *Equation (9)* provides the empirical relationship for average specific cake resistance. Here $\alpha_0$, *kc*, and *m* are empirical parameters.

*Equation (8)* is solved for each time step considering the generic initial condition $\Delta P = \mu R_m q$, at t = 0 and $\Delta P_c = 0$, at t = 0. Boundary conditions are set to correspond to conditions seen with real experiments, which is the case when $\Delta P$ = 4.3 bar, at t = end.

Depending on the various parameters, *Equation (8)* is solved for each time step. Considering typical values presented in the book for membrane filtration of $CaCO_3$, the normalized permeability is plotted versus volume for different suspension concentrations are presented in *Figure 3.2.a*. The reason for plotting normalized permeability versus volume will be addressed in more detail in the following chapter). What is important here are two observations: a) Less volume is needed to impair the permeability with a high concentration compared to a low concentration, b) When multiplying the volume with the concentration, the mass of suspended solids is obtained. *Figure 3.2.b* illustrates that by performing this simple multiplication, one single master curve is obtained. In other words, plotting normalized permeability versus mass injected demonstrates one master curve which scales with concentration.

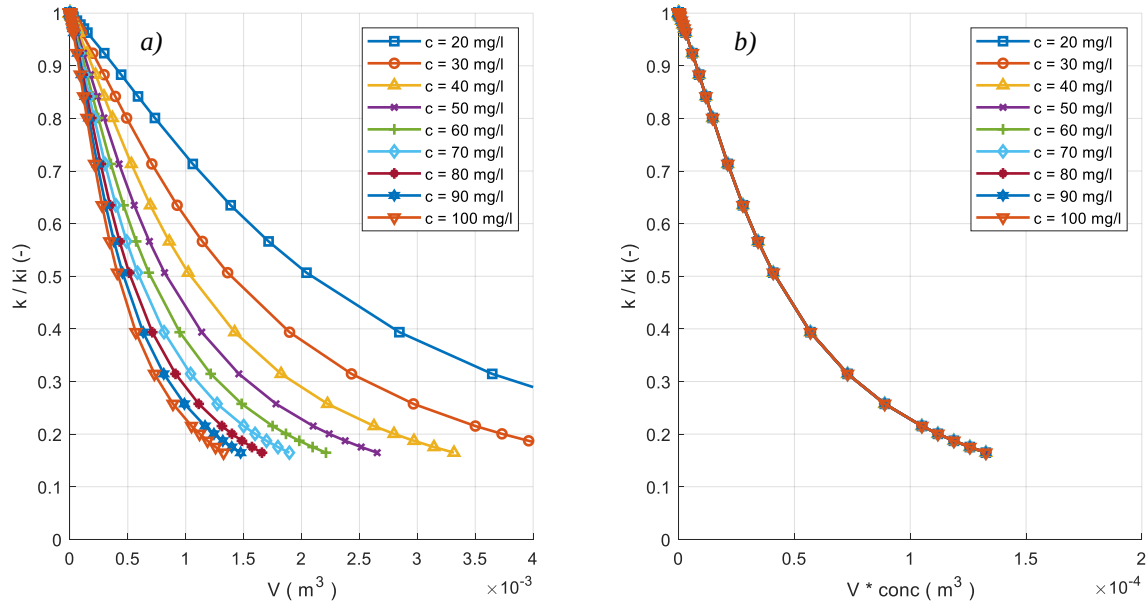


Figure 3.2: Model results for standard porous medium filtration parameters. a) Normalized permeability plot plotted versus volume and b) normalized permeability plotted against volume times concentration.

### 3.3.2 Constant Pressure Filtration

Considering constant pressure filtration, the general filtration equation is rearranged in the same manner as seen in previous section, allocating the parameters in the following form:

$$\frac{t}{V} = \frac{\mu \alpha_{av} c}{2 \Delta P A^2} V + \frac{\mu R_m}{A \Delta P} \tag{10}$$

*Equation (10)* is solved for each time step considering the initial condition $V = 0$, at t = 0 and $\Delta P_c = 0$, at t = 0. The boundary condition can be chosen for total volume $V$ flowed, at t = end.

Plotting $t/V$ versus $V$, also known as the Ruth plot, illustrates that the problem can be approached by solving *Equation (10)* in the form of y = $a$x + $b$. Here $a$ (the slope during cake

filtration) is equal to $\frac{\mu \alpha_{av} c}{2\Delta P A^2}$, which is also known as the Modified fouling index (MFI). *Figure 3.3* demonstrates the typical profile found with constant pressure filtration and illustrates three different regimes: Blocking filtration, cake filtration and cake compression. In the linear part illustrated in the Cake filtration regime, the MFI is determined.

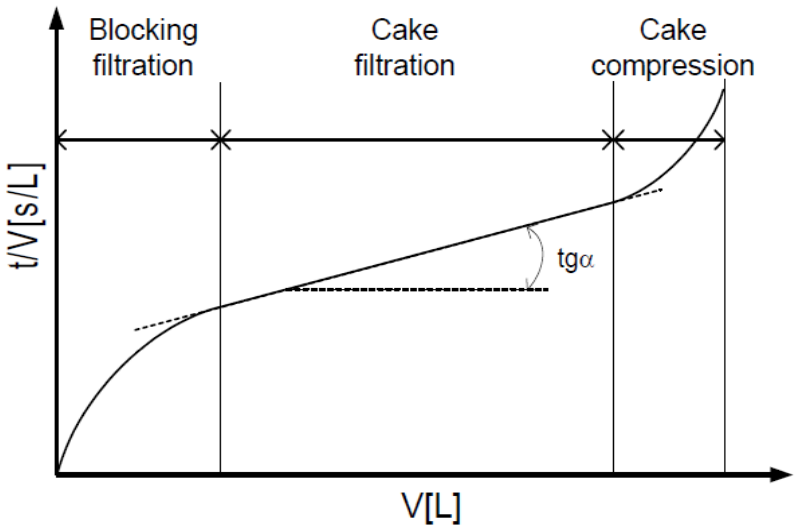


Figure 3.3: Ruth plot, plotting t/V versus volume with the indication of different filtration regimes considering constant pressure filtration [31].

# 4 Experimental Methods

## 4.1 Porous Medium

To study the effect of water quality on formation damage into the subsurface reservoir, different porous media types are tested and compared. Throughout this report, some terminology is used in referring to the porous media 'types' used in this research. The two types of porous media tested are:

- Membrane Filters (MF)
- Porous thin disc (PTD)

Membrane filters are thin porous media which are commonly known and used for water quality tests and the porous thin discs resemble to a large extent the cores used in Special Core Analysis (SCAL)[4] representing the porous media found in the reservoir.

### 4.1.1 Membrane filters

One of the applications in the usage of membrane filters is Micro-filtration. Micro-filtration is represented by particle and/or micro-organism filtration above a pore size of 0.1 $\mu$m. In this study, the membrane filters of interest are the mixed cellulose esters (MCE) and polycarbonate (PC) filters, both commonly used in Micro-filtration. Both types are available in a range of different pore sizes. However, the selected pore size is chosen to align with common usage in on-site water quality tests and filtration of synthetic brine practices. The MCE and PC filters originate from Merck Millipore Ltd. under the name of MF-Millipore™ and Isopore™ membrane filters, further referred to as MF0.45 and IP0.4, respectively. The membrane filter characteristics from the supplier are given in *Table 4.1*. The MF0.45 filters have a fibre/sponge-like structure with high porosity, visible in *Figure 4.1.a*. The IP-0.4, on the other hand, has a perforated structure, visible in *Figure 4.1.b*.[5]

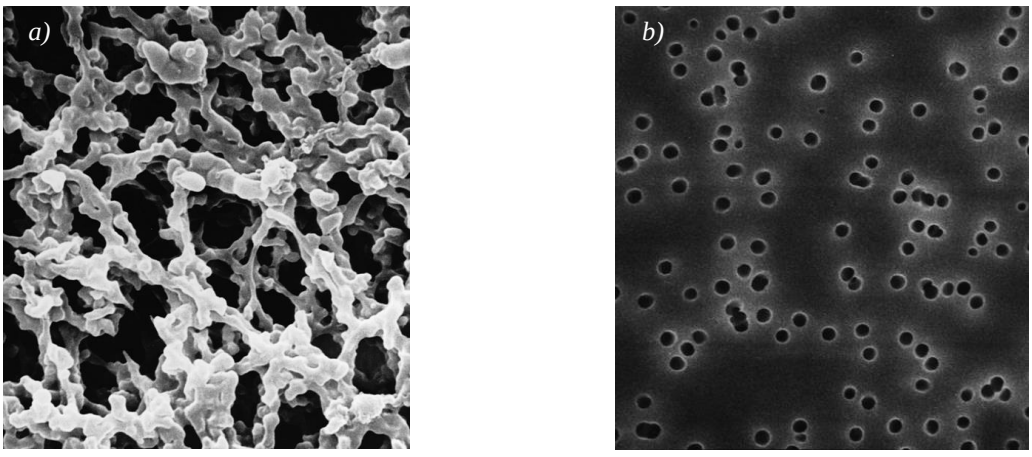


Figure 4.1: SEM images of a) Mixed cellulose esters (MCE), MF0.45 structure. b) Polycarbonate (PC) IP0.4, filter structure. Scale not available, nonetheless, the pores given in black should indicate 0.45 and 0.4 $\mu$m pore sizes.

[4] More information on SCAL: https://www.scores-panterra.nl/

[5] Images available from: https://www.merckmillipore.com/NL/en/life-science-research/chromatography-sample-preparation/microfiltration-membranes/FqCb.qB.7ZkAAAFBDQZlvzJE,nav

Table 4.1: Membrane filter specifications and characteristics.

| Name | Filter type & Code | Pore size [$\mu$m] | Diameter [mm] | Thickness [$\mu$m] | $\varphi$ [%] | Water flowrate [ml/min x cm$^2$] |
|---|---|---|---|---|---|---|
| MF0.45 | MCE (HAWP) | 0.45 | 47 | 150 | 79 | 60 |
| IP0.4 | PC (HTTP) | 0.4 | 142 | 10 | 10-20 | >50 |

### 4.1.2 Porous thin discs

The second porous media type are the porous (sandstone) thin discs. Two sandstones from different outcrops are used: Bentheimer Sandstone block 11 (BH11) and Berea Sandstone block 18 (BER18). Both are characterized by X-ray diffraction (XRD) analyses for their mineral composition and a Mercury Injection Capillary Pressure ("MICP") measurements to obtain pore throat size distribution.
Cylindrical cores are drilled from the two sizeable cubical sandstone blocks with a 35 mm drill bit using tap water as a lubricant. From the cylindrical cores, 8mm thick, thin discs are cut with a struers-Accutom-100 precision saw. To remove any contamination from the freshly cut porous media, e.g. sawing dust and/or oil-water lubricants, the discs were put in a Soxhlet extraction bath for 15 hours and subsequently dried in an oven at 60 °C for 3 hours. Permeability tests were carried out on each of these thin discs with filtered synthetic brine prior to the suspension flow experiment.

#### 4.1.2.1 Bentheimer sandstone (BH11)

One of the two porous media types is Bentheimer sandstone, chosen because of the high homogeneity and lateral continuity throughout the sandstone. It is also a well-known sandstone and widely used in literature [20], [32]–[34]. BH11 mainly consists of silica with a low amount of minerals with a constant grain size distribution. The BH11 block is taken from an outcrop in Bad Bentheim/Nordhord, Germany, which is in terms of deposition a shallow marine formation descending from Zechstein, Lower Cretaceous times.

##### 4.1.2.1.1 BH11 Mineral Composition

The mineral composition of the sandstone is obtained by performing XRD analysis on test samples from the cubical block BH11. This analysis gives the semi-qualitative results of the rock fraction and mineral content of the sample. In literature, the Bentheimer sandstone has been extensively analyzed for the mineral composition and the XRD-analysis. These results [20], [32], [33] are given along the results of this study, presented in *Table 4.2*. The XRD-analysis results show that the composition exists mainly out of quartz with small amounts of clay and feldspar.

Table 4.2: XRD analysis results of Bentheimer sandstone sample (BH11) and results found in literature [20], [32], [33].

| Mineral | This Study [wt. %] | Peksa et al. (2015) [wt. %] | Maloney et al. (1990) [wt. %] | A. Murtaza (2017) [wt. %] |
|---|---|---|---|---|
| Quartz | 98 | 91.7 | 97.5 | 92 |
| Kaolinite (Clay) | 1 | 2.5 | 0.5 | 2.8 |
| Microcline (Feldspar) | 1 | 4.9 | 2 | 4.5 |
| Other | Trace | 0.8 | Trace | 0.7 |
| **Total** | **100** | **100** | **100** | **100** |

#### 4.1.2.1.2 BH11 Pore characteristics

The porosity of the test samples is determined by using the mercury buoyancy method. This is a method where the grain volume and bulk volume is obtained by immersing a dry sample in mercury. From the volumes, the porosity is calculated. The weight of the sample is obtained by weighing the samples saturated with chloroform under vacuum. From the microscopic image presented in *Figure 4.3* and grain size distribution (GSD) shown in *Figure 4.2*, display the grain size which varies between the 70-400 $\mu$m (D50 grain size of approximately 200 $\mu$m). A MICP measurement is done to obtain the Pore-Throat size Distribution (PTSD), presented next to the grain size distribution shown in *Figure 4.2*. From this figure, one can observe the median pore throat diameter (D50) equals about 32 $\mu$m.

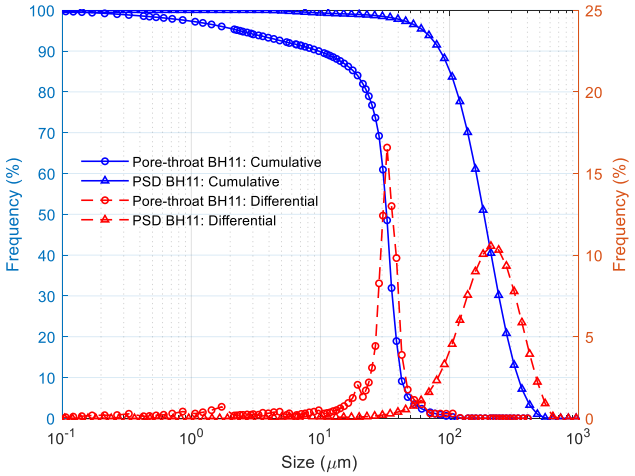


Figure 4.2: Pore-throat and grain size distribution BH11.

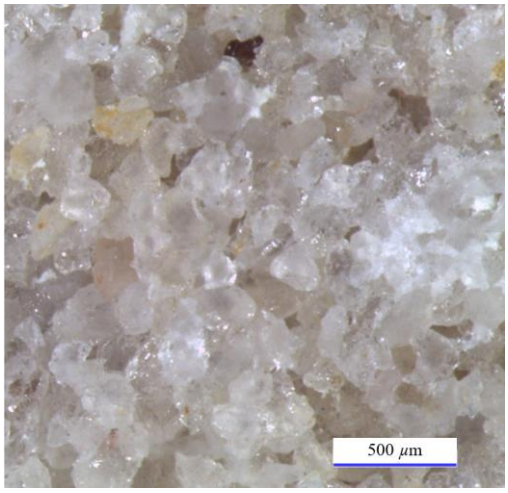


Figure 4.3: Microscopic image of BH11 PTD

### 4.1.2.2 Berea sandstone (BER18)

Berea sandstone samples originate from Pennsylvania (USA) outcrop and is a light grey to buff coloured river delta formation rock descending from Upper Devonian age. The block BER18 is in the form of siltstone and fine to medium grain sandstone.

#### 4.1.2.2.1 BER18 Mineral composition

The mineral composition of BER18 is determined by using XRD analyses, where the results are presented in *Table 4.3*. The results show that the composition also exists mainly out of quartz with some small amounts of clay and feldspar, which is similar as found in literature [33]. BER18 has a higher clay and feldspar weight percentage compared to BH11 sandstone.

Table 4.3: XRD analysis results of Berea sandstone sample (BER18) and results found in literature [33].

| Mineral | This Study [wt. %] | Maloney et al. (1990) [wt.%] |
|---|---|---|
| Quartz | 91 | 94 |
| Kaolinite (Clay) | 4 | 2 |
| Microcline (Feldspar) | 3 | 3 |
| Other | 1 | 1 |
| **Total** | **100** | **100** |

#### 4.1.2.2.2 BER18 Pore Characteristics

The porosity, grain volume and bulk volume are determined in the same manner as for BH11, i.e. the mercury buoyancy method. A MICP test was performed to obtain the pore throat size distribution, which is given alongside the results of the grains size distribution presented in *Figure 4.5*. From this figure follows that the median pore throat diameter (D50) is around 18 $\mu$m, which is about half of the BH11 median pore throat size. From *Figure 4.4* and *Figure 5.5*, one can conclude that the grain size varies between the of 100-300 $\mu$m, with the median (D50) of 180 $\mu$m.

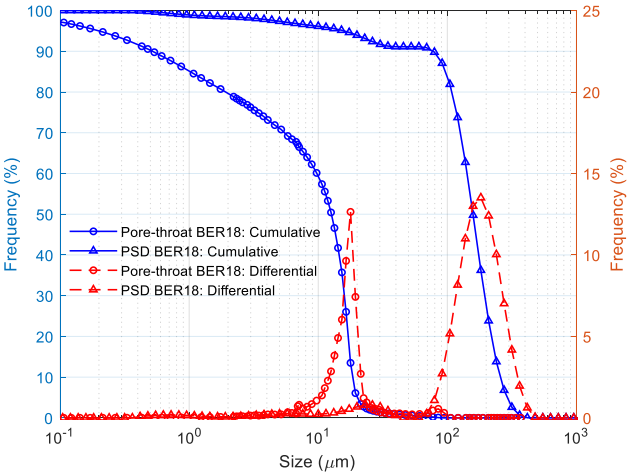


Figure 4.4: Pore-throat and Grain size distribution BER18.


Figure 4.5: Microscopic image of BER18

### 4.1.3 Porous thin discs preparation and mounting

After a Soxhlet cleaning and drying procedure, the discs are cooled and the length, width and weight are measured. Subsequently, the discs are wrapped in PTFE Bonfix Teflon tape to make a tight fit in the modified membrane filter setup to prevent fluid bypassing/leakage. This ensures fluid conformance during a suspension flow experiment. Adding a silicon disc on top fixates the thin disc and acts as a seal constraining the inflow fluid flow cross-sectional area for the thin disc ($A_{TD}$) to the reduced effective area ($A_{eff}$). A schematic cross-section is given in *Figure 4.6*. All discs are labelled on the side to referencing the core ID, slice number as well as the used mounting orientation. For example, TD-F1 stands for Thin Disc, core F, slice 1. After being wrapped and labelled, the discs are saturated under vacuum with FSB. Subsequently, the discs are cleaned utilising an ultrasonic bath for 30 min to remove any loosely connected material from the sand face areas of the discs. Core holder and discs are submerged in brine during mounting to prevent air entrapment within the flow cell.

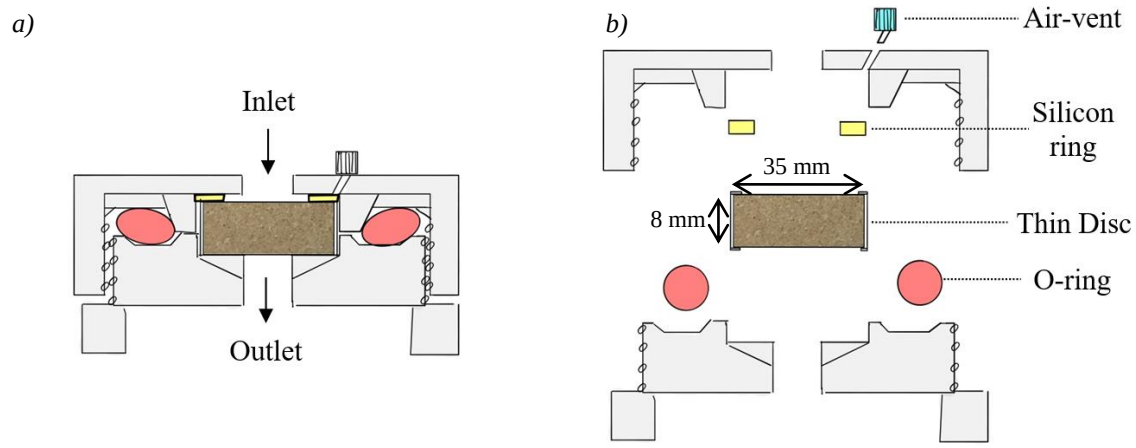


Figure 4.6: Schematic drawing of a closed (a) and open (b) thin disc holder.

## 4.2 Synthetic Brine preparation

Specific amounts of salts are prepared and added to demineralized water (demi water). This is done to create a synthetic brine with an ionic composition resembling a known seawater recipe. Two brine concentrates are made, where small volumes from these two concentrate batches can be added to a large volume of demi water to obtain the ionic composition intended eventually.

### 4.2.1 Ten times concentrated brine preparation

Two batches of brine concentrates are prepared, concentrate A and concentrate B, separating the calcium/magnesium salts from the sulphate salts. These are separated to ensure that no salt precipitation takes place in the form of calcium-/magnesium sulphate, which is commonly the case if brine is stored for a longer time. Two calibrated volumetric flasks of 5 L (A and B) are cleaned and filled up to 3 L with demi water. Next, each salt of weight given in *Table 4.4* is added in the given order for concentrate A and B. When all the salts are added, demi water is added until the 5 L mark is reached. Afterwards, a magnetic stirrer is added and is continuously stirred.

### 4.2.2 Filtered Synthetic Brine preparation

To create a flow experiment batch, a 10 L volumetric flask is cleaned and filled with 5 L of demi water. Two 500 ml volumetric glasses are prepared, one filled with concentrate A and one with concentrate B. Both 500 ml volumetric glasses are added to the 10 L volumetric glass and filled up to the calibrated mark with demi water. The concentration of ions from this batch is given in *Table 4.5*. A magnetic stirrer is added, and after stirring, the sample is filtered through an IP-0.4 filter using an overpressure resulting in the filtered synthetic brine (FSB).

Table 4.4: Weight of each salt added to demineralized water to create the ten times concentrate synthetic brine.

| | Total Conc. [10 L] | Conc. A [5 L] | Conc. B [5 L] |
|---|---|---|---|
| Salts | Weight (g) | Weight (g) | Weight (g) |
| NaCl | 2350 | 1175 | 1175 |
| KCl | 74 | 74 | 0 |
| $MgCl_2.6H_2O$ | 1040 | 1040 | 0 |
| $CaCl_2.2H_2O$ | 140 | 140 | 0 |
| $Na_2SO_4.10H_2O$ | 910 | 0 | 910 |

Table 4.5: Concentration of ions in the Filtered Synthetic Brine (FSB)

| Ions | Concentration [PPM] |
|---|---|
| $Na^+$ | 10543 |
| $K^+$ | 388 |
| $Mg^{2+}$ | 1243 |
| $Ca^{2+}$ | 382 |
| $Cl^-$ | 18911 |
| $SO_4^{2-}$ | 2,713 |
| **Total** | **34180** |

## 4.3 Particle Characterization

Baracarb2 ($CaCO_3$), provided by Baroid (Halliburton), is chosen as a model substance to represent fluid contaminant. In literature, $CaCO_3$ has been extensively used as a suspended particle fluid substance [9], [34], [35]. However, in literature, extended details regarding the mixing procedure, PSD and mineral composition typically are sparse or incomplete. Therefore, this aspect is given substantial attention. Baracarb2 is made from ground marble with a density of 2.71 g/cm$^3$ and engineered to specific particle size. Baracarb can be ordered in different sizes, i.e. Baracarb2/5/10/25/100, where the number in the name should indicate the nominal median particle size (D50). However, in literature, it is found that this is not necessarily the case [34], [35]. This study will confirm this. Calcium carbonate is a natural

substance found in subsurface fluids, and it's a common practice to use it in drilling applications, for increasing water density and as bridging agent [36].

### 4.3.1 Mineral composition Baracarb2

In this section, the findings of the mineral composition of Baracarb2 are presented. First, an acid solubility test is performed on Baracarb2 to identify non-calcium carbonate content, as calcium carbonate should be fully dissolvable in acid. Therefore, an 18% HCl solution is added to a prepared suspension until al calcium carbonate is dissolved. Thereafter the residue is filtered with an MF0.45 and weighed after drying in an oven. Interestingly, 7.8 wt.% is non-calcium carbonate. Subsequently, Baracarb2 is analyzed for mineral composition by performing XRD analysis and Scanning Electroscope Microscopy (SEM) imaging. The XRD results are given in *Table 4.6* and show that Baracarb2 exist mainly out of calcite (calcium carbonate) with minor quartz*, clinoptilolite* and smectite* traces. The marked* substances represent the insoluble content observed in the acid solubility test. *Figure 4.7* presents an SEM image of the as-received dry Baracarb2 particles. From this image, a rough estimation is made for the particle range, which is 2 – 20 $\mu$m. The particles have a variating form in which can be classified as sub-rounded to sub-angular.

Table 4.6: XRD results of Baracarb2.

| Mineral | Baracarb2 Composition [wt. %] |
|---|---|
| Calcite | 95.5 |
| Quartz | 1.9 |
| Clinoptilolite | 1.7 |
| Smectite | 0.9 |
| **Total** | **100** |

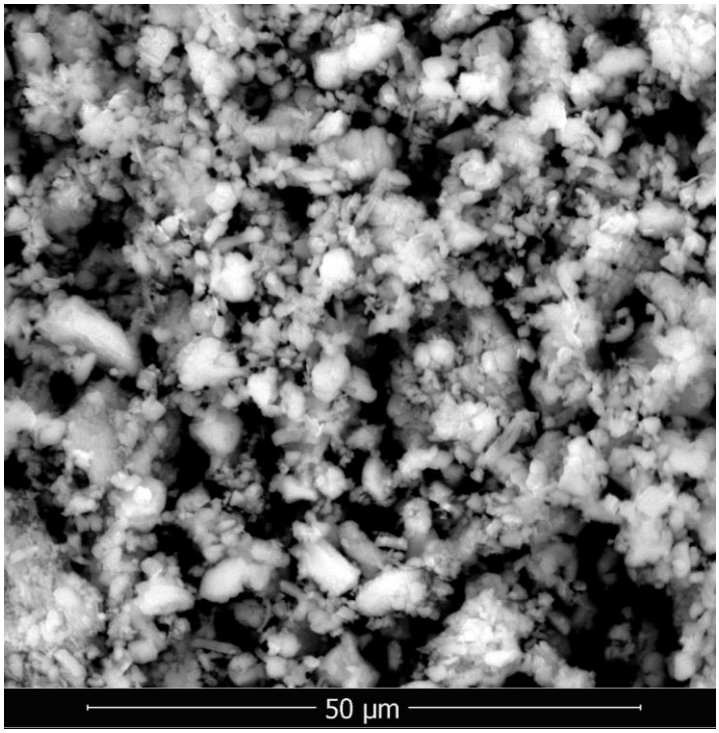


Figure 4.7: SEM imaging of Baracarb2

## 4.4 Suspension Stability Study

After characterization of the Baracarb2 particles, a stability study is carried out to analyse the behaviour of these particles in the prepared FSB. This was done in four ways; calcium saturation test, turbidity measurements for concentration identification, sedimentation experiments and particle analysis using laser diffraction method. It is important that the particles remain in suspension and no sedimentation takes place in flow lines or connection points during a flow experiment. Therefore, the Baracarb2 suspensions are always continuously stirred with a magnetic stirrer at a rate of 100 rpm.

### 4.4.1 Calcium saturation in synthetic brine

Baracarb2 particles are added to the FSB to create a suspension with a specific concentration. However, knowing that the composition given in *Table 4.5* is calcium undersaturated, some of the calcium carbonate will dissolve until an equilibrium is reached. The amount of calcium that dissolves in the FSB is estimated using the OLI software package and is experimentally tested for three different concentrations of Baracarb2, namely 20, 50 and 100 mg/l. Also, the salinity impact on solubility is tested using two salinities; Brine type 1 and 2. These correspond to 0% and a 50% diluted FSB. The test results are given in *Table 4.7*. From these results, one can conclude that at least 10 mg/l of the calcium carbonate will dissolve when Baracarb2 added to the FSB. The method of experimentally determining the amount of dissolved Baracarb2 is quite an error-prone process, considering possible losses of containment during the experimental steps. From *Table 4.7*, it is seen that about the same amount of Baracarb2 dissolves considering the two brine types and the OLI estimated values.

Table 4.7: Baracarb2 dissolution test in calcium undersaturated brine at room temperature.

| Batch # | Brine type | Salinity [PPM] | Baracarb2 Concentration [mg/l] | Baracarb2 dissolved experimentally measured [mg/l] | Baracarb2 Dissolved OLI simulated [mg/l] |
|---|---|---|---|---|---|
| 1 | 1 | 34180 | 100 | 16 | 10.1 |
| 2 | 1 | 34180 | 50 | 18 | 10.1 |
| 3 | 1 | 34180 | 20 | 14 | 10.1 |
| 4 | 2 | 17090 | 100 | 15 | 10.4 |
| 5 | 2 | 17090 | 50 | 11 | 10.4 |
| 6 | 2 | 17090 | 20 | 11 | 10.4 |

### 4.4.2 Turbidity

Before each flow experiment, turbidity measurements are taken on the samples of Baracarb2 suspension and FSB to identify the maximum and minimum turbidity range. This is done for all experiments to enable calibration of the turbidity to concentration values as well as enabling calculating the normalized turbidity. The turbidity is measured with a Hanna Instruments (HI-93414) turbidity meter[6]. This instrument measures turbidity in the three ranges: 0.00-9.99 NTU, 10.0-99.9 NTU and 100-1000 NTU. Each range has a different resolution: 0.01 NTU, 0.1 NTU and 1 NTU, respectively to the given ranges. The accuracy tends to be ± 2% of reading plus an absolute error of 0.02 NTU. *Figure 4.8* illustrates how the turbidity differs between the varying suspensions.

The turbidity and pH measurements for different concentrations are given in *Table 4.8*, where all suspensions are found to have a pH of about 8.7. The turbidity of FSB showed similar values for all measurements and ranges between the 0.06-0.1 NTU, respectively. The turbidity is measured for multiple suspensions with varying concentration. These turbidity results are plotted against the corresponding suspension concentration, resulting in *Figure 4.9*. From these data points, a linear regression line is fitted, which illustrates a linear trend between turbidity and concentration. The linear regression line intercepts the x-axis at 10 mg/l, which indicates that adding 10 mg/l to FSB gives a response of zero turbidity. This is in line what is found in section *4.4.1*, i.e. 10 mg/l of calcium carbonate dissolves when added to

[6] The extended specifications for the Hanna Instruments (HI-93414) can be found at https://www.hannainst.dk/epa-compliant-turbidity-and-free-total-chlorine-meter-with-fast.html#specifications

FSB. The pH is also measured for the suspension as well as the original FSB finding repeatable outcomes.

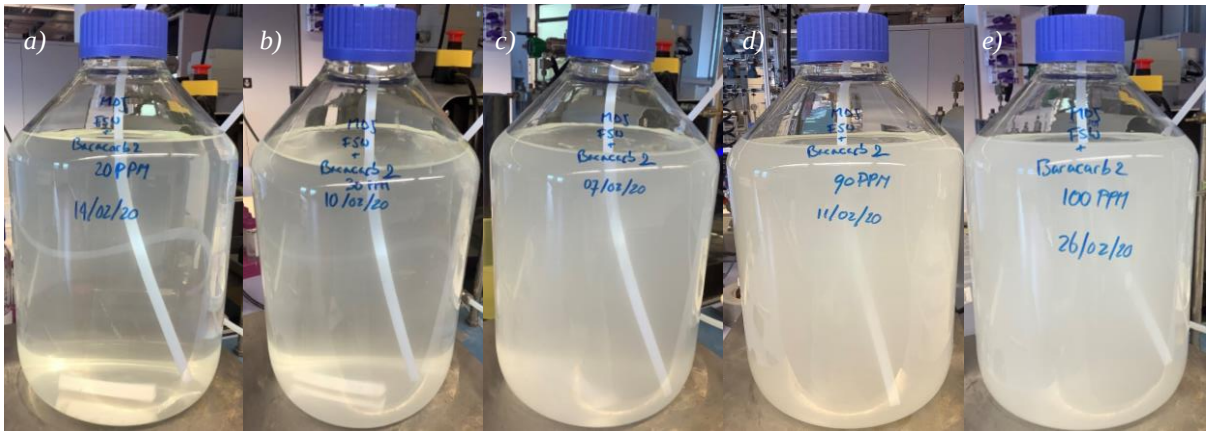


Figure 4.8: Baracarb2 suspensions in a 10 L reservoir tank with varying concentration: a) 20 mg/l. b) 30 mg/l. c) 50 mg/l. d) 90 mg/l. e) 100 mg/l.

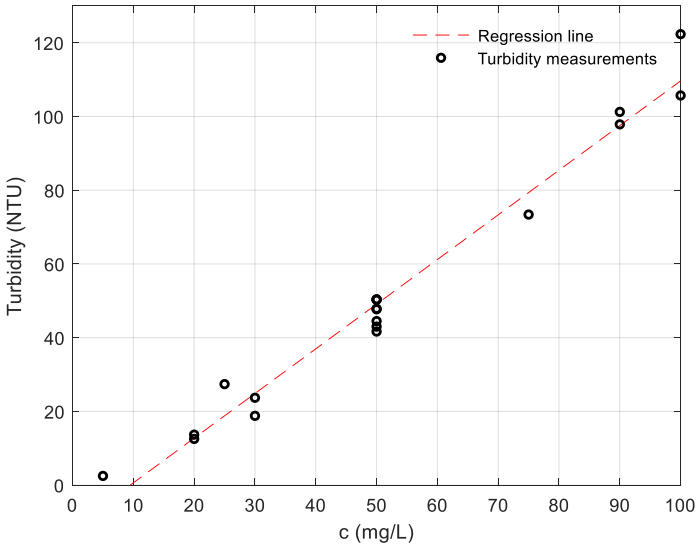


Figure 4.9: Turbidity measurements of suspensions at different concentration with regression indicating a trend between turbidity and concentration

Table 4.8: Baracarb2 suspension turbidity measurements for different concentrations with additional pH measurement determined before the flow experiments.

| Baracarb2 Concentration [mg/l] | Turbidity [NTU] | *pH* |
|---|---|---|
| 100 | 106 | 8.6 |
| 90 | 100 | 8.8 |
| 50 | 49 | 8.6 |
| 30 | 21 | 8.6 |
| 20 | 13 | 8.7 |

### 4.4.3 Particle size analysis

To analyse the particle size distribution (PSD) and the stability of the suspended Baracarb2 particles over time, the Malvern Hydro 2000G is used. This device makes use of a high-speed rotating laser scanning a small volume flowing through a flow cell, where some of the light is blocked/obscured by the particles in suspension. By measuring the time of obscuration and rotary speed of the laser, the particle diameter is determined by the Laser Obscuration Time (LOT) principle. As a result, an accurate measurement is made of the particle size distribution [37]. In literature, similar tests are found attempting to capture the particle size distribution of Baracarb2 and Barcarb5 [34], [35]. Dogon and Golombok (2015) show that it is important to measure the particle size distribution of Baracarb2 and Baracarb5 for an extended time, as the duration of the test influences the particle size measurements. They also show that shearing of the fluid results in orthokinetic agglomeration of the Barcarb2 and Baracarb5 particles in suspension. Therefore, consideration of keeping stirring speeds fixed for all experiments is necessary.

In conducting the particle size distribution experiments, two types of methods are considered;

- *Method 1.* First, FSB is added to the tank for an initial measurement to establish a baseline. Next, 100 mg/l Baracarb2 suspension is poured in the tank using small amounts. At the same time, the live feed obscuration measurements are recorded on the Malvern computer software. The suspension is added until the obscuration level is within the predefined operational range. In the tank, a stirrer is present to keep particulates in suspension, and a pump ensures circulation through the flow cell.

- *Method 2.* First, a baseline measurement is conducted with FSB, like in 'Method 1'. By draining the tank with a hose, the FSB is subsequently removed. Hereafter, the tank is refilled with 1 L of 50 mg/l Baracarb2 suspension. It must be mentioned that the ultrasonic probe was not operating throughout the experiment.

Five particle size distribution (PSD) tests are conducted;

- Three tests of diluted Baracarb2 suspension differing in creation time via 'Method 1'
  - One day stirred at 100 rpm (Figures in *Appendix A*)
  - Three days stirred at 100 rpm (Figures in *Appendix A*)
  - Six days stirred at 100 rpm (Figures in *Appendix A*)

- Two tests which include testing a suspension of Baracarb2, via 'Method 2'
  - 50 mg/l (*Figure 4.10*)
  - 50 mg/l buffered at a pH of 8.5. (*Figure 4.11*)

For all the above-described PSD experiments, the same test is run using the Malvern software. This includes taking 20 sequential measurements at a sampling rate of 6 per hour. *Figure 4.10* shows the results of the 50 mg/l test, where the ascending time is indicated with using a colour bar. *Figure 4.10.a* gives the cumulative graph of the particle size distribution. The differential from this cumulative graph distribution function is presented in *Figure 4.10.c*. *Figure 4.10.b* provides the measured obscuration at each time step and *Figure 4.10.d* shows the results of the pH and temperature meters measured additionally.

*Figure 4.10.a*, *Figure 4.10.c*, *Figure 4.11.a* and *Figure 4.11.c* show typical size distributions of Baracarb2 in FSB in the range of 1-40 $\mu$m. Note the observed artefacts in the form of few small air bubbles observed in the 200-500 $\mu$m particle size range.

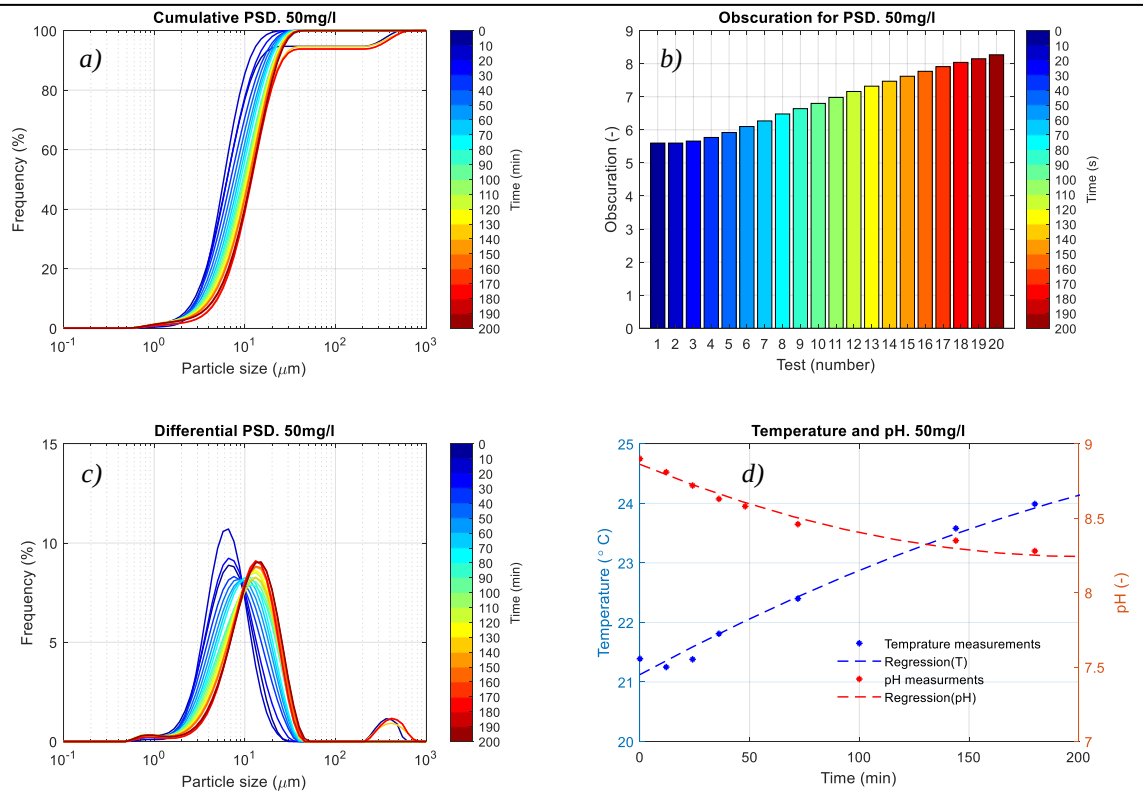


Figure 4.10: a) Cumulative particle size distribution of 50 mg/l Baracarb2 in FSB over time. b) Obscuration measured at each timestep. c) The differential particle size distribution of 50 mg/l Baracarb2 in synthetic brine over time. d) pH and temperature over time measured additionally.

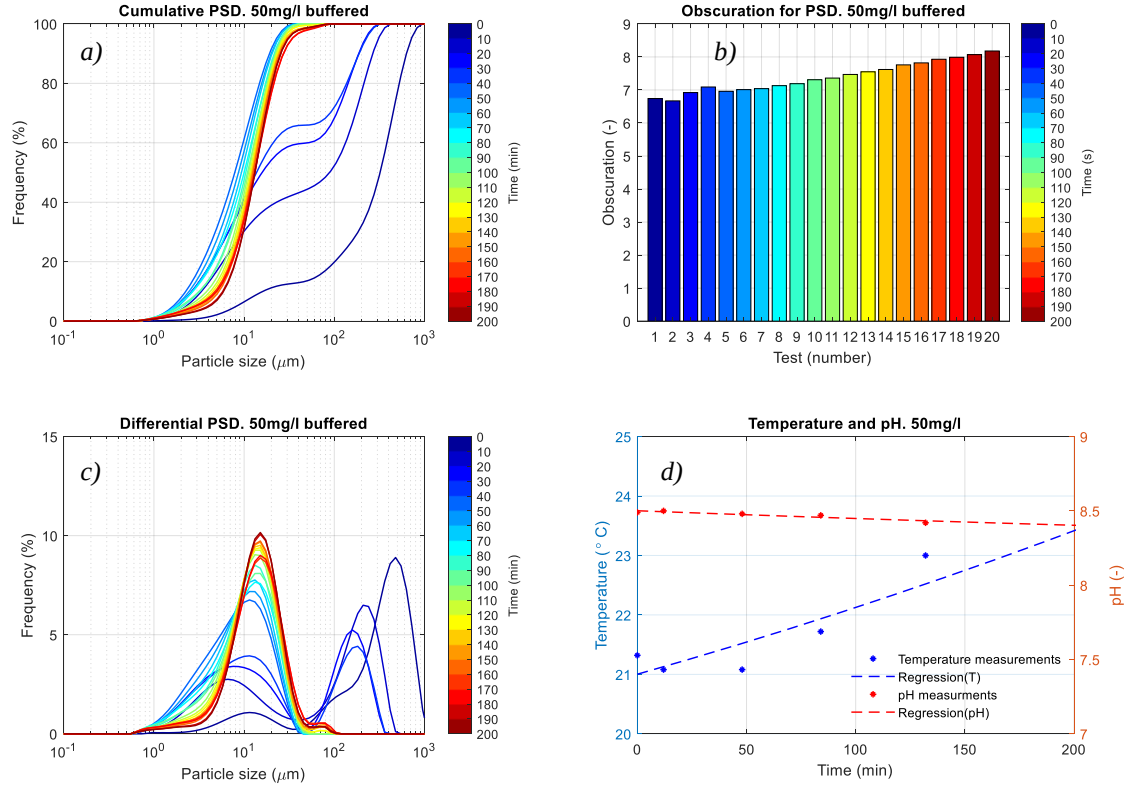


Figure 4.11: a) Cumulative particle size distribution varying with time of a 50 mg/l Baracarb2 suspension with buffered FSB at pH 8.5. b) Obscuration measured at each timestep. c) Differential particle size distribution varying with time of a 50 mg/l Baracarb2 suspension with buffered FSB at pH 8.5. d) pH and temperature over time measured additionally.

From the results presented in *Figure 4.10.a* and *Figure 4.10.c*, it is observed that the general trend shifts towards the right, indicating that particle size increases with time. The increasing obscuration signal shown in *Figure 4.10.b* illustrates that more light gets blocked over time, suggesting an increasing concentration or particle size. The latter is more evident as no particles are added additionally, and contamination of the flow cell is not considered to have a significant impact on the obscuration. Combining these results with the particle size range with visual inspection of the SEM images, it is proposed that particle agglomeration takes place. Considering *Figure 4.10.d*, a 3 °C temperature increase is measured. This is explained by the mechanical work done within the Malvern device resulting in dissipative heat loss to the suspension. The *pH* measurements give a downward trend, which is not adequately understood at this moment in time but might be related to $CO_2$ exchange between the solution and gasses within the ambient atmosphere.

To demonstrate the influence of *pH*, a similar suspension of 50 mg/l is created with a buffered FSB at *pH* 8.5, which is in the range of the equilibrium *pH* measured with Baracarb2 suspensions presented in *Table 4.8*. The same experiment is conducted with results shown in *Figure 4.11*, where *Figure 4.11.d* demonstrates that the buffer is active as the *pH* stays reasonably constant. Comparing the results presented *Figure 4.10* and *Figure 4.11*, it is seen that the distribution is in the same range and follows the same particle size increase with time.

The median particle size (D50) at each time step for all five tests is presented in *Figure 4.12*. From this figure, it is seen that a similar trend is given with a different starting point varying between the 4 and 8 $\mu$m. An interesting observation is, irrespectively the age of the suspension, following 'Method 1' results in the same trend with minor differences. *Figure 4.12* illustrates that the mean particles size given for a time frame of 50 to 100 min, the particle size distribution increases from 9 to 11 $\mu$m. This range is highlighted as in this time frame the actual flow experiments are conducted.

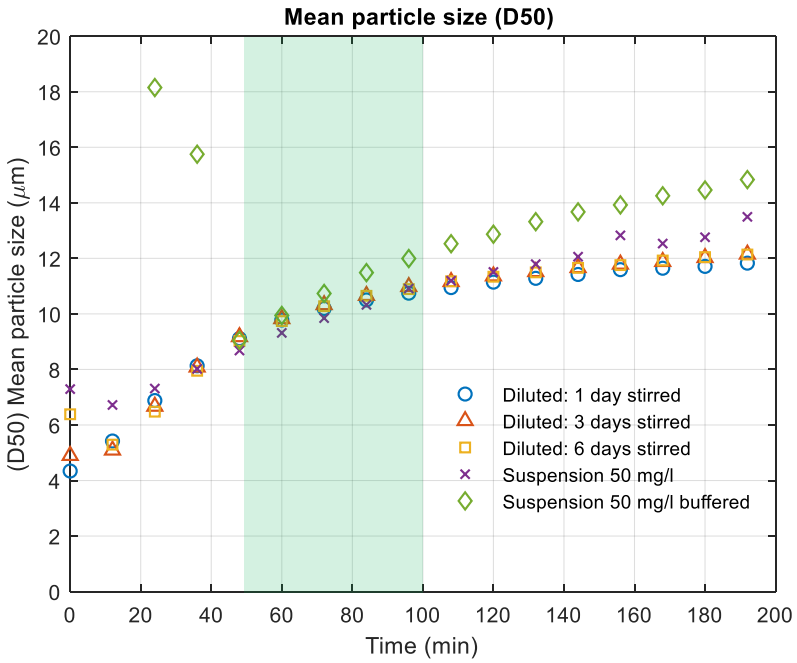


Figure 4.12: Median particle sizes (D50) at different time steps for five PSD experiments. A green section is highlighted, which indicates the operating window when experiments are conducted.

## 4.5 Experimental Setup

The experimental setup consists of the Con-vergence Hydra with some external modifications and is located at Shell Technology Centre Amsterdam (STCA).

### 4.5.1 Con-vergence Hydra unit

The Con-vergence Hydra, further in this report referred to as Hydra, is generally used for SDI/MFI water quality analysis. Basically, SDI and MFI, are methods of analyzing membrane fouling and cake filtration. For this study, the Hydra membrane holder is modified to cater for an 8 mm thick porous thin disc instead of the conventional membrane filter. The Hydra set-up contains a feed pump, two flowmeters, two pressure and temperature meters. The experimental setup is given in *Figure 4.14*. The system is controlled by the software program *Osmo-inspector*, available with the included Con-vergence laptop. This application runs pre-programmed filtration test scripts where several control settings can be programmed. In more detail, the system consists of:

- *Feed Pump.* The feed pump is a KNF diaphragm liquid pump, model NF 1.600. This pump operates based on the oscillating displacement pump principle. The pump is driven at a particular power by setting a constant rate or constant pressure set point in the pre-programmed script.

- *Flowmeter.* The experiments in this study are conducted only with the high flowmeter (FT-1), which is a Coriolis M15 type. The flowmeter is manufactured to operate within the range of 5-3000 ml/min (0.3-180l/hr).

- *Pressure and Temperature meters.* The pressure and temperature meters within the Hydra are of type 500 series. The pressures meters, P1 and P2, are placed before and after the setup, calculating a pressure gradient by subtracting P2 from P1. The operational range is limited between 0-4 barg.

- *Flow lines.* All flow lines external to the Hydra are (fluoropolymer) PFA tubing, which can withstand high temperature and pressures of 200 °C and 12 bar.

- *Three-way valve and external tubing.* Two sets of fluid batches are created in each experiment. One batch contains the filtered synthetic brine and one batch the suspension brine. Both batches are connected with 3/8-inch PFA tubing to a three-way valve, to create the possibility to switch between batches. This is done either during or after an experiment. From the three-way valve, a 3/8-inch PFA tubing is connected to the Hydra. The permeate tubing leaving the hydra for disposal is also a 3/8-inch PFA tubing.

- *Effluent sampling.* From the permeate line, samples are collected in 15 ml tubes during experiments for turbidity measurements.

### 4.5.2 Membrane holder and Thin Disc holder

The feed and permeate tubing entering and leaving the thin disc/membrane holder are both 3/8-inch PFE tubing, both fitted with a ¼-inch straight threat to 3/8-inch pneumatic tube fittings. These pneumatic tube fittings were specifically ordered at ERIKS. The usage of pneumatic tube fittings facilitates in rapid switching between the thin disc holder and the

membrane holder, while submerged in FSB. Both schematic overviews of the membrane setup and thin disc setup can be found in *Appendix B.*

### 4.5.3 Stability region Hydra

The feed pump, flowmeters and pressure meters are bound to specific operating ranges. These ranges are stated in *Figure 4.14*. However, these operating windows are different for each porous media. This is because the permeability of each porous media type (BH11, BER18 or MF0.45) is different. Considering Darcy's law, the pressure gradient multiplied by the permeability is proportional to the flowrate, hence with a fixed flow rate, the pressure increases when permeability decreases. This was also observed when testing membrane filters with different pore sizes, i.e. with a constant fixed rate, the pressure drop increased when a smaller pore size was used.

In the proof of concept phase, each porous media type is tested for multiple constant rates where the pressure gradient response was examined. The results show that the Hydra's maximum rate is obtained at 65.4 l/hr. At the other end, the minimum pressures and minimum rates are bounded by the pump capacity. It was found that if the pressure drop was below a certain threshold, say 0.1 bar, the rate would give an unstable response. This is illustrated for thin discs of 2mm (not to be confused with the 8mm porous thin discs in the following chapters) in *Figure 4.13*.

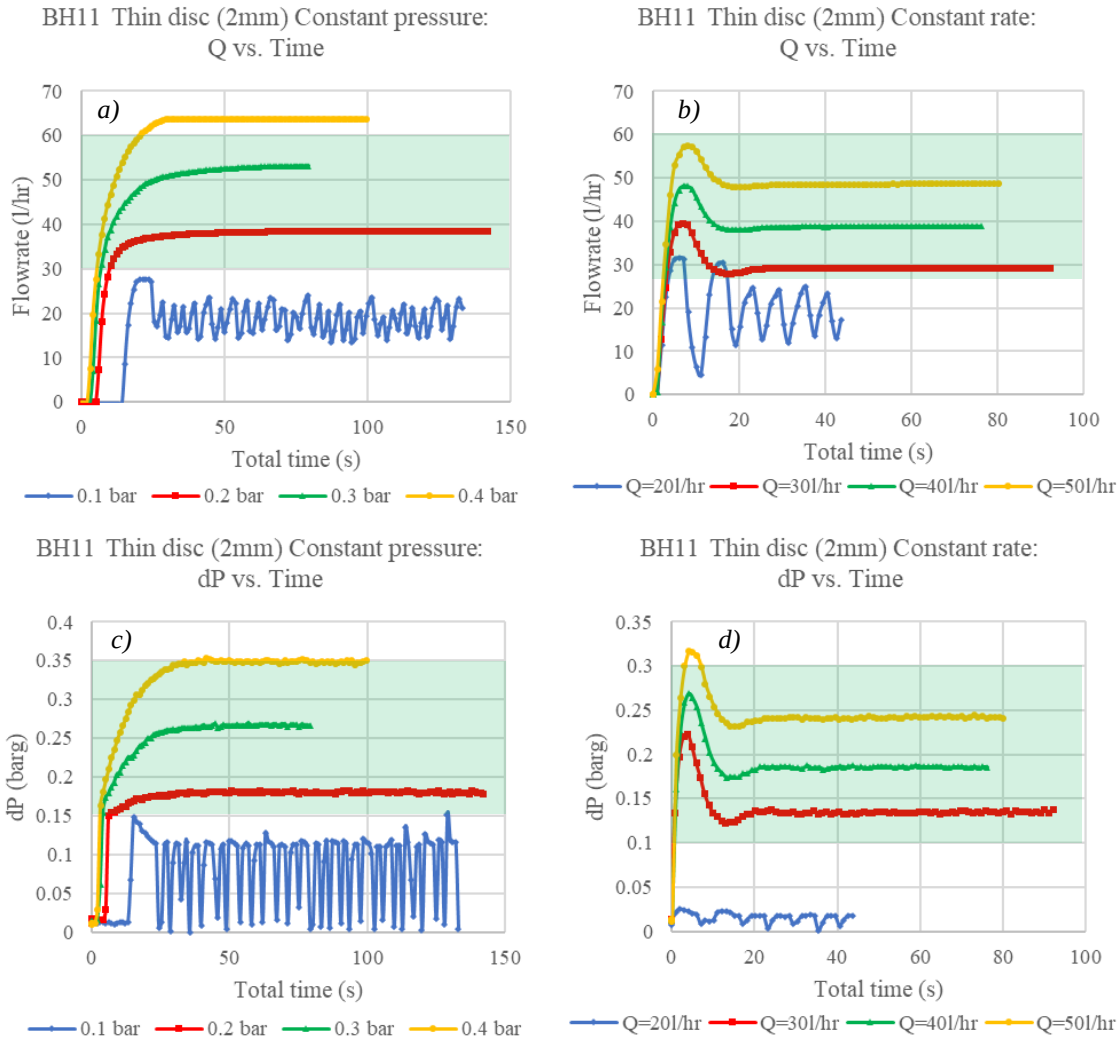


Figure 4.13: Identification of the stability operating window of the Hydra indicated with a green transparent section.

### 4.5.4 Experimental Setup Diagram

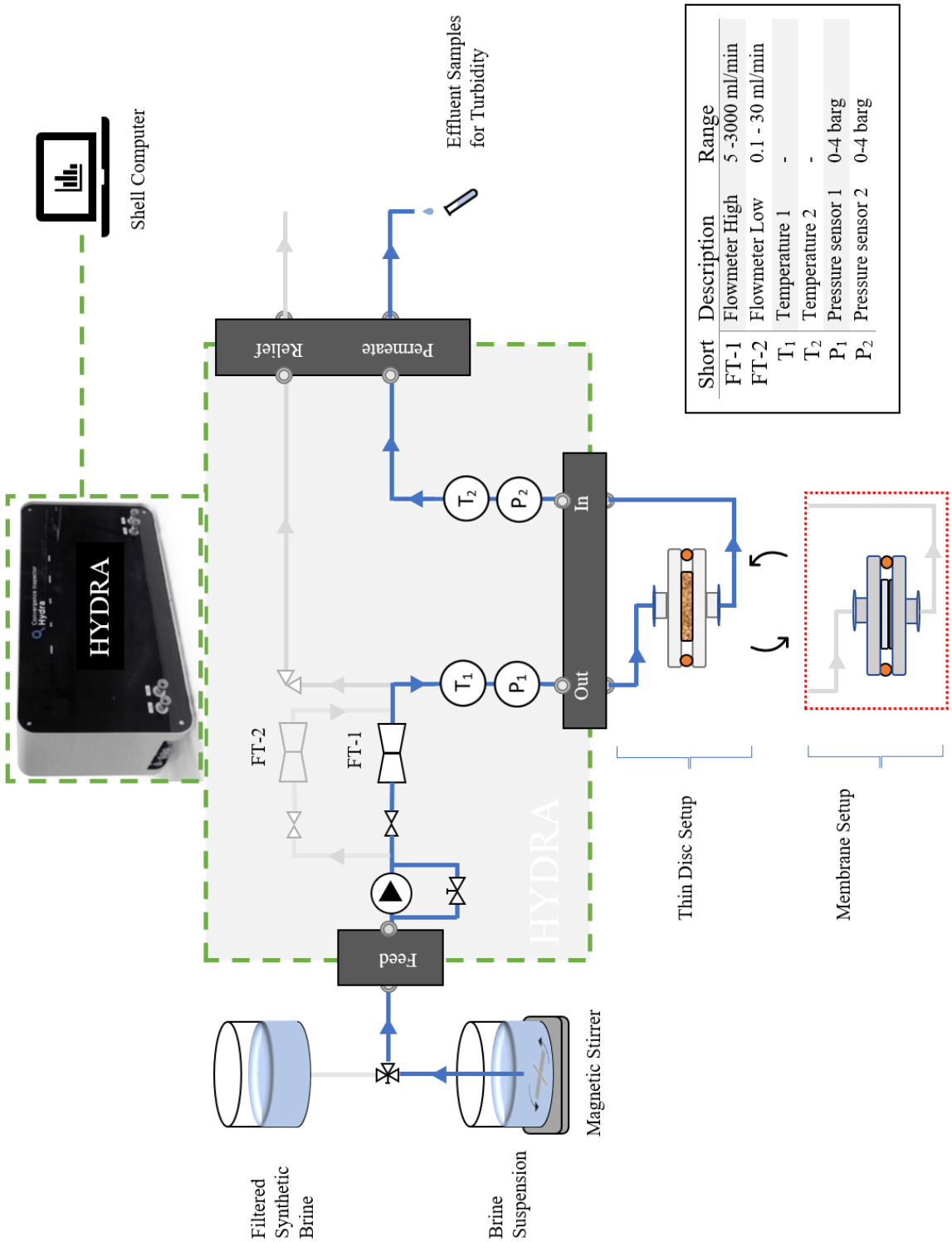


Figure 4.14: Experimental setup diagram, which shows the equipment internally and externally of the Con-vergence Hydra.

## 4.6 Experimental Procedure

Before each experiment, the Hydra is cleaned according to the cleaning procedure given in *Appendix C*. The dead volume, which is referred to as the volume from the PFA injection line inlet until the face of porous media is measured for both feed lines equals approximately 185 ± 5 ml. All lines are flushed with FSB to ensure every line is saturated with brine before each suspension flow experiment. The experimental procedure encompasses three parts; porous medium preparation, permeability tests and suspension injection test. For each test the process is the same and is as given in the following steps;

- *Porous medium preparation*
  1. The thin disc sample is saturated with FSB under vacuum, to prevent air entrapment.
  2. The thin disc is mounted in the sample holder cell while submerged in brine, which is kept in a 5 L bin filled with FSB. Sequentially, an MF0.45 filter is mounted in a membrane setup while submerged in brine in the same bin.
  3. The thin disc setup is connected to the Hydra feed line and permeate line while submerged in brine.
  4. The outside of the sample is dried with a paper towel and checked for leakage. The feed lines are also checked for air bubbles.

- *Permeability test*
  5. A glass of 5 litres is prepared and filled with FSB.
  6. When the thin disc is in place, a pre-programmed Hydra script is prepared to run. This script contains a constant flowrate program for several rates. Starting with a high rate, a stepwise procedure lowers the rate every 50 seconds until a low rate is reached. When the low rate is reached, the rate increases with the same steps back to the original high rate.

- *Suspension injection test: porous thin disc*
  7. A glass of 10 L is prepared and is filled with a calibrated 10 L of FSB. A magnetic stirrer is added and set to 250 rpm. Baracarb2 with a specific weight is prepared and added to the 10 L of synthetic. After 5 minutes of stirring at a rate of 250 rpm, the stirring speed is lowered to 100 rpm and continuously stirred for ~55 minutes.
  8. With the thin disc still in place, a constant rate script is prepared to run.
  9. During the experiment, the effluent is sampled in 15 ml tubes. Subsequently, the samples are tested for turbidity. Additionally, the FSB and suspension are sampled for turbidity and pH measurements

- *Suspension injection test: membrane filter*
  10. After completion of the thin disc suspension injection, the inline thin disc setup is switched with the membrane setup. This is done to perform a membrane filtration experiment with the same suspension.
  11. After completion of the experiments and the porous media is removed, all lines are flushed with demi water, and the cleaning procedure is started.

### 4.6.1 Post-analyses Thin discs

#### 4.6.1.1 Formation damage mitigation and Post Ultrasonic Bath (PUB) analysis

As stated by Porter (1989): “Formation damage is not necessarily reversible” and “what gets into porous media does not necessarily come out.” This is also described by Porter as “the reverse funnel effect”[38]. Knowing this phenomenon, it is worthwhile to test to what extent the permeability is recoverable after a suspension flow experiment. As explained in the subsequent section, the formation permeability is severely damaged due to particle plugging of suspended particles in suspension. From literature, it is known from analyzing cores that suspended particles enter the porous medium and can be retained by deep bed filtration mechanisms. In most cases, the damage is most significant in the first 1 cm and appears to decrease exponentially along the core. Different mitigation measures exist to restore the permeability, such as backflow or acid treatments. Aforementioned treatments are also mechanisms used with real injector wells [5]. In this research, a post ultrasonic bath (PUB) cleaning step is applied. Recovery of permeability is tested by putting the porous thin disc sample in an ultrasonic bath for 30 min. Subsequently, the porous discs and disc holder are submerged in FSB and are back flowed with 1L of FSB. Once this is done, a permeability test is performed to obtain the PUB permeability.

#### 4.6.1.2 SEM imaging & Micro-CT scan

To image the significance and depth of damage with the thin discs, both externally as well as internally, some of the porous thin discs are post analyzed with Micro-CT scans and SEM imaging techniques. In this research, Micro CT scans are made from some porous thin disc prior to the suspension flow experiment, obtaining an initial image which is referred to as the ‘clean’ porous thin disc. After a suspension injection experiment, the porous thin discs are air-dried and scanned again. The micro CT scan operates by creating an image which depends on density difference. Unfortunately, the density difference is only 2.6% due to silica and Baracarb2 having specific densities of 2.64 and 2.71 g/cm$^3$, respectively. Unlike hematite [28], this results in a limited contrast difference between both images making a clear identification between Baracarb2 and the silica porous medium more challenging. Nevertheless, subtracting the subsequently clean porous thin discs images from the post-experiment porous thin discs images was done by carefully aligning the thin discs and overlaying them in Aviso. Using the present distinctive mineral features as markers shown within both scans enabled the 3D visualisation of the Baracarb2 damage.

Next to the Micro-CT scan, SEM imaging is used for the same purpose, i.e. image the significance and depth of the damage within the porous thin discs. Therefore, a thin disc is broken in half along the diagonal and polished to get a flat surface. Thereafter, an SEM image was made, which shows in detail how the porous medium is filled with particles.

## 4.7 Experimentally generated data

When conducting a flow experiment, the Hydra generates flow rate, pressure drop and temperature data. This data is visualized during an experiment via the live feed in the Osmo-inspector software. Subsequently, the data is available in a .csv excel spreadsheet at the end of an experiment. Before showing any experimental results, it is useful to explain a simplified representation of the results seen from conducting a suspension flow experiment with the Hydra. This simplified representation is presented in *Figure 4.15*. In most cases, the results in *Chapter 5* and *Chapter 6* are presented in the same manner as seen in this figure. Here four windows are shown, where *Figure 4.15.a* and *Figure 4.15.c* presents the flow rate and pressure drop plotted against volume injected, respectively. From the flowrate results,

pressure drop results and other pre-determined parameters, the permeability ($k$) is calculated considering Darcy's law. Knowing the initial permeability ($k_i$) at the start of the experiment, the permeability is normalized by dividing over its initial permeability ($k/k_i$), which is plotted against volume injected in *Figure 4.15.b.* The impedance ($J$), which is plotted against volume injected in *Figure 4.15.d,* is calculated in the same manner as the normalized permeability and is equal to the initial permeability divided by the permeability results ($k_i/k$).
For all figures given in *Figure 4.15,* a dotted line is presented at a certain volume ($V_{BC}$), which discriminates two regimes: constant rate (CR) and constant pressure (CP) domain.

*'Constant rate (CR)'.* All experiments are initially started with a specific constant rate ($Q_0$) given in *Figure 4.15.a.* Considering Darcy's law, this initiates a pressure drop ($dP_0$) over the porous medium shown in *Figure 4.15.c.* As a response to suspended solids damaging the porous medium, the pressure drop increases. This increase follows an exponential trend until the maximum pressure ($dP_{max}$) at a certain volume ($V_{BC}$) is achieved, indicating that the maximum allowable power of the Hydra pump is reached. At this specific point, shown with the dotted line, the CR regime is switched to CP regime.

*'Constant pressure (CP)'.* When the maximum pressure is reached, it can be observed that in *Figure 4.15.c,* the pressure drop becomes constant and the rate given in *Figure 4.15.a* starts to decline. Due to the suspended solids continuously damaging the porous media, thereby decreasing the permeability, increasing work performed by the pump after reaching the pressure constraint results in a decline of the overall flow rate.

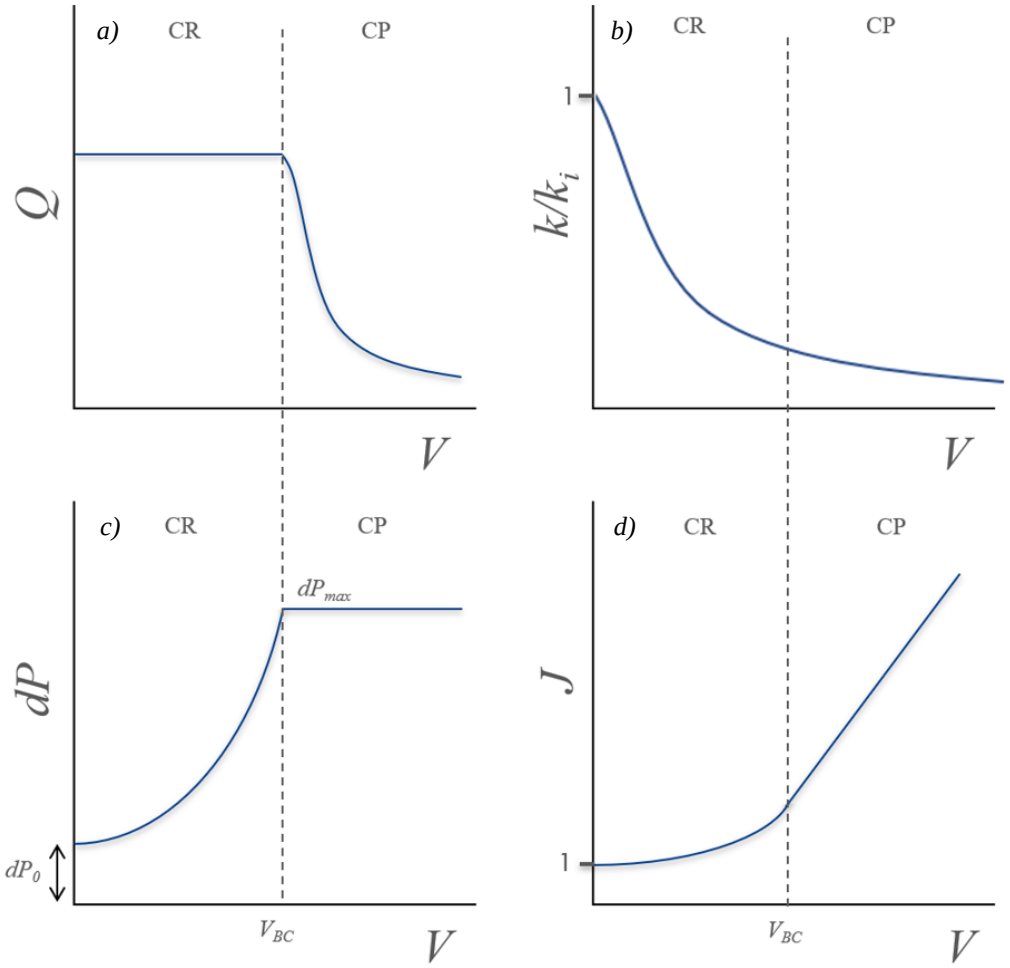


Figure 4.15: Schematic representation of typical experimental results conducted with porous thin discs and the Hydra. a) Flowrate, b) Normalized permeability, c) Pressure drop and d) Impedance.

Considering the normalized permeability and the impedance plots versus volume in *Figure 4.15.b* and *Figure 4.15.d*, it can be seen that within the CR domain, both the trends follow a decreasing and increasing exponential trend, respectively. When in the CP domain, the normalized permeability plot shows that there is very little change in terms of permeability as it reaches a certain threshold (later explained as cake permeability). This part is best described in the impedance plot, showing a linear trend.

The switch from the CR to the CP regime occurring at the maximum allowable pressure drop ($dP_{max}$) at a particular volume ($V_{BC}$) usually generates a sharp transition in pressure drop ($dP$), indicated in *Figure 4.16*. It is not entirely clear why this phenomenon occurs, as it may represent a cake disturbing feature or a pressure meter artefact. *Figure 4.16* illustrates the typical phenomenon which can be observed in the experimentally generated data.

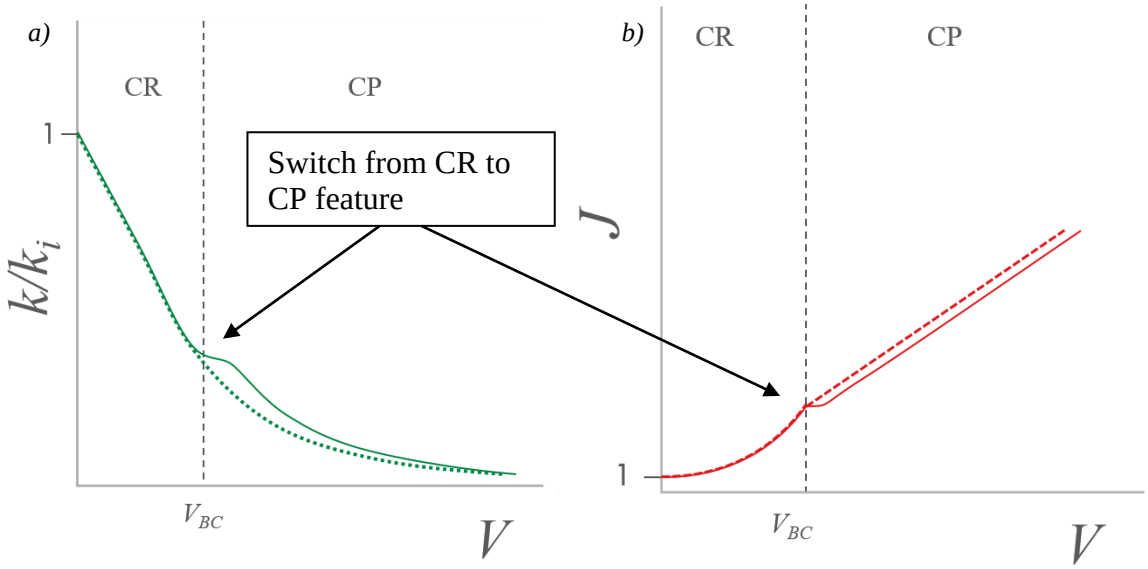


Figure 4.16. Schematic representation of the experiments plotted versus volume, with the illustration of the CR to CP regime shift feature seen in most experiments and expected trend course. a) Normalized permeability and b) Impedance.

# 5 Results

In this chapter, the WID results using the Hydra are presented, investigating the effect of water quality on formation damage using porous thin discs and membrane filters according to the experimental procedure detailed in section *4.6*. All experiments are conducted with the use of the Hydra, which has multiple internal sensors (described in section *4.5*). Pressure drop, flow rate, and temperature data are measured during all WID experiments. Additionally, effluent samples are collected during the experiment to determine the effluent turbidity and *pH*. Sequentially tested are the following porous media types: porous thin discs of 8mm (BH11 and BER18) and membrane filters (MF0.45).

The structure of this chapter is as follows: Section *5.1* contains the characterization of the thin discs in terms of their static and dynamic parameters. After characterization, suspension injection tests are performed with each porous medium. Section *5.2.1* proves, to a large extent, the reproducibility of the executed experimental flow tests. Subsequently, multiple suspension injection tests are reported using concentrations between the 20 mg/l and 100 mg/l of Baracarb2 in FSB. Every porous thin disc experiment is followed by an MF0.45 filter experiment. Post-experiment characteristics are obtained for a few thin discs.

## 5.1 Porous media characteristics

### 5.1.1 Porous thin discs

As discussed in section *4.1.2*, the porous thin discs are characterised in terms of their initial chemical composition and spatial dimensions. *Table 5.1* summarises the measured spatial characteristics of the different type of porous thin discs labelled according to the convention as detailed in section *4.1.3*. Using a Mitutoyo digital calliper (with an accuracy of ± 0.01 mm) each porous thin disc is measured. The table contains the following columns: a reference to the original sandstone block, length, diameter as well as the calculated cross-sectional area. Using the method detailed in section *4.1.2*, the porosity and pore volumes are determined. The volumes and porosity have a measurement error of 0.01 ml and 0.5%, respectively.

Table 5.1: Porous thin discs, static information and static characteristics.

| Sample ID | Porous media Type | $L_{TD}$ [mm] | $D_{TD}$ [mm] | $A_{TD}$ [mm$^2$] | $V_p$ [ml] | $\varphi_{eff}$ [%] |
|---|---|---|---|---|---|---|
| TD-C3 | BH11 | 7.99 | 34.85 | 953.9 | - | 24.0 |
| TD-D1 | BH11 | 8.01 | 34.87 | 955.0 | - | 24.0 |
| TD-F1 | BH11 | 8.09 | 34.85 | 953.9 | 1.83 | 24.0 |
| TD-F2 | BH11 | 8.09 | 34.87 | 955.0 | 1.82 | 24.0 |
| TD-F3 | BH11 | 8.08 | 34.85 | 953.9 | 1.82 | 24.2 |
| TD-F4 | BH11 | 8.10 | 34.85 | 956.1 | 1.83 | 24.0 |
| TD-F5 | BH11 | 7.73 | 34.89 | 954.4 | 1.75 | 24.2 |
| TD-F6 | BH11 | 8.07 | 34.87 | 955.0 | 1.82 | 24.0 |
| TD-G1 | BER18 | 8.09 | 34.56 | 938.1 | 1.55 | 20.7 |
| TD-G2 | BER18 | 8.10 | 34.56 | 938.1 | 1.55 | 20.7 |
| TD-G3 | BER18 | 8.09 | 34.59 | 939.7 | 1.55 | 20.7 |
| TD-G4 | BER18 | 8.10 | 34.74 | 947.9 | 1.55 | 20.6 |
| TD-G5 | BER18 | 8.07 | 34.61 | 940.8 | 1.53 | 20.5 |
| TD-G6 | BER18 | 8.10 | 34.55 | 937.5 | 1.55 | 20.7 |

After saturating under vacuum with FSB, the porous thin discs are mounted in the setup submerged in FSB. Subsequently, a rate step test is performed to determine the initial permeability. An important feature to mention, as discussed earlier in section *4.1.3,* is that the cross-sectional inflow area is reduced due to the use of the additional silicon ring. Consequently, the thin disc cross-sectional area ($A_{TD}$) of 9.5 x $10^{-4}$ $m^2$ is reduced to the effective inflow area ($A_{eff}$) of 5.7 x $10^{-4}$ $m^2$. This applies only to the thin disc experiments. For the membrane filter tests, no silicon ring is added.

*Figure 5.1* shows the typical results for the permeability test flow sequence, which includes flowing FSB through a porous thin disc at different rates. *Figure 5.1* provides an example of the procedure and shows a stepwise decreasing and successively increasing V-shaped rate pattern with time. Each flowrate results in a corresponding pressure drop enabling comparing the successive identical rate steps and identification of potential inconsistencies. The results of pressure drop response is plotted against the corresponding rate, resulting in the 'blue' data points visible in *Figure 5.1.b*. Considering Darcy's law, plotting rate versus pressure drop, the slope quantifies the permeability for each porous thin disc (*Appendix D*). Linear regression results and calculated permeability values are given in *Table 5.2*.

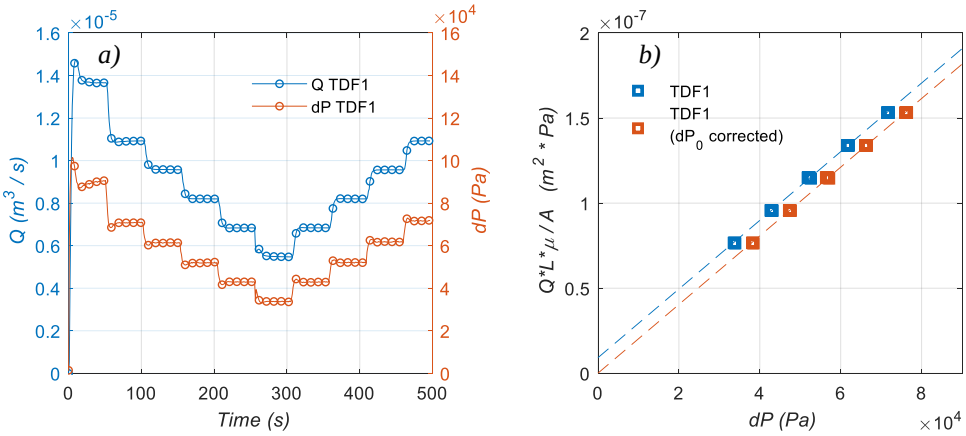


Figure 5.1: Thin disc $dP_0$ correction procedure: a) Flowrate ($Q$) and pressure drop ($dP$) data generated by the permeability test of porous thin disc TD-F1. b) Darcy plot TD-F1.

Table 5.2: Regression slope, permeability calculation and pressure drop ($dP_0$) correction for each porous thin disc.

| Sample ID | Porous media type | Regression slope [$m^2$] | $k_i$ [Darcy] | $dP_0$ correction [Pa] |
|---|---|---|---|---|
| TD-C3 | BH11 | 2.05 x $10^{-12}$ | 2.060 | 5000 |
| TD-D1 | BH11 | 2.01 x $10^{-12}$ | 2.010 | 6200 |
| TD-F1 | BH11 | 2.03 x $10^{-12}$ | 2.059 | 4100 |
| TD-F2 | BH11 | 2.00 x $10^{-12}$ | 2.027 | 5800 |
| TD-F3 | BH11 | 2.04 x $10^{-12}$ | 2.060 | 6100 |
| TD-F4 | BH11 | 1.88 x $10^{-12}$ | 1.902 | 6900 |
| TD-F5 | BH11 | 2.13 x $10^{-12}$ | 2.069 | 5400 |
| TD-F6 | BH11 | 1.79 x $10^{-12}$ | 1.800 | 6100 |
| TD-G1 | BER18 | 1.72 x $10^{-13}$ | 0.169 | 4500 |
| TD-G2 | BER18 | 1.75 x $10^{-13}$ | 0.168 | 3000 |
| TD-G3 | BER18 | 1.85 x $10^{-13}$ | 0.176 | 4000 |
| TD-G4 | BER18 | 1.65 x $10^{-13}$ | 0.161 | 4500 |
| TD-G5 | BER18 | 1.57 x $10^{-13}$ | 0.154 | 3500 |
| TD-G6 | BER18 | 1.53 x $10^{-13}$ | 0.152 | 3500 |

The linear line should intersect the x and y-axis at the origin, as no flow should result in a pressure drop of zero. By this means, a pressure drop correction is applied. Typical $dP_0$ correction values lie between the 3000 and the 6300 Pa (0.03 and 0.063 bar). Without the $dP_0$ correction, the permeability values tend to be 5-10% lower than with $dP_0$ correction.

### 5.1.2 Membrane filters

Membrane filter properties are assumed to be the same throughout all MF0.45 experiments, as discussed in section *4.1.1*. A rate step test is performed in the same manner as with the porous thin discs to determine the permeability resulting in *Figure 5.2.a*. In this figure, particularly at the last (increasing) rate step, the pressure is observed to continue to increase with time or injected volume. This can be explained as follows: a) the porous medium is slightly compressible and becomes less permeable due to deformation at high rates, and/or b) the injected fluid already contains particles causing plugging of the porous medium and reducing the permeability. The permeability is estimated at 0.015 Darcy for all membrane filters. The pressure drop correction is calculated by determination of the interception with the x-axis and is 12000 Pa (0.12 bar).

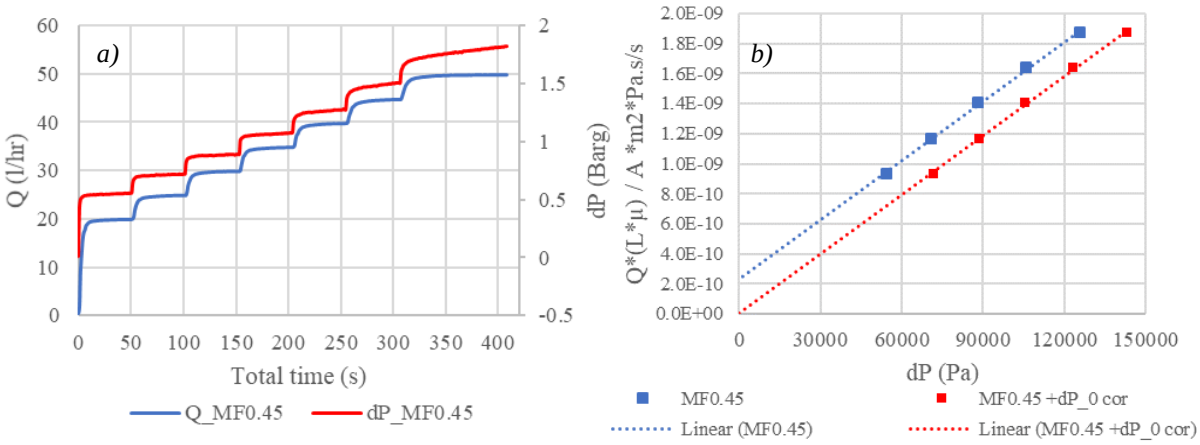


Figure 5.2: Membrane $dP_0$ correction procedure: a) Flowrate ($Q$) and pressure drop ($dP$) data generated by the permeability test of MF0.45. b) Darcy plot MF0.45.

## 5.2 Suspension flow experiments

The suspension flow experiments are conducted sequentially on porous thin discs and membrane filters, where porous thin disc experiments are listed in *Table 5.3* and the membrane filter experiments in *Table 5.4*. For convenience, the name of the experiment equals the concatenation of the sample ID (porous thin disc or membrane filter ID) and the experiment index. For example, TD-F1 is followed up with a membrane filter experiment MF-F1. As described in section *4.7*, all experiments are performed at constant flowrate until the maximum allowable pressure ($dP_{max}$) is achieved. From that point onwards, the mechanism boundary changes from constant rate (CR) to constant pressure (CP). Once in the constant pressure regime, the flowrate can decline as a result. The starting flow rate is chosen such that the rates fall within a stable region of the operating window of the Hydra, as explained in section *4.5.3*. The stable region differs for each porous media type. In addition to the stable region, the choice of initial flow rate is such that it resembles near-wellbore region injection rate conditions typically in the order of $10^{-3}$ and $10^{-2}$ m/s [39].

The experiments are categorized into two groups:

- *Initial reproducibility experiments*. Initial repeating suspension injection experiments with a fixed concentration of 50 mg/l suspension.
  - **BH11:** TD-C3, TD-D1
  - **BER18:** TD-G1, TD-G2
  - **MF0.45:** MF-G1(1), MF-G1(2)

- *Water Quality (WQ) variation*. Suspension injection test with a variety of concentrations of suspended particles.
  - **BH11:** TD-F1 – TD-F5
  - **BER18:** TD-G2 – TD-G5
  - **MF0.45:** MF-F1 – MF-F5, MF-G2 – MF-G5

Table 5.3: Porous thin disc suspension injection specifications.

| Experiment ID | Porous media type | $Q_0$ [l/hr] | Brine type | $c$ [mg/l] | pH [-] | Duration [min] | $V_{inj}$ [L] |
|---|---|---|---|---|---|---|---|
| TD-C3 | BH11 | 30 | 1 | 50 | - | 31.3 | 4.84 |
| TD-D1 | BH11 | 30 | 1 | 50 | - | 35.3 | 5.37 |
| TD-F1 | BH11 | 20 | 1 | 50 | 8.6 | 40.1 | 5.59 |
| TD-F2 | BH11 | 20 | 1 | 30 | 8.6 | 33.0 | 6.62 |
| TD-F3 | BH11 | 20 | 1 | 90 | 8.8 | 20.0 | 3.06 |
| TD-F4 | BH11 | 20 | 1 | 20 | 8.5 | 42.0 | 9.95 |
| TD-F5 | BH11 | 20 | 1 | 100 | 8.7 | 30.2 | 3.30 |
| TD-F6 | BH11 | 20 | 1 | 50 | 8.6 | 35.1 | 4.81 |
| TD-G1 | BER18 | 10 | 2 | 50 | 8.8 | 11.4 | 0.78 |
| TD-G2 | BER18 | 10 | 2 | 50 | 8.7 | 11.7 | 0.88 |
| TD-G3 | BER18 | 10 | 2 | 90 | 8.8 | 9.3 | 0.71 |
| TD-G4 | BER18 | 10 | 2 | 30 | 8.6 | 11.4 | 1.01 |
| TD-G5 | BER18 | 10 | 2 | 20 | 8.6 | 10.2 | 0.99 |
| TD-G6 | BER18 | 10 | 1 | 50 | 8.6 | 8.1 | 0.76 |

Table 5.4: Membrane filter suspension injection specifications.

| Experiment ID | Porous media Type | $Q_0$ [l/hr] | Brine type | $c$ [mg/l] | pH [-] | Duration [min] | $V_{inj}$ [L] |
|---|---|---|---|---|---|---|---|
| MF-F1 | MF0.45 | 20 | 1 | 50 | 8.6 | 23.0 | 4.35 |
| MF-F2 | MF0.45 | 20 | 1 | 30 | 8.6 | 13.3 | 3.35 |
| MF-F3 | MF0.45 | 20 | 1 | 90 | 8.8 | 16.4 | 2.59 |
| MF-F5 | MF0.45 | 20 | 1 | 100 | 8.7 | 12.1 | 2.21 |
| MF-G1(1) | MF0.45 | 10 | 2 | 50 | 8.8 | 37.2 | 4.83 |
| MF-G1(2) | MF0.45 | 10 | 2 | 50 | 8.8 | 29.7 | 4.22 |
| MF-G2 | MF0.45 | 20 | 2 | 50 | 8.7 | 12.2 | 2.87 |
| MF-G3 | MF0.45 | 10 | 2 | 90 | 8.8 | 26.4 | 3.22 |
| MF-G4 | MF0.45 | 10 | 2 | 30 | 8.6 | 24.8 | 4.09 |
| MF-G5 | MF0.45 | 20 | 2 | 20 | 8.6 | 14.6 | 4.00 |

### 5.2.1 Initial Reproducibility Experiments

The method of performing suspension flow experiments on porous thin discs with the use of the Hydra has not been done before. Therefore, some work is conducted prior to the results shown in this report, also referred to as the 'proof of concept phase'. Hence, the proof of concept phase results: TD-A# until TD-E#, are not shown, except for TD-C3 and TD-D1. TD-C3 and TD-D1 represent the first reliable experiments from following the applied experimental procedure.

Obtaining experiment reproducibility is pivotal to achieve reliable results. In other words, repeating an experiment following the same experimental procedure, should give similar results/trends, i.e. within a specific experimental error range due to, for example, sample heterogeneity. In the following sections, the results are provided from the initial experiments on each porous media type, to indicate the level of reproducibility. The reproducibility experiments include performing a constant rate (fixed concentration) test.

#### 5.2.1.1 TD-C3 and TD-D1

The first experiments were conducted with BH11 porous thin discs: TD-C3 and TD-D1. These thin discs originate from two cores ("C" and "D") drilled next to each other in the BH11 block. The porous thin disc properties and suspension injection specifications are given in *Table 5.5*. From these results, it can be stated that the thin discs have very similar hydrodynamic characteristics. The two experiments are conducted at a constant rate of 30 l/hr ($8.33 \times 10^{-6}$ $m^3/s$) and a fixed suspension concentration of 50 mg/l. Results are presented in *Figure 5.3*. *Figure 5.3*, where *Figure 5.3.a* and *Figure 5.3.c* show the measured flow rate and pressure drop versus volume injected for both experiments, respectively. As discussed before in section *4.7*, starting with a constant rate, the pressure drop builds up until a maximum pressure drop ($dP_{max}$) is reached, which is in this case 4.3 bar and occurs typically around the 2.5 L of total suspension volume injected. From that point onwards, the rate declines as a response to the constant pressure regime.

Knowing the initial permeability ($k_i$) at the start of the experiment, determined with clean FSB experiment beforehand, the permeability results from the suspension flow experiments are normalized by dividing over its initial permeability (see section *4.7* for more details), resulting in the normalized ($k$ / $k_i$) graph of *Figure 5.3.b*. The impedance ($J$) given in *Figure 5.3.d* is the inverse of *Figure 5.3.b*. Both *Figure 5.3.b* and *Figure 5.3.d* are plotted against suspension volume ($V_s$) injected, which is the total volume ($V_t$) injected minus the estimated dead volume ($V_d$), i.e. only from the point of suspension arrival onwards.

*Figure 5.3.a* shows both experiments starting initially at a constant rate declining a bit until the switch from CR towards the CP regime. Within the CP regime, both rate curves follow the same declining trend. From *Figure 5.3.c*, it can be seen that the pressure drop build-up for both experiments are very similar and follow the same trend. Considering the normalized permeability in *Figure 5.3.b*, the similarity of both curves is striking, underpinning the same kind of permeability damage is occurring in both experiments. From the impedance plot in *Figure 5.3.d*, it can be seen that within the constant pressure regime, both experiments follow a linear trend and are very similar.

Table 5.5: Porous thin disc, operational conditions and suspension specifications of the reproducibility experiments TD-C3 and TD-D1.

| Experiment ID | Porous media Type | $Q_0$ [l/hr] | Brine type | $c$ [mg/l] | Duration [min] | $V_{inj}$ [L] | $\varphi_{eff}$ [%] | $k_i$ [Darcy] |
|---|---|---|---|---|---|---|---|---|
| TD-C3 | BH11 | 30 | 1 | 50 | 31.3 | 4.84 | 24.0 | 2.060 |
| TD-D1 | BH11 | 30 | 1 | 50 | 35.3 | 5.37 | 24.0 | 2.010 |

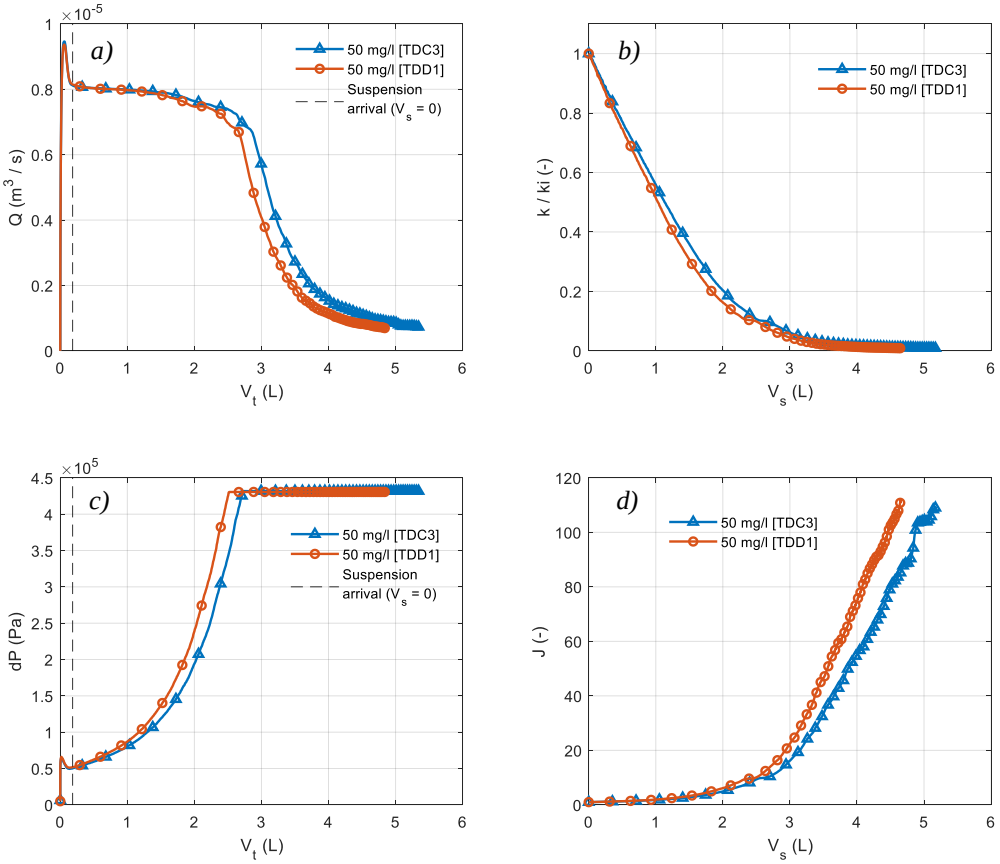


Figure 5.3: a) Results of experiments TD-C3 and TD-D1 plotted versus volume injected: a) Flowrate, b) Normalized permeability, c) Pressure drop and d) Impedance.

When conducting a constant rate experiment with the Hydra, the start features an overshoot of the rate taking approximately 20 seconds (≈ 170 ml considering a rate of 30 l/hr) to find the setpoint flowrate, visible in both *Figure 5.3.a* and *Figure 5.3.c*. Fortunately, the dead volume as previously discussed section *4.5.1* and visible in *Figure 4.14*, equals approximately 185 ± 5 ml of FSB, so the first part of a suspension flow experiment is always preceded by the FSB dead volume. When the suspension arrives at the porous medium injection face, it is referred to as suspension arrival ($V_s = 0$) indicated in *Figure 5.3.a* and *Figure 5.3.c* with the dotted line.

### 5.2.1.2 TD-G1 and TD-G2

The second set of reproducibility experiments uses BER18 porous thin discs: TD-G1 and TD-G2. Both thin discs are cut from the same core "G", drilled from the BER18 block. The approach is the same as with previous reproducibility experiments, where two similar experiments are conducted with a fixed suspension concentration of 50 mg/l. As seen from *Table 5.2*, the BER18 permeabilities are one order of magnitude lower than the BH11 permeabilities. Therefore, a lower rate of 10 l/hr (2.778 x $10^{-6}$ $m^3$/s) is used to maintain within the stable operating window of the Hydra. Given the suspension injection specifications in *Table 5.6*, the results for TD-G1 and TD-G2 are presented in *Figure 5.4*. Here *Figure 5.4.a*, *Figure 5.4.b*, *Figure 5.4.c*, *Figure 5.4.d* show the measured flowrate, normalized permeability, pressure drop and impedance versus suspension volume injected,

respectively. To mitigate against the initial overshoot discussed in section *5.2.1.1*, BER18 thin discs are subjected to a suspension free FSB flow lasting 60 seconds before manually switching using a valve switch from the FSB line to the suspension line. In this section, only the part of suspension arrival ($V_s$ = 0) onwards is presented. In section *5.2.2.2*, the FSB flow and valve switch before the suspension arrival is discussed in detail.

The pressure drop build-up seen in *Figure 5.4.c* is quite rapid and reaches $dP_{max}$ after flowing of about 0.12 L of suspension for both experiments. Because this rapid pressure drop increase, a rate decline is observed during the "constant rate" regime. When the $dP_{max}$ is reached, the rate decreases following a robust declining trend. The normalized permeability presented in *Figure 5.4.b* illustrates a very similar trend for both experiments, starting with a rapid (linear) decline to the 40% within the first 0.15 L. Subsequently, the normalized permeability seems to stabilize at around 10%. Considering the impedance results for both experiments presented in *Figure 5.4.d*, the trend is very similar until 0.3 L of suspension flowed. Hereafter, it is observed that the trends diverge from each other. When in the constant pressure domain, which is initiated from about 0.12 L of suspension volume flowed, the impedance does not follow a linear trend as observed with the BH11 reproducibility experiments. Subsequently, the trend seems to follow an s-shape curve.

Table 5.6: Porous thin disc, operational conditions and suspension specifications of the reproducibility experiments TD-G1 and TD-G2.

| Experiment ID | Porous media Type | $Q_0$ [l/hr] | Brine type | $c$ [mg/l] | Duration [min] | $V_{inj}$ [L] | $\varphi_{eff}$ [%] | $k_i$ [Darcy] |
|---|---|---|---|---|---|---|---|---|
| TD-G1 | BER18 | 10 | 2 | 50 | 11.4 | 0.78 | 20.7 | 0.169 |
| TD-G2 | BER18 | 10 | 2 | 50 | 11.7 | 0.88 | 20.7 | 0.168 |

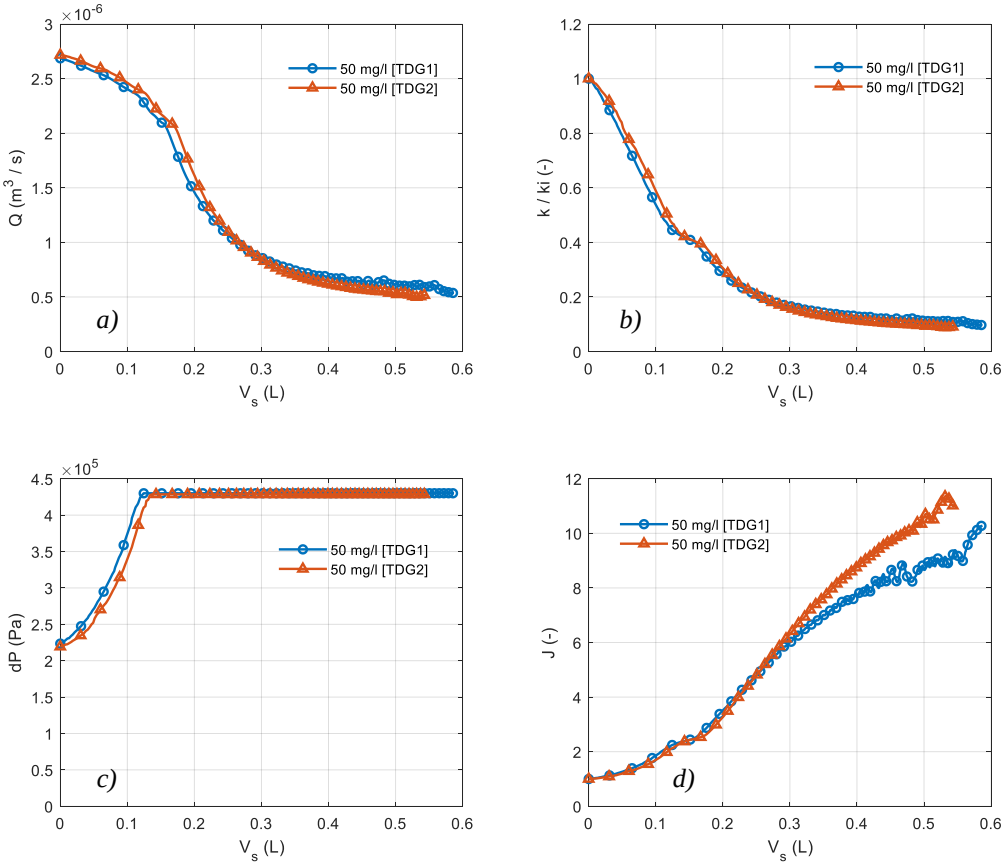


Figure 5.4: Results of experiments TD-G1 and TD-G2 plotted versus suspension volume injected: a) Flowrate, b) Normalized permeability, c) Pressure drop and d) Impedance.

#### 5.2.1.3 MF0.45

Reproducibility experiments with membrane filters are performed with suspension injection tests at two rates: 20 l/hr and 10 l/hr, corresponding to the rates of porous thin discs BH11 and BER18. The operational conditions, as well as the specifications for the four reproducibility experiments with membrane filters, are given in *Table 5.7*. With these reproducibility experiments, the concentration is fixed at 50 mg/l. Initial permeabilities are estimated to be 0.015 Darcy, as stated in section *5.1.2*. The permeabilities are also calculated from the initial rates and pressure drop responses at the start of each test and show similar values. As no cleaning procedure is done between the thin disc and membrane filter experiments, the lines still contain the suspension of the previous experiment. Therefore, when starting the MF0.45 experiment, the suspension arrival is instantaneous.

Results of experiments MF-F1 and MF-G2 are presented in *Figure 5.5*, where four windows are shown. Here *Figure 5.5.a*, *Figure 5.5.b*, *Figure 5.5.c*, *Figure 5.5.d* show the measured flowrate, normalized permeability, pressure drop and impedance versus suspension volume injected, respectively. The permeability of the MF0.45 is estimated by doing a back on the envelope calculation. Considering Darcy's law, inserting initial flow rate, pressure drop response, as well as the remaining parameters into Darcy's equation, results in a value very similar to the initial permeability (section *5.1.2*);

$$k = \frac{Q \cdot \mu \cdot L}{A \cdot (dP_0 + dP_{cor})} = \frac{5.556 \cdot 10^{6} \cdot 0.001 \cdot 150 \cdot 10^{-6}}{8.33 \cdot 10^{-4} \cdot \left(0.5 \cdot 10^{5} + 0.12 \cdot 10^{5}\right)} = 0.016 \text{ Darcy}$$

*Figure 5.5.c* illustrates the pressure drop build-up with the two experiments at a rate of 20 l/hr. The results from both experiments are very similar in terms of their shape. The build-up starts at 0.5 bar and proceeds to follow an upward trend towards $dP_{max}$. Considering the same phase in *Figure 5.5.a*, the rate starts its decline right away and decreases by about 10% within the CR regime. *Figure 5.5.b*, when reaching the CP regime, the rate decline for both experiments is almost identical. The permeability follows a rapidly declining trend from 100 to 15% within the first 1 L of injected suspension. Subsequently, the decline seems to stabilize. Considering *Figure 5.5.d*, the impedance results in the constant pressure regime illustrate a linear trend, which follows a similar slope.

Two experiments with a fixed concentration of 50 mg/l are also conducted at a rate of 10 l/hr and are presented in *Figure 5.6*. Within all windows, an unstable response occurs during the first 0.3 L injected suspension. This is a typical example of what happens when performing an experiment outside the stability window of the Hydra. Over time the permeability of the medium impairs due to plugging of suspended solids, resulting in a pressure drop increase. This pressure drop increases until the pressure enters the stability region, which from that point onward gives a stable response. The start of the experiment displays a very noisy signal. Nevertheless, the data after the unstable results are still valuable. Very similar trends are observed with both experiments in terms of rate, pressure drop, normalized permeability and impedance.

Table 5.7: Membrane filter, operational conditions and suspension specifications of the reproducibility experiments MF-F1 and MF-G2.

| Experiment ID | Porous media Type | $Q$ [l/hr] | Brine type | $c$ [mg/l] | Duration [min] | $V_{inj}$ [L] | $\varphi$ [%] | $k_i$ [Darcy] |
|---|---|---|---|---|---|---|---|---|
| MF-F1 | MF0.45 | 20 | 1 | 50 | 23.0 | 4.35 | 79.0 | 0.015 |
| MF-G2 | MF0.45 | 20 | 2 | 50 | 12.2 | 2.87 | 79.0 | 0.015 |
| MF-G1(1) | MF0.45 | 10 | 1 | 50 | 37.2 | 4.83 | 79.0 | 0.015 |
| MF-G1(2) | MF0.45 | 10 | 1 | 50 | 29.7 | 4.22 | 79.0 | 0.015 |

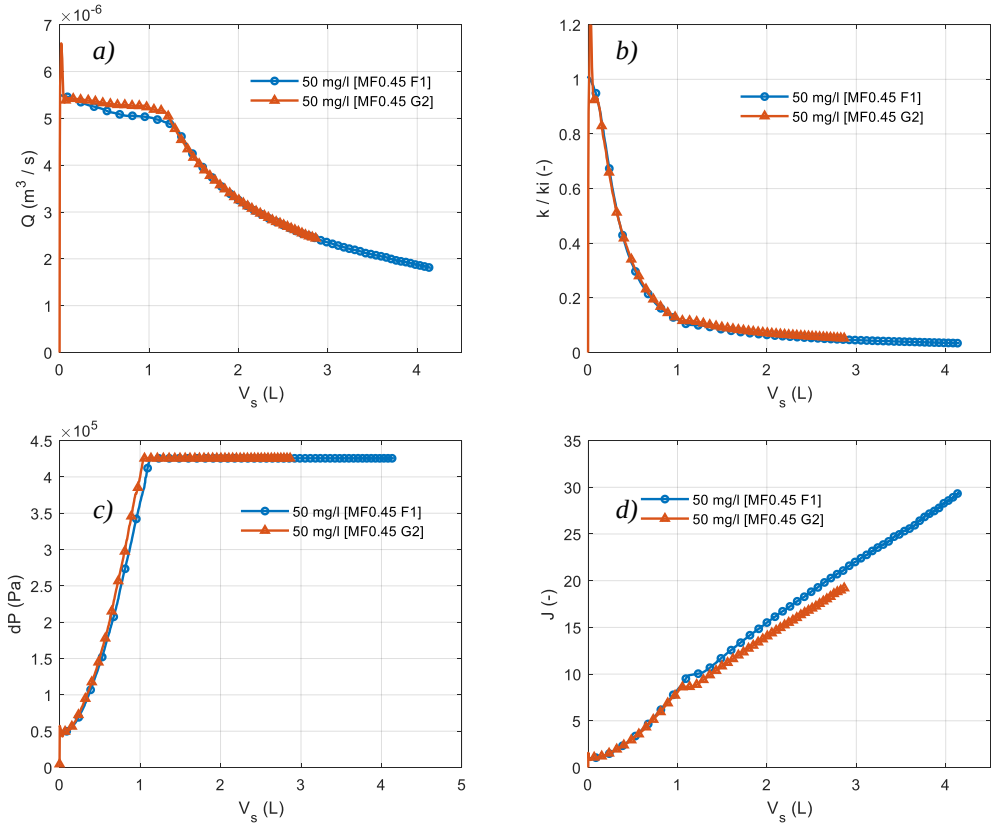


Figure 5.5: Results of experiments MF-F1 and MF-G2 (20 l/hr) plotted versus suspension volume injected: a) Flowrate, b) Normalized permeability, c) Pressure drop and d) Impedance.

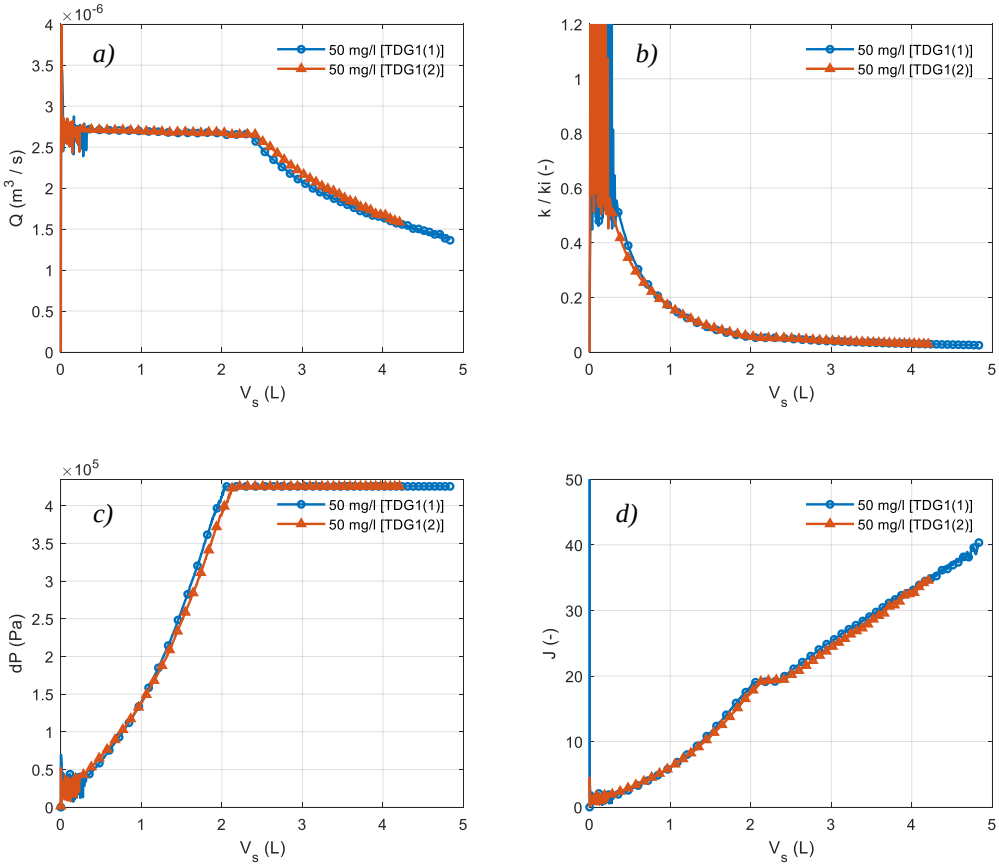


Figure 5.6: Results of experiments MF-G1(1) and MF-G1(2) (10 l/hr) plotted versus suspension volume injected: a) Flowrate, b) Normalized permeability, c) Pressure drop, d) Impedance.

### 5.2.2 Water Quality (WQ) Variation

After the initial tests, experiments are conducted on each porous media type for varying suspension concentrations, or in other words, varying the WQ. This is done by keeping the operational conditions and experimental procedure identical, except for the suspension concentration. Experiments with porous media type BH11 are all conducted by performing a constant rate test as detailed in section *4.7*. As stated earlier, each BH11 suspension flow experiment is preceded by a suspension free FSB dead volume passing through the thin disc until suspension arrival. Compared to the BH11 experiments, the BER18 experiments have a small addition in the experimental procedure. The constant rate experiments with porous media type BER18 are first subjected to an FSB flush to prevent the device from overshooting. Basically, after 60 seconds a valve switches from FSB line to suspension line.

*Calcium undersaturation and "actual" suspension concentration*
As discussed in section *4.4.1*, the FSB is calcium undersaturated, resulting in losing approximately 10 mg/l of Baracarb2 due to dissolution into the FSB. This estimate was obtained through MF0.45 absolute filtration and subsequent micro mass balance measurements as well as through OLI estimates (section *4.4.1*). Knowing this feature, the suspension "actual" fouling concentrations are the subtracting the dissolved 10 mg/l, e.g. 20 mg/l becomes 10 mg/l. To prevent any confusion, suspension concentrations always refer to the total suspension Baracarb2 concentration being either present as solid as well as in the liquid phase. As an example: 500 mg of Baracarb2 is added to 10 L of FSB resulting in a suspension of 50 mg/l.

#### 5.2.2.1 BH11

After confirming experimental reproducibility, experiments with BH11 discs are conducted for various suspension concentrations (*c*) and are listed in *Table 5.8*. In this table, the experiments are now ordered from low to high suspension concentration, i.e. high WQ to low WQ, respectively. From the results of *Table 5.1* and *Table 5.8*, it is seen that the BH11 thin discs have very similar dynamic characteristics. The initial permeability for all experiments is about 2.0 D, with minor differences seen in permeability with TD-F4 and TD-F5. The duration of an experiment is controlled by setting a volume limit of 10 litres, which is also the size of the suspension reservoir tank. The limit is not always achieved, as most of the experiments are stopped manually. The aim in all executed experiments is to capture the CR as well as the CP regime response while saving enough suspension for the subsequent MF0.45 test. For most experiments, both porous thin disc and membrane filter test are performed with one suspension tank of 10 L, except for TD-F4. This experiment required all the suspension contained in the reservoir tank. The duration of the BH11 tests is usually between the 20 and 40 minutes and injection volumes range between the 3-10 L depending on water quality. The lower the water quality, the faster damage occurs, which thereby reduces the duration and volume injected. The rate, normalized permeability, pressure drop and impedance results for the BH11 experiments with the various concentrations are presented in *Figure 5.7.a*, *Figure 5.7.b*, *Figure 5.7.c* and *Figure 5.7.d*. As previously discussed, a constant rate and a constant pressure (corresponding to $dP_{max}$) regime are distinguished. With each experiment, the volume at which the regime shift occurs ($V_{BC}$) is different and is captured in *Table 5.8*.

From the $V_{BC}$ results presented in *Table 5.8*, it becomes evident that increasing the suspension concentration decreases the required total amount of suspension volume to reach $dP_{max}$. The pressure drop results are shown in *Figure 5.7.c*. This figure indicates the impact of the suspension concentration on the *dP* trend within the CR regime. Here it is observed that increasing suspension concentration increases the slope of this exponential trend. This is discussed in more detail in the next chapter. *Figure 5.7.a* illustrates that, while in the CR

regime, the rates for all experiments are rather constant until reaching the $dP_{max}$. Subsequently, the rate declines more rapidly for a high concentration as compared to a low concentration experiment.

From *Figure 5.7.b,* it becomes apparent that the normalized permeability rapidly decreases (semi) linearly from 100-20% as compared to its initial value. As before, increasing suspension concentration decreases the required suspension volume for the permeability to drop. In more detail, the permeability tends to flatten towards a particular value of ~2% of the normalized permeability. This corresponds to a permeability of 0.04 Darcy. *Figure 5.7.d* shows the impedance to follow an exponential trend during the constant rate regime. While in the constant pressure regime, the impedance for all experiments follows a linear trend.

Table 5.8: Porous thin disc, operational conditions and suspension specifications of the concentration variation experiments TD-F1 - TD-F5.

| Experiment ID | Porous media Type | $Q_0$ [l/hr] | Brine type | $c$ [mg/l] | Duration [min] | $V_{inj}$ [L] | $\varphi_{eff}$ [%] | $k_i$ [Darcy] | $V_{BC}$ [L] |
|---|---|---|---|---|---|---|---|---|---|
| TD-F4 | BH11 | 20 | 1 | 20 | 42.0 | 9.95 | 24.0 | 1.902 | 6.90 |
| TD-F2 | BH11 | 20 | 1 | 30 | 33.0 | 6.62 | 24.0 | 2.027 | 3.96 |
| TD-F1 | BH11 | 20 | 1 | 50 | 40.1 | 5.59 | 24.0 | 2.059 | 3.00 |
| TD-F3 | BH11 | 20 | 1 | 90 | 20.0 | 3.06 | 24.2 | 2.060 | 1.66 |
| TD-F5 | BH11 | 20 | 1 | 100 | 30.2 | 3.30 | 24.2 | 2.069 | 1.63 |

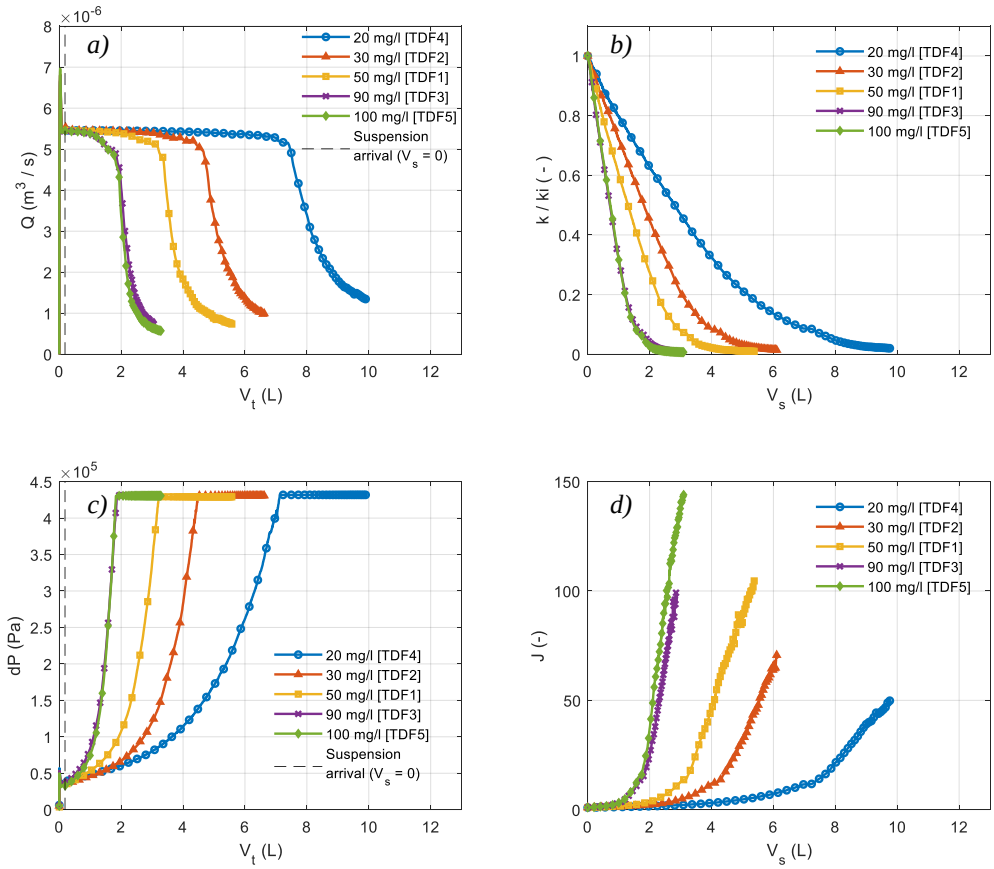


Figure 5.7: Results of experiments TD-F1 to TD-F5, where the concentration is varied between the 20 mg/l and 100 mg/l plotted versus suspension volume injected. a) Flowrate, b) Normalized permeability, c) Pressure drop and d) Impedance.

#### 5.2.2.1.1 BH11 Turbidity Effluent measurements

Effluent samples are taken from the permeate line in a 15 ml tube, where each effluent sample has the same volume. Effluent samples are taken manually, where the time of sampling and amount of measurements differ for each experiment. The turbidity is measured for the effluent samples, as well as for the suspension samples, where the turbidity measurements for all experiments are given in *Appendix F*. The turbidity data is normalized by dividing the effluent turbidity over the initial injected suspension turbidity.

To facilitate data interpretation and result discussion, the corresponding rate and pressure drop data are presented alongside the turbidity data in *Figure 5.8*. For each experiment, the effluent turbidity measurements start with a low percentage and within the CR regime rapidly increases towards a plateau at about 60% of the injected turbidity during the CR regime phase. Depending on the suspension concentration, the normalized turbidity stays at a plateau until $dP_{max}$ is reached. Interestingly, the decrease of the injection rate occurring towards reaching the CP regime results in a decline in turbidity along with the rate decline.

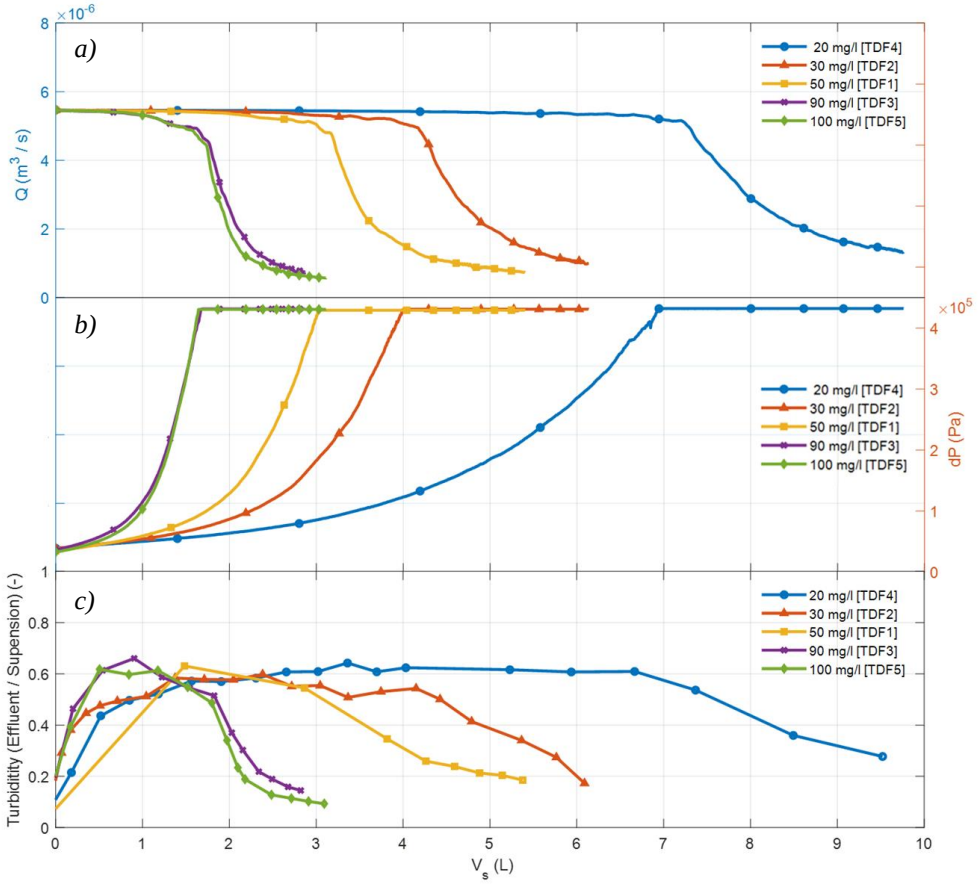


Figure 5.8: BH11, a) Flow rate versus suspension volume injected for various concentrations. b) Pressure drop versus suspension volume injected for various concentrations c) Normalized effluent turbidity versus volume. Stacked figures for visualization of process at each concentration experiment.

### 5.2.2.2 BER18

Experiments with varying suspension concentration are also conducted with porous thin discs of type BER18. The specifications of these experiments are given in *Table 5.9* and are ordered by suspension concentration, or in other words ordered by WQ. The porous thin discs have very similar permeability, ranging in between the 159 and 187 mD. Compared to the BH11 thin discs, the permeability is in the order of 10 lower than the permeability of the BER18. Therefore, a lower flow rate of 10 l/hr is chosen, which is half the rate of the

experiments with the BH11 porous thin discs. This lower rate is chosen to ensure the pressure drop starts in the stability region of the Hydra.

The rate, normalized permeability, pressure drop, and impedance results of the BER18 experiments are given in *Figure 5.9*. In *Figure 5.9.a* and *Figure 5.9.*c, three sections can be distinguished, indicated by the dotted lines. The experiments with the BER18 porous thin discs are initially subjected to a clean FSB flow, where after 60 seconds ($V_t \approx 0.15$ L) a three-way valve is manually switched from FSB line to suspension line. After the valve switch, the dead volume passes through the sample, until the suspension arrives at the thin discs sand face ($V_t \approx 0.33$ L and $V_s = 0$). This sequence of clean brine flow and a valve switch is carried out to illustrate that flowing with clean brine, results in a stable response in terms of flow rate and pressure drop for all the BER18 porous thin discs. *Figure 5.9.*c illustrates a difference in the level of pressure drop in the volume range of 0.15 and 0.33 L. This demonstrates slight permeability differences between the samples, resulting in small differences in pressure drop responses with the same rate.

From *Table 5.9* it is seen that the duration of experiments is between the 9 and 11 minutes and the total fluid volume injected varies in between the 0.7 and 1 L. All experiments are manually stopped as the volumes flowed are far lower than the maximum capacity of the suspension reservoir tank. Considering the part of suspension arrival onwards ($V_s = 0, \rightarrow$), the total suspension volume flowed is between the 0.35 and 0.7 L. These are quite low volumes and indicate rapid impairment of the porous medium. Compared to BH11, the duration and volumes used with BER18 experiments are substantially lower. From $V_{BC}$ results presented in *Table 5.9,* it is seen that, with a higher concentration, less volume is needed to reach the $dP_{max}$. The pressure drop results shown in *Figure 5.9.c* demonstrates the impact of concentration on the *dP* trend within the constant rate regime. Similarly observed with the BH11 experiments, it is found that, the higher the concentration, the higher the slope of this exponential trend. *Figure 5.9.a* demonstrates that the rate declines during the 'constant rate' regime, making the constant rate regime not so constant.

*Figure 5.9.b* presents the normalized permeability results, where an s-shape trend is observed. Here holds, the higher the concentration of particles in suspension, the less suspension volume is needed for the permeability to drop. Subsequently, in the constant pressure regime, the permeability tends to flatten towards a certain value of ~15% of the normalized permeability. This corresponds to a permeability of 0.03 Darcy, which is in the same range as observed with the BH11 endpoint permeabilities. From *Figure 5.9.d,* it is seen that the impedance shows an exponential trend while in the constant flow regime. While in the constant pressure regime, the trend does not follow a linear trend as observed with the BH11 experiments. Instead, a curvature is seen indicating a less increasing slope.

Table 5.9: Porous thin disc, operational conditions and suspension specifications of the reproducibility experiments TD-G2 to TD-G5.

| Experiment ID | Porous media Type | $Q_0$ [l/hr] | Brine type | $c$ [mg/l] | Duration [min] | $V_{inj}$ [L] | $\varphi_{eff}$ [%] | $k_i$ [Darcy] | $V_{BC}$ [L] |
|---|---|---|---|---|---|---|---|---|---|
| TD-G5 | BER18 | 10 | 2 | 20 | 10.2 | 0.99 | 20.5 | 0.154 | 6.90 |
| TD-G4 | BER18 | 10 | 2 | 30 | 11.4 | 1.01 | 20.6 | 0.161 | 3.96 |
| TD-G2 | BER18 | 10 | 2 | 50 | 11.7 | 0.88 | 20.7 | 0.169 | 3.00 |
| TD-G3 | BER18 | 10 | 2 | 90 | 9.3 | 0.71 | 20.7 | 0.176 | 1.66 |

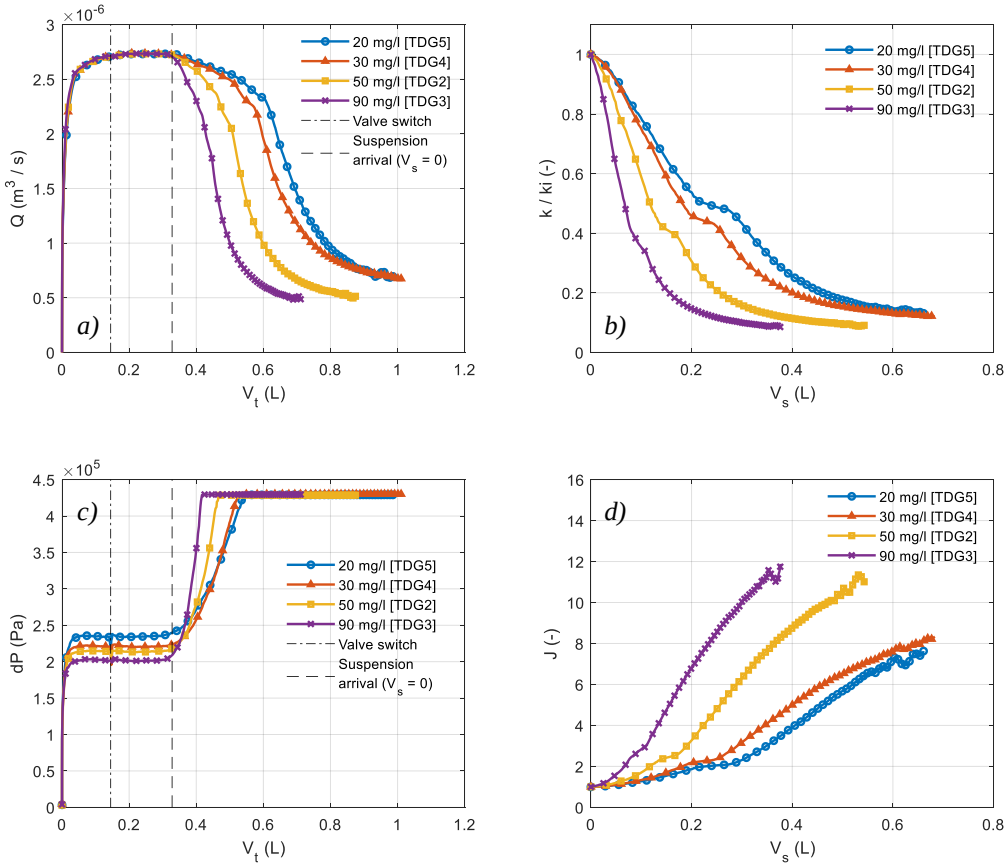


Figure 5.9: Results of experiments TD-G2 to TD-G5, where concentration is varied. a) Flowrate versus volume injected with the indication of an FSB flow and valve switch. b) Normalized permeability versus suspension volume injected. c) Pressure drop versus volume injected with the indication of an FSB flow and valve switch. d) Impedance versus suspension volume injected.

#### 5.2.2.2.1 BER18 Turbidity Effluent measurements

Effluent samples are taken from the permeate line in a 15 ml tube during the BER18 experiments. These effluent samples, as well as additional suspension samples, are measured for turbidity. From the start, it was observed that the effluent samples show a very low turbidity value throughout the experiment, i.e. between the 0.1 and 0.7 NTU. This is seen with all BER18 effluent turbidity measurements, as illustrated in *Appendix F*. The turbidity data is normalized by dividing the effluent turbidity over the suspension turbidity. The results for all BER18 turbidity measurements are presented in *Figure 5.10*, alongside the corresponding rate and pressure drop data. These results illustrate that the normalized turbidity is around 1-2%, during the whole experiment and demonstrate that very little of the total particles in suspension passes through the BER18 thin discs.

With one MF0.45 test, effluent samples are taken, which are measured for turbidity in the same manner as done with the porous thin discs. Turbidity results of this test are in the same order as the BER18 effluent turbidity measurements. Assuming nothing passes through the MF0.45 filter, all turbidity readings of effluent MF0.45 samples should indicate the bottom turbidity range of the Hydra. As the results of the MF0.45 and BER18 turbidity measurements are almost the same, it is assumed that nothing passes through the BER18 thin discs.

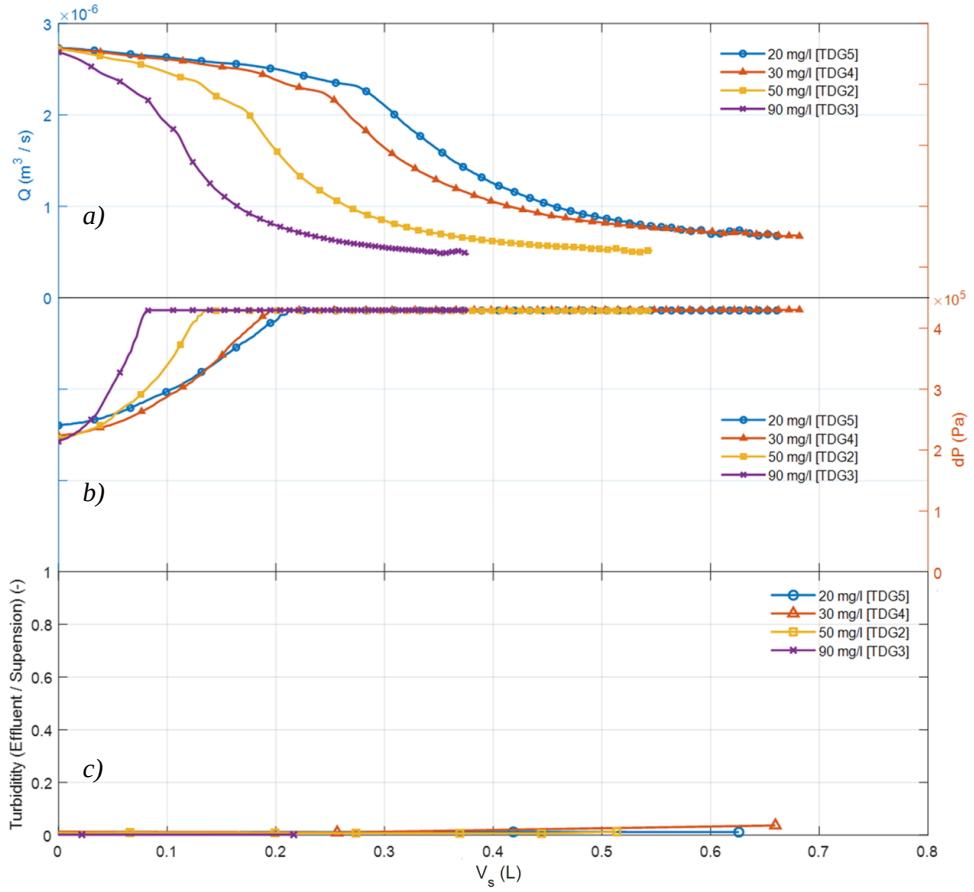


Figure 5.10: BER18 a) Flow rate versus suspension volume injected for various suspensions. b) Pressure drop versus suspension volume injected for multiple suspensions. c) Normalized effluent turbidity versus volume. Stacked figures for visualization of process at each concentration experiment.

### 5.2.2.3 MF0.45

As detailed earlier, each thin disc experiment is followed by an MF0.45 test and is carried out using the same suspension. As a result, experiments with an MF0.45 are conducted with various concentrations (*c*). In *Table 5.10*, the experiments are ordered from low to high suspension concentration, i.e. high to low WQ, respectively. The experiments are conducted at a rate of 20 l/hr, to maintain in the stable region of the hydra. As previously stated, the characteristics of the MF0.45 are not experimentally determined and are taken from the product information available from the supplier, with the assumption that they are similar for all MF0.45. Initial permeabilities are estimated to be 0.015 Darcy, as stated in section *5.1.2*. The duration of an experiment is manually controlled, varying between the 12 and 23 min. The injection volumes range between the 2.2 - 4.4 L, depending on water quality.

The rate, normalized permeability, pressure drop and impedance results for the MF0.45 experiments with various concentrations are presented in *Figure 5.11.a*, *Figure 5.11.b*, *Figure 5.11.c* and *Figure 5.11.d*. From these results, the same constant rate and constant pressure regime are distinguished as stated earlier, with the regime shifting point achieved when $dP_{max}$ is reached at a specific volume flowed ($V_{BC}$). With each experiment, the volume at which the regime shift occurs ($V_{BC}$) is different and is presented in *Table 5.10*. Once more, it is seen that the higher the concentration, the lower the amount of suspension volume is needed to reach $dP_{max}$. The results presented in *Figure 5.11.c* illustrates an exponential trend towards $dP_{max}$. Considering the flow rate results in *Figure 5.11.a* in the constant rate regime,

the rate is relatively constant for the low concentration suspension experiments. However, with increasing concentration, the rate falls with 10% in the constant rate regime.

The normalized permeability results presented in *Figure 5.11.b* illustrate a rapid decline to 20%. Hereafter a threshold is reached, and the results demonstrate that there is very little decline while in the constant pressure regime. The impedance results presented in *Figure 5.11.d*, illustrate a linear slope with suspension volume.

Table 5.10: Membrane filter information, operational conditions and suspension specifications of the reproducibility experiments MF-G5, MF-F2, MF-F1, MF-F3 and MF-F5.

| Experiment ID | Porous media Type | $Q_0$ [l/hr] | Brine type | $c$ [mg/l] | Duration [min] | $V_{inj}$ [L] | $k_i$ [Darcy] | $V_{BC}$ [L] |
|---|---|---|---|---|---|---|---|---|
| MF-G5 | MF0.45 | 20 | 2 | 20 | 14.6 | 4.00 | 0.015 | 1.88 |
| MF-F2 | MF0.45 | 20 | 1 | 30 | 13.3 | 3.35 | 0.015 | 1.37 |
| MF-F1 | MF0.45 | 20 | 1 | 50 | 23.0 | 4.35 | 0.015 | 1.11 |
| MF-F3 | MF0.45 | 20 | 1 | 90 | 16.4 | 2.59 | 0.015 | 0.64 |
| MF-F5 | MF0.45 | 20 | 1 | 100 | 12.1 | 2.21 | 0.015 | 0.72 |

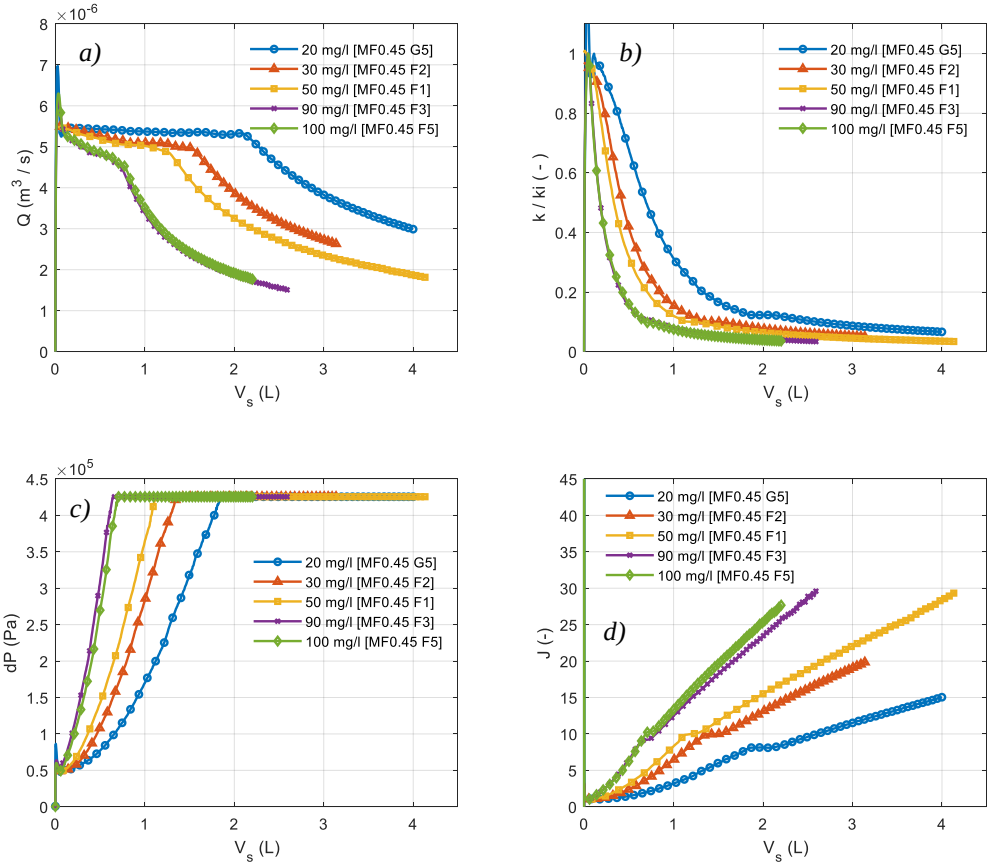


Figure 5.11: Results of experiments MF-G5, MF-F2, MF-F1, MF-F3 and MF-F5, where concentration is varied and plotted versus suspension volume injected a) Flowrate, b) Normalized permeability, c) Pressure drop, d) Impedance.

## 5.3 Post analysis Thin Discs

After a suspension flow experiment, some thin discs are analyzed to determine the severity of the formation damage. SEM imaging or micro-CT scan measurements are done to visualise

the core face as well as in-depth damage within the porous thin discs. The reversibility of the formation damage is analyzed by core flow permeability measurements of the damaged thin disc after an ultrasonic bath as explained in detail in section *4.6.1.1*.

### 5.3.1 SEM post-analysis TD-F5

Sample TD-F5's cross-section is visualised by assembling multiple SEM images. Unfortunately, SEM imaging is a surface characterisation technique, and consequently, 3D pathways cannot be investigated. A screenshot of the about 1.6 GB sized total SEM is presented in *Appendix G*. Prior to SEM, the following preparation steps are made: Firstly, without disturbing the cake formed on the top, the disc is carefully removed from the disc holder and is air-dried in a sealed storage place. Secondly, once dry, the thin discs are broken into two pieces along the diagonal. This is done by first cutting a small incision in the bottom side, to create a breaking plane. Subsequently, the thin disc is polished on the broken side to create a flat surface for optimal SEM imaging. Finally, the thin disc is covered with a carbon coating, and multiple SEM images are made from the side section of the thin disc. *Figure 5.12* illustrates the white-ish EFC formed on top unevenly distributed on the surface. The damage clearly bounded to the $A_{eff}$ area, and the outer area remains undamaged due to the silicon ring. *Figure 5.12.b* illustrates this in detail, where the damaged zone is indicated with a red shade. The EFC appears to concentrate at certain inflow areas and is certainly not one (thick) homogenous layer. Since the Baracarb2 particles deposited within the pores are too small to be observed with the naked eye, SEM imaging enables making high-resolution images from very small sections of the thin disc.

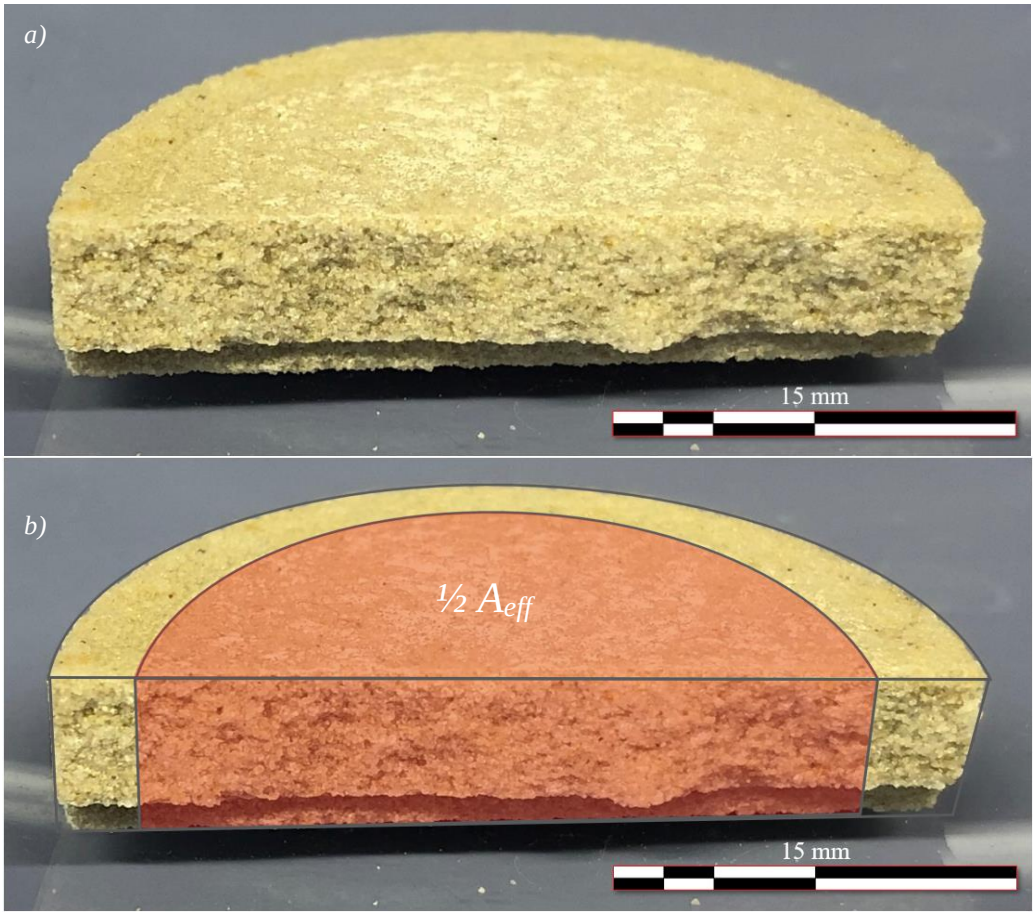


Figure 5.12: TD-F5 cross-section through the broken in half thin disc. a) Damaged sample and, b) Identification of the damaged zone.

*Figure 5.13.a*, as well as the zoomed-in *Figure 5.13.b*, enables a closer look at the formation damage process and EFC. In *Figure 5.13.a*, the distribution of the sand grains is seen alongside with the Baracarb2 particles within the pores. The zoomed-in area indicates the damage is primarily limited to the upper part of the thin disc, i.e. 3 to 4 grains deep. However, there are also pores throughout the thin disc which are fully or partially filled with Baracarb2 particles, indicating formation of IFC. For the BH11 porous rock, this is expected since the effluent turbidity results showed a high amount of suspension material was able to pass through. As the SEM image only illustrate a 2D cross-section, the flow paths through the thin disc are not fully captured. Therefore, the damage tends to pop-up at certain places within the porous thin disc.

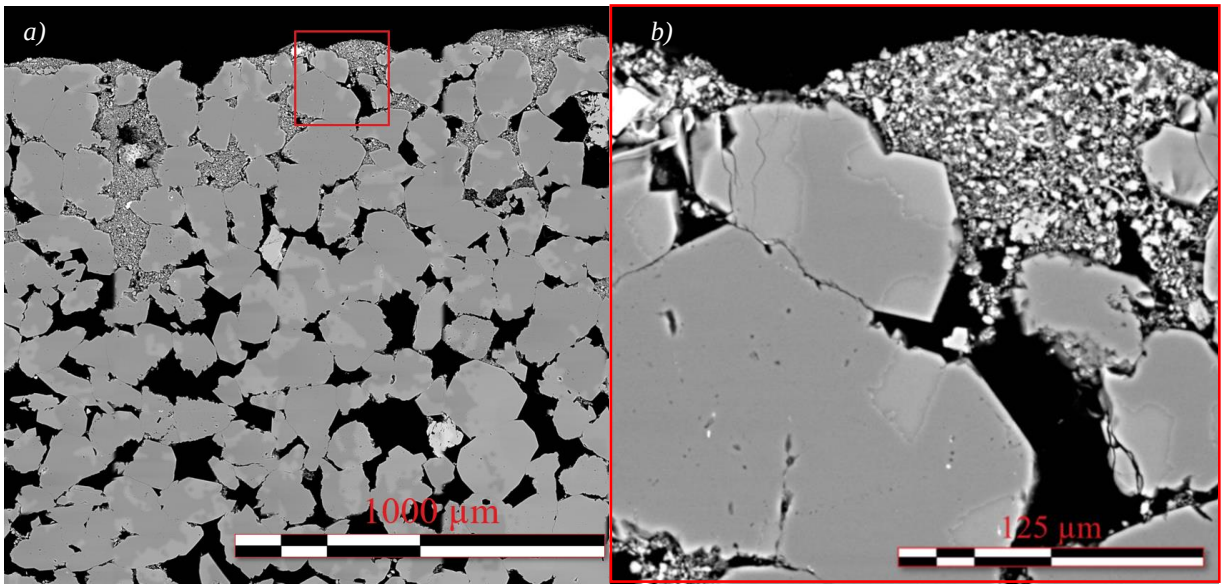

Figure 5.13: TD-F5 (Post experiment) SEM imaging results, with identification of Baracarb2 particles in the porous medium. a) SEM image snapshot capturing multiple grains and depth of damage. b) SEM image zoom in onto EFC formed at the sand face.

### 5.3.2 Micro-CT Scan post analyses TD-D1

The TD-D1 is chosen for post-analysis by constructing images from the Micro-CT scans of the damaged and clean thin disc, which are given in *Appendix G*. The results are presented in *Figure 5.14*, where the method of obtaining these images is detailed in section *4.6.1.2*. *Figure 5.14.a* illustrates the EFC formed on top of TD-D1, while preserving the sandstone grains in place. In *Figure 5.14.b*, the sandstone grains are removed by image processing. In this way, the significance of the formation damage is demonstrated in a 3D view. As detailed in section *4.6.1.2*, the images are constructed by performing a subtraction method, meaning that the difference between the damaged and clean disc are given, including that all differences are presented. The images are made with the Teflon tape still in place, which damages in the process of mounting and dismounting from the disc holder. It is believed that, considering the highlighted areas outside of the $A_{eff,}$ some artefacts are present, which are not considered damage due to suspended Baracarb2 particles.

A cross-sectional 3D image from TD-D1 is presented in *Figure 5.15*, enabling imaging of the damage depth within the thin disc to a certain extent. One can conclude from *Figure 5.14.b* and *Figure 5.15* that the damage is mainly present as EFC in the top section of the thin disc, with some IFC throughout the thin disc. This is in line what is seen with the SEM images seen with TD-F5 in the previous section. Cake thickness is estimated at 0.4 to 0.8 mm.

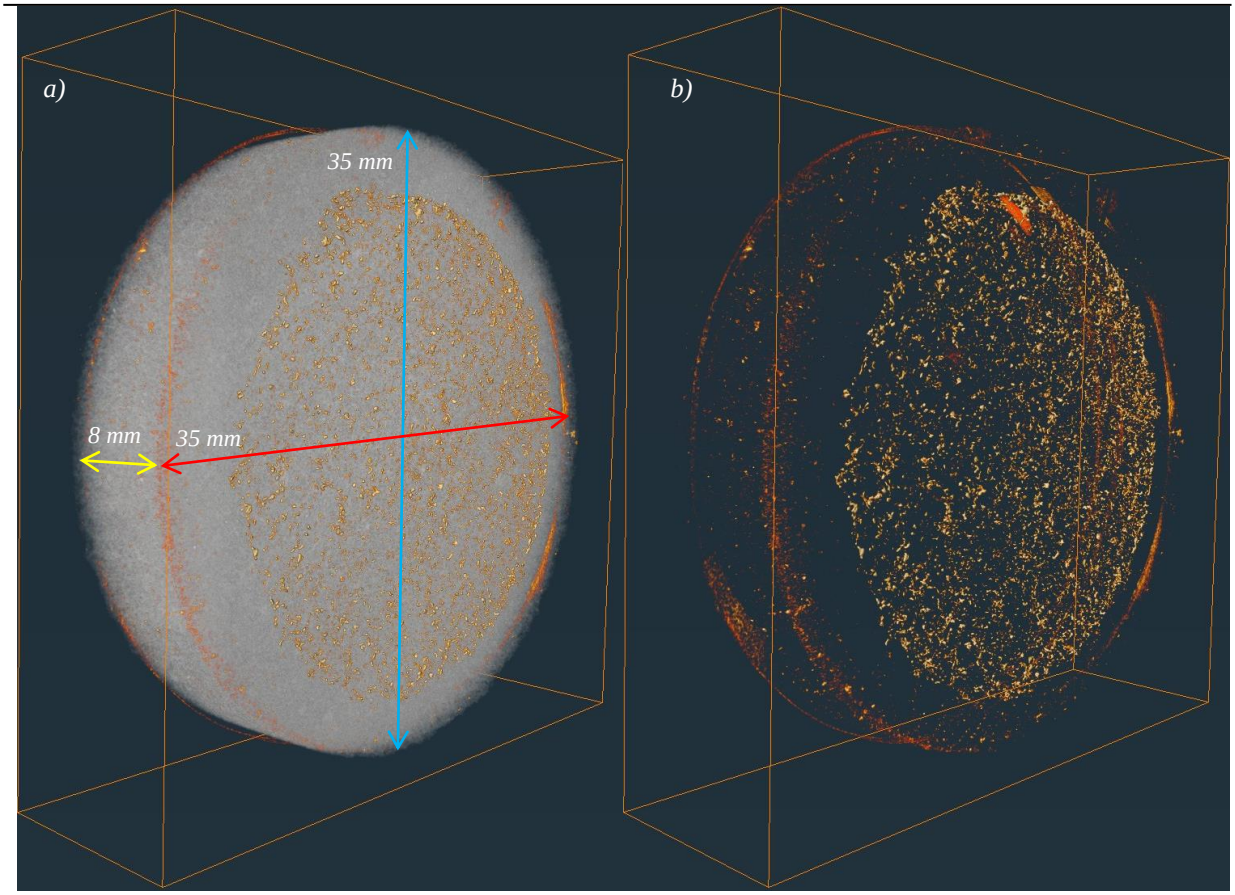

Figure 5.14: 3D view of a Micro-CT scan of TD-D1. a) Baracarb2 damage on top of the clean disc is seen in one picture. b) Micro-CT scan of the resulting damage visible by subtracting the clean disc from the damages disc scans.

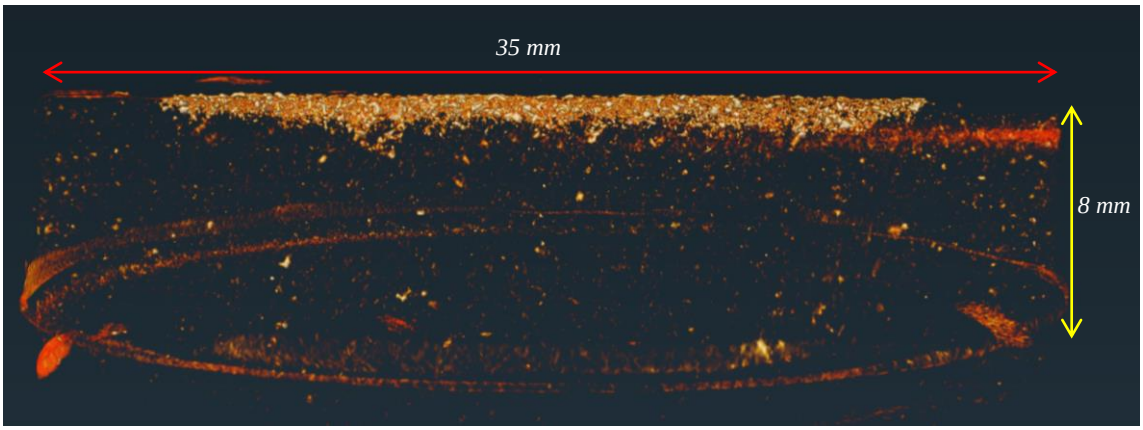

Figure 5.15: Side view of the Micro-CT scan of TD-D1

### 5.3.3 Post-Ultrasonic Bath (PUB)

Some of the porous thin discs of type BH11 and BER18 are tested for reversibility of the formation damage, in other words, re-establishment of the permeability. This is done by post treating the thin discs with an ultrasonic bath and back flowing the thin disc with 1 L before starting a rate step test, as detailed in section *4.6.1.1*. The initial permeability ($k_i$) of the clean thin discs, as well as the final the permeability ($k_{end}$) at the end of a suspension injection test combined with the partially restored permeability ($k_{PUB}$), is presented in *Table 5.11*. The data visualised in *Figure 5.16*, as well. By using this method, about 90% of the permeability is found to be recoverable, and consequently, the remaining 10% of the damage appears to be irreversible.

Table 5.11: Thin disc permeability damage and restoration cycle: before the experiment ($k_i$), at the end of the suspension flow experiment ($k_{end}$) and post-treated using an ultrasonic bath ($k_{PUB}$) with 1L backflow.

| Sample ID | Porous media type | $k_i$ [Darcy] | $k_{end}$ [Darcy] | $k_{PUB}$ [Darcy] | Reversible recovery [%] |
|---|---|---|---|---|---|
| TD-F1 | BH11 | 2.059 | 0.020 | 1.816 | 88 |
| TD-F2 | BH11 | 2.027 | 0.028 | 1.905 | 94 |
| TD-F3 | BH11 | 2.060 | 0.021 | 1.833 | 89 |
| TD-F4 | BH11 | 1.902 | 0.038 | 1.737 | 91 |
| TD-G2 | BER18 | 0.169 | 0.015 | 0.152 | 90 |
| TD-G4 | BER18 | 0.161 | 0.020 | 0.148 | 92 |

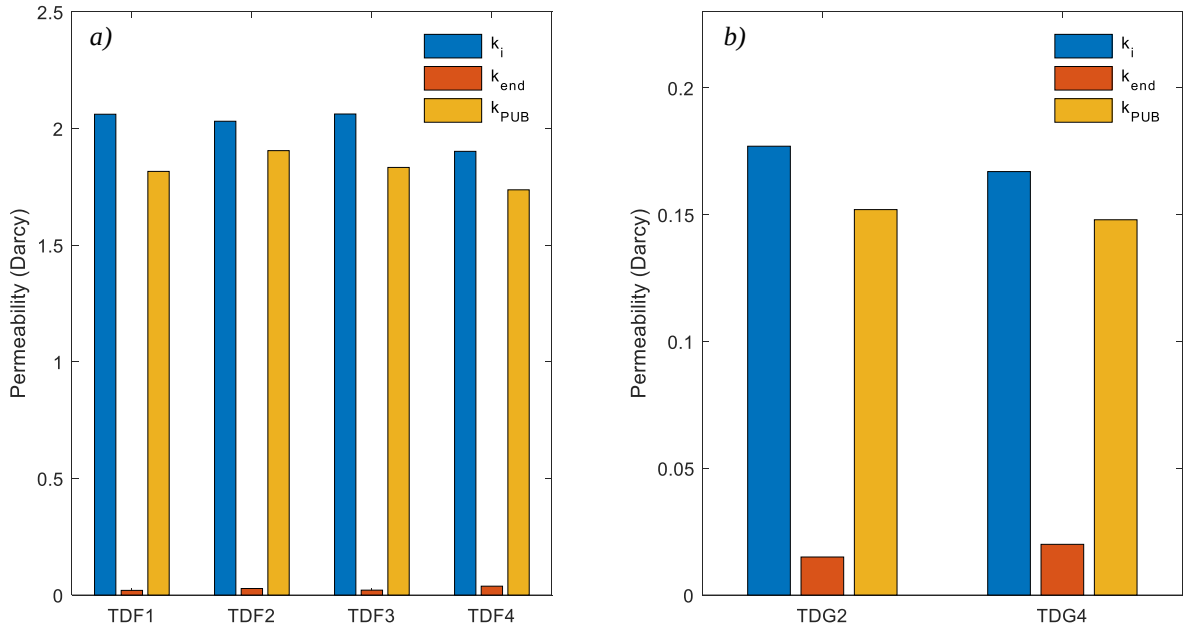


Figure 5.16: Bar plot of the permeability: before experiment ($k_i$), at the end of suspension flow experiment ($k_{end}$) and post-treated with a ultrasonic bath ($k_{PUB}$) with 1L backflow. a) BH11 and, b) BER18.

# 6 Discussion

The findings and results from sections *4* and *5* are discussed, where results are explained by the underlying mechanisms and emphasized whether the results are in line with the expectations or not. This chapter consists of five sections structured in the logical order of data acquisition; Section *6.1* discusses the experimental findings of the porous media, and Section *6.2* comprises a discussion about the stability of particles within synthetic brine. Section *6.3* discusses the combination of the medium and fluid in a dynamic sense, namely the results on suspension flow experiments. Within section *6.3*, the reproducibility and the underlying damage mechanisms of the fixed concentration experiments of 50 mg/l Baracarb2 suspension are discussed. Subsequently, the results on varying WQ (i.e. TSS) is discussed. Consequently, in section *6.4*, the post-experimental results are discussed. Lastly, a final reflection is done.

## 6.1 Porous media characteristics

In order to increase our understanding of formation damage due to suspension filtration, it is essential to have enough experimental control. Therefore, the thin discs from the same sandstone block need to have roughly similar permeability. The average permeability of BH11 and BER18 are 2.00 and 0.170 Darcy, respectively. From *Table 5.1* and *Table 5.2*, thin discs within each porous media type class have very similar dimensions, pore volumes and effective porosities. The homogenous nature resonates with findings in literature [32], [33]. Comparing the different rock types BH11 and BER18, the latter has smaller pore volumes and lower porosity values, which is consistent with the grain size and pore-throat size results. The $dP_0$ pressure correction term is consistently in the same order of magnitude. Membrane filter characteristics are assumed to be identical for that specific type of filter used. The permeability of the MF0.45 is estimated at 0.015 Darcy, which looks quite low at first sight. However, with a thickness of 150$\mu$m and a porosity of 79%, the pressure drop response with a specific rate is in fact in the same range as the BH11 thin discs.

## 6.2 Particle stability study

Stability of the fluid during experiments is vital. Therefore, experimental control on the particle behaviour in synthetic brine is required. XRD results of Baracarb2 demonstrate that roughly 5% is non-calcium carbonate, which is higher than expected. Especially with widespread usage of Baracarb in literature where the assumption is made that Baracarb is pure calcium carbonate. The same holds for the dissolution of 10 mg/l of calcium carbonate in synthetic brine, which may give a suspension concentration lower than intended.

Several tests are performed where the particles are analyzed for size distribution, which shows reproducible results of size between the 1 and 30 $\mu$m, with the mean (D50) particle size of 10 $\mu$m. It is observed the particles increase over time, i.e. D50 mean particle size increases from 8 to 12 $\mu$m over the time period resonating with the suspension flow experiment time. From the PSD, obscuration and SEM imaging, it is assumed that particle agglomeration takes place over time. Some research on analyzing Baracarb2 show either results in a limited time frame or do not capture the operational conditions which seem crucial in understanding the behaviour of the calcium carbonate particles. Results show that the above-described characters are essential to incorporate to eventually understand the impact of these particles on forming formation damage.

## 6.3 Suspension flow experiments

This section is divided into the serval parts. First, the pore-throat size distribution (PTSD) measurements of the porous medium are compared with the particle size distribution (PSD) of Baracarb2. Subsequently, the results and standard deviation are given for the reproducibility tests for a fixed concentration of 50 mg/l for each porous medium type, e.g. BH11, BER18 and MF0.45. From these reproducibility results, the trend and damage mechanisms are described for each porous medium. Subsequently, the suspension concentration is varied, resulting in an experiment for different water quality.

### 6.3.1 PSD Baracarb2 and PTSD Porous media

The results from the Baracarb2 PSD given in section *4.4.3* and PTSD of BH11 provided in section *4.1.2.1.2* are combined and presented in *Figure 6.1.a*. The same is done with the BER18 PTSD, shown in *Figure 6.1.b*. In both figures, the overlapping areas of the Baracarb2 PSD and the porous medium PTSD are highlighted. From *Figure 6.1.a* and *Figure 6.1.b*, it is evident that the Baracarb2 PSD has a greater overlapping area with the BER18 PTSD as compared to the BH11 PTSD. Consequently, the suspension filtration and damage mechanism differ for BH11 as compared to BER18. More specifically, the BER18 thin discs act as a more 'efficient filter' causing particles to be retained by size exclusion (also known as straining [24]) resulting in the rapid formation of an EFC as compared to the BH11 sample. Consequently, the turbidity of the BER18 effluent samples (see section *5.2.2.2.1*) is slightly above the detection limit turbidity apparatus as compared to BH11, transmitting about 50% of the injected concentration. Early establishment of an EFC results in cake ripening (enhances the rejection coefficient) and consequently has a big influence on the duration of the experiment and subsequently on the suspension volume injected. With membrane filters (MF0.45), the pore-throat size is around the 0.45 $\mu$m (as provided by the supplier), causing all particles to be retained as EFC on the surface of the MF0.45 filter. This is also observed in *Figure 4.1.a*.

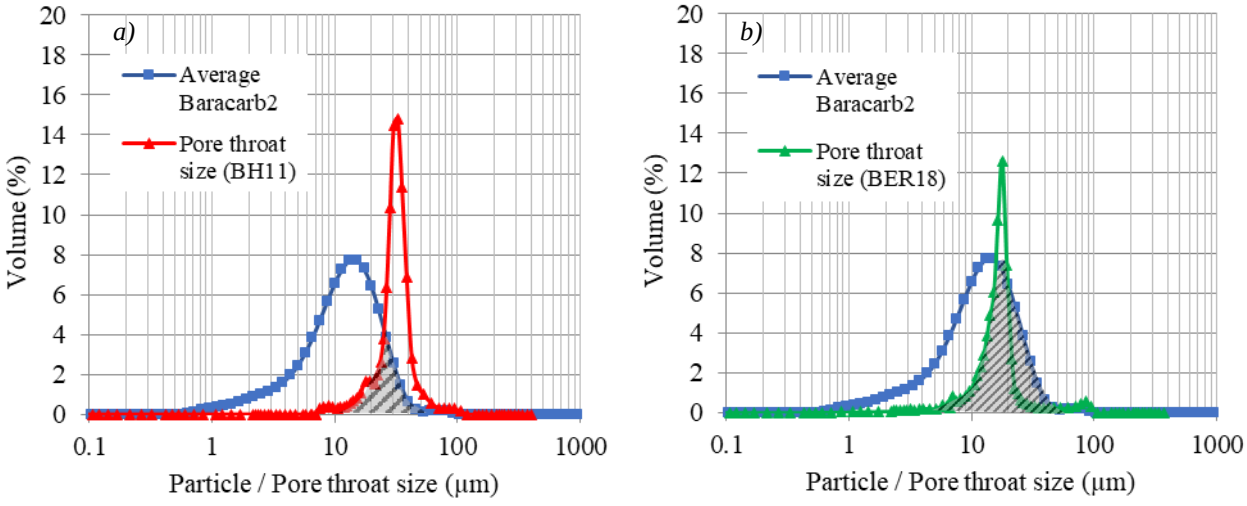


Figure 6.1: The particle size distribution of Baracarb2 given along the results of the pore throat size distribution of BH11 (a) and BER18 (b).

### 6.3.2 Reproducibility tests

The reproducibility of the 50 mg/l experiments given in section *5.2.1* is satisfactory for each porous media type. Similar trends are observed for the two different thin disc samples. In *Figure 6.2*, the errors are presented along the data curves to illustrate the error bound. *Figure 6.2.a* and *Figure 6.2.b* show a mean normalized permeability plot composed of the two

experiments with error bars (3 times the ~0.5 standard deviation) for BH11 and BER18 samples, respectively. Membrane filters show similar reproducibility. Though, it must be stated that permeability impairment in the starting phase is difficult to compare due to possible inconsistencies with initial conditions. Also, the cake filtration, i.e. constant pressure (CP) part is of interest, not necessarily the permeability impairment (CR part).

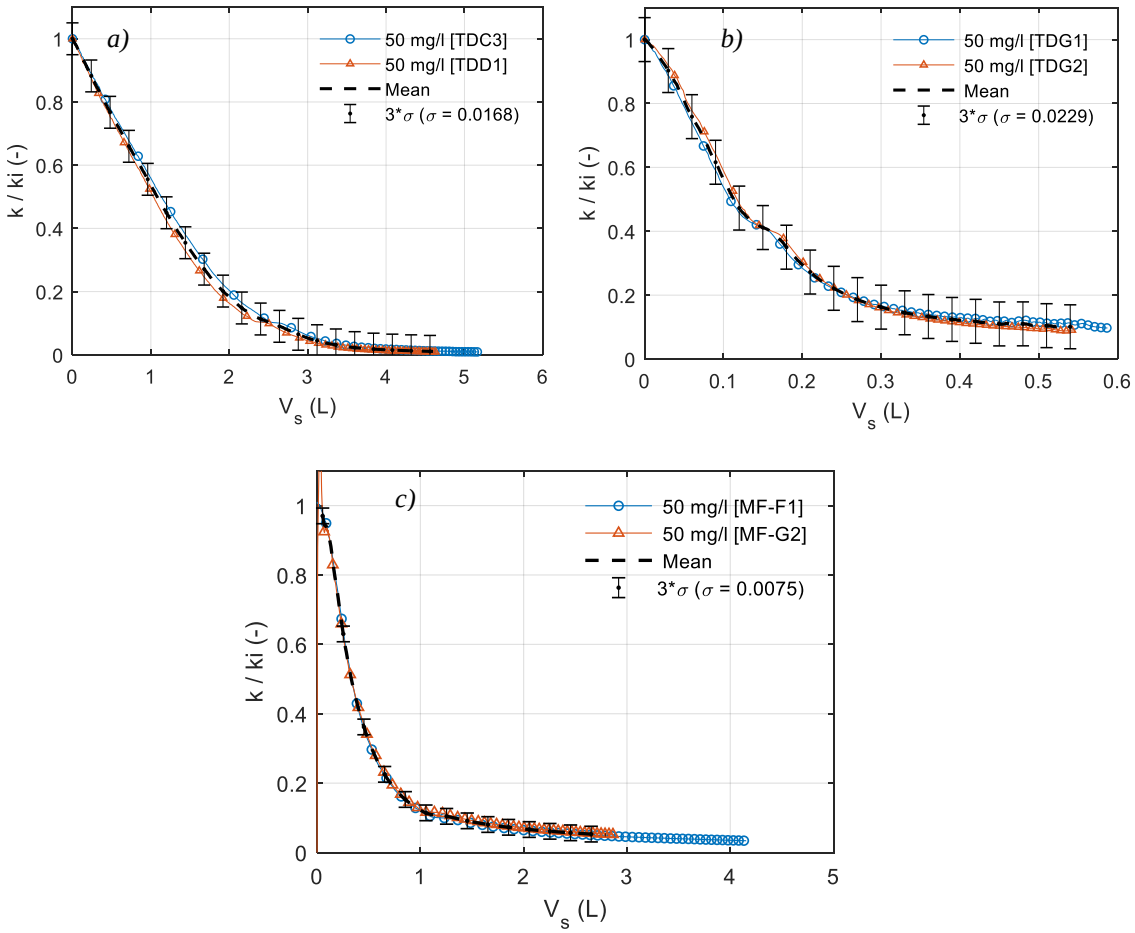


Figure 6.2: Normalized permeability reproducibility results with the calculated error. a) BH11, b) BER18 and c) MF0.45 (20 l/hr).

### 6.3.3 Trend behaviour and damage mechanisms

In this section, the trend behaviour from BH11, BER18 and MF0.45 (porous) media sample, during a 50 mg/l suspension injection test, are compared. These curves are obtained by simply drawing a simplified representation of the trends seen in the reproducibility section. These simplified representations from the normalized permeability and impedance are presented in Figure 6.3. There are some similarities between the porous media types and some differences that can be stated. One can observe that the curves have roughly the same shape as described in section *4.7*.

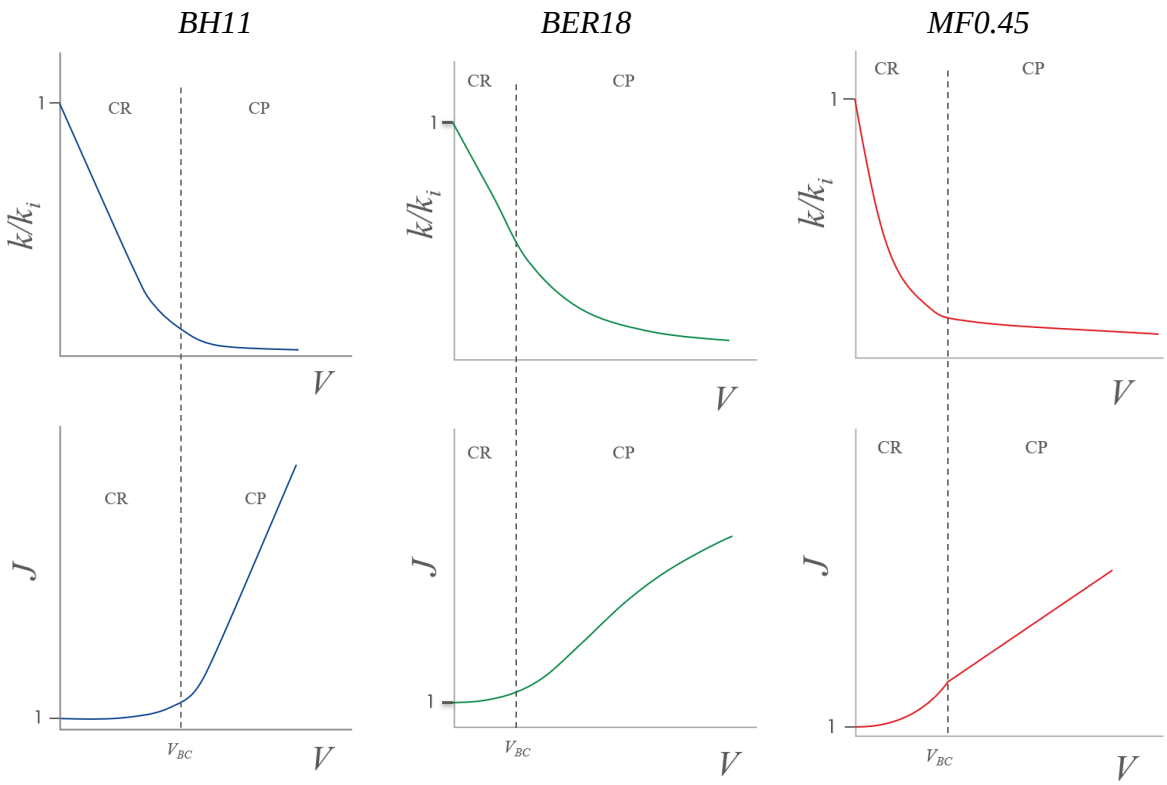


Figure 6.3: Simplified representation of the results from 50 mg/l Baracarb2 suspension flow experiments for the investigated media.

*Constant rate (CR) domain:*
In the constant rate domain, the normalized permeability drop is declining linear in the first part of all the experiments. It is proposed that within this part, the IFC forms within the discs and/or transition is initiated of forming an EFC on the porous medium. It depends on the porous medium type how long this trend stays linear and what the gradient of the slope is (more information in the following section *6.3.4*). This seems to relate to how fast the transition from IFC to fully established EFC takes place as well as the initial permeability of the medium. With the BER18 thin discs, very low volumes are needed for a very significant decrease (>60%) of normalized permeability, so it can be assumed that the IFC phase is very small and EFC is rapidly formed. Note that the suspension volumes for the BER18 experiments are in the order of 10 lower than seen with the BH11 and MF0.45 experiments. Also, due to the very low turbidity effluent readings, it is assumed that mainly EFC formation is responsible for the permeability impairment occurring in the BER18 experiments.

The normalized turbidity effluent reading of 60% obtained for the BH11 thin disc experiments, on the other hand, seem to facilitate DBF and indicate that formation damage can be attributed to IFC formation. This is assumed to occur in high flow passage areas in three up following sequences (1 to 3), illustrated in a schematic drawing presented in *Figure 6.4*. From the normalized turbidity data, the particle throughput is estimated, and it is assumed that a significant number of particles are retained by absorption in the first section as well as in the second section. Subsequently, a slightly declining plateau is maintained where particles are allowed to pass through the porous medium as presented in the latter part. Here it is hypothesized that particles follow high passage areas through the thin discs without large retainment until a threshold is reached.

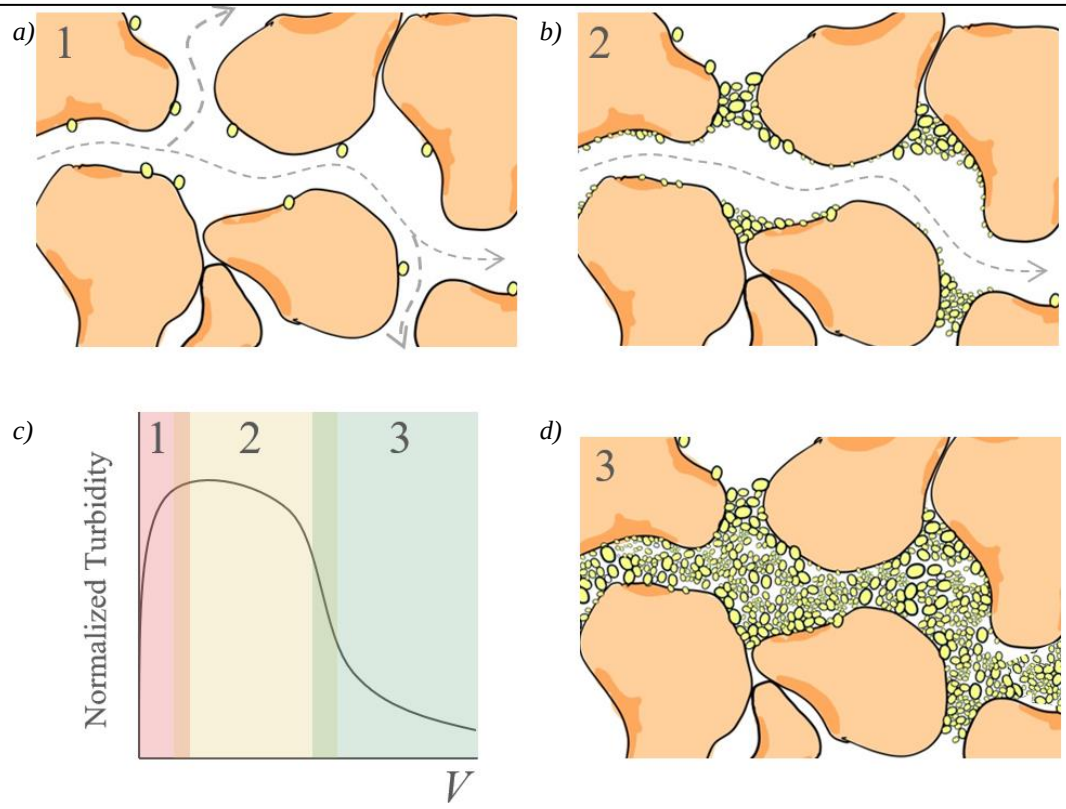


Figure 6.4: Schematic drawing of IFC and EFC forming within thin disc with up following formation damage sequences given along the normalized turbidity plot.

*Constant pressure (CP) domain:*
Subsequently, after a certain volume (which is not necessarily $V_{BC}$) an exponential decay towards a base value is observed. This exponential decay towards a base value can be interpreted as a transition from IFC to EFC (*Figure 6.4.b* to *Figure 6.4.d)*. Eventually, the internal accumulation is building outwards (upstream) forming an EFC. As a result, the overall flow through the thin discs becomes controlled by the flow path through the cake, instead of initial flow occurring through the pores of the grains. The part where the cake is fully formed is best visualised by the impedance results and corresponds to the part where the curve follows a linear slope. For visualization, a schematic drawing of a porous thin disc is presented in *Figure 6.5*. This illustrates the formation damage (and therefore the permeability impairment) due to suspended solids, before and after a suspension injection test.

For the BER18 thin discs, the impedance results in the CP part follows a somewhat different trend as compared to BH11 and MF0.45 results. This trend is different in the manifestation of an S-shape. Due to the limited injected volume at $V_{BC}$, it appears as if the EFC is not entirely formed when $dP_{max}$ is reached. In summary, possibly the linear trend is not fully visible yet because the duration of the experiment is too short.

With membrane filters, on the other hand, it is assumed that from the start, EFC starts to develop. However, this is difficult to compare to the thin disc because of the high porosity and engineered (fibre like) surface. As particles retain on the surface, the cake is compressed during filtration. It is striking that IFC forming in thin discs and EFC compressible behaviour seen with membrane filters present very similar trends.

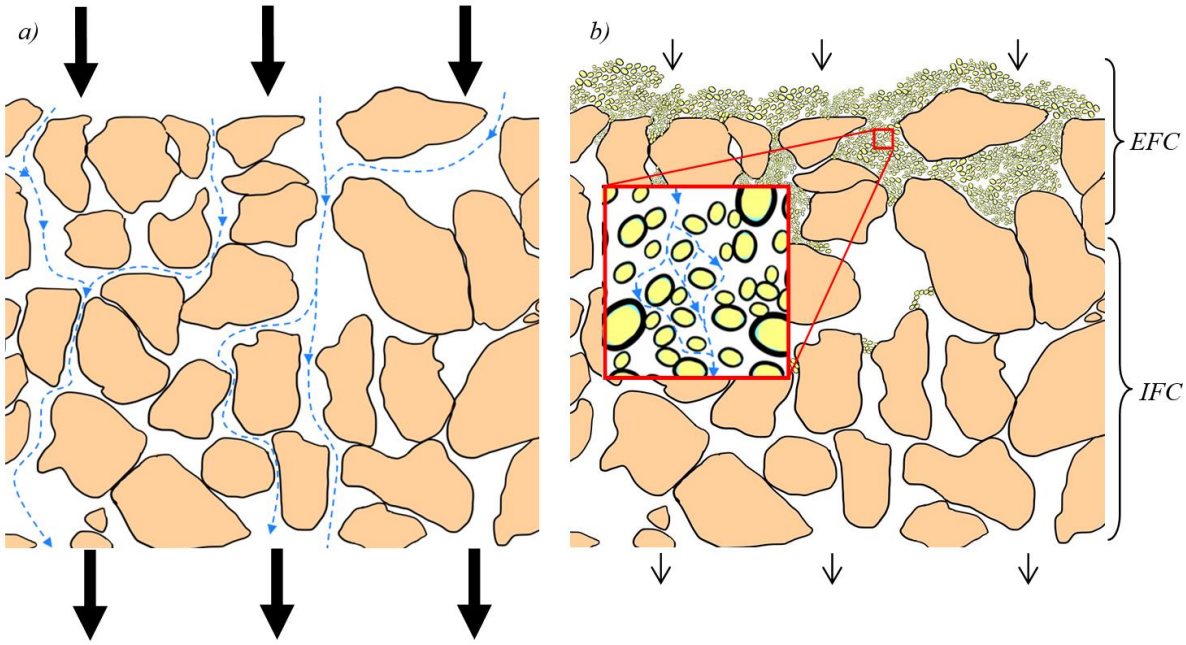


Figure 6.5: Schematic drawing of a thin disc, before (a) and after (b) a suspension injection test. The black arrow size indicates the flowrate.

### 6.3.4 TSS / Water Quality variation

As explained in section 2.2.2, WQ is interpreted as TSS. In this section, the results from WQ variation experiments are evaluated for each porous media type. Subsequently, the effect of varying water quality on formation damage is presented. A 'similarity transformation' is applied to investigate the scaling behaviour of the permeability decrease due to formation damage as a function of suspension concentration of Baracarb2. With all WQ variation experiments presented in the results section, either the full trend is illustrated, or the trend is separated in either a CR or a CP regime.

From a **Reservoir Engineering point of view**, it is important to predict in what stage the permeability impairment is situated, at a specific time (or in this case with a certain volume injected). By this means, the best remediation can be chosen in the form of prevention or stimulation. A usual approach is to identify the number of volumes injected needed until the permeability is halved, (i.e. $k/k_i = 50\%$).

From a **Production Technologist / Chemist point of view**, usually, the focus is on the cake filtration part, in order to determine the TSS and thereby the influence on formation damage. Within the CP part of the experiment, it is assumed that the EFC is fully established when the impedance versus volume demonstrates a linear trend. As discussed in the model section (section *3.3.2*), plotting impedance versus volume injected provides information of the formed cake. Accurately, the Modified Fouling Index (MFI) can be determined by calculating the slope of the impedance versus volume for each concentration (Ruth plot).

#### 6.3.4.1 Master curve and similarity curve collapse

One can expect experiments to follow one single master curve which scales (more or less) with suspension concentration, which is demonstrated in the model section *3.3*, where the filtration curve scales perfectly with concentration. To illustrate the scaling collapse, the normalized permeability, impedance and normalized turbidity effluent measurements versus suspension volume injected for multiple suspension concentrations are repeated in *Figure 6.6* (*a*, *c*, and *e*) as well as the corresponding transformed curves (*b*, *d* and *f*). Each experiment,

irrespective of the suspension concertation, appears to follow the same typical declining trend but differs with respect to the volume injected. To investigate this further, the suspension volumes of each experiment are scaled with a specific 'scaling factor', to manually overlay the normalized permeability trends on top of each other. The scaling factors are presented in *Table 6.1*, along with the suspension concentration values. By introducing the same scaling factor with the impedance and turbidity data, a 'master curve' is obtained. Especially from the turbidity plot curve collapse, it now becomes evident that this data also follows one master curve. Subsequently, plotting the applied scaling factors against the suspension concentration in *Figure 6.15* (at the end of this chapter) indicates that the scaling value roughly equals the suspension concentrations (*c*). The spread of the data can mainly be explained by the effect of heterogeneity in the porous media.

Table 6.1: WQ experiment where concentration and scaling factor are given for BH11.

| Experiment ID | Porous media Type | *c* [mg/l] | Scaling factor [%] |
|---|---|---|---|
| TD-F4 | BH11 | 20 | 21 |
| TD-F2 | BH11 | 30 | 36 |
| TD-F1 | BH11 | 50 | 48 |
| TD-F3 | BH11 | 90 | 88 |
| TD-F5 | BH11 | 100 | 93 |

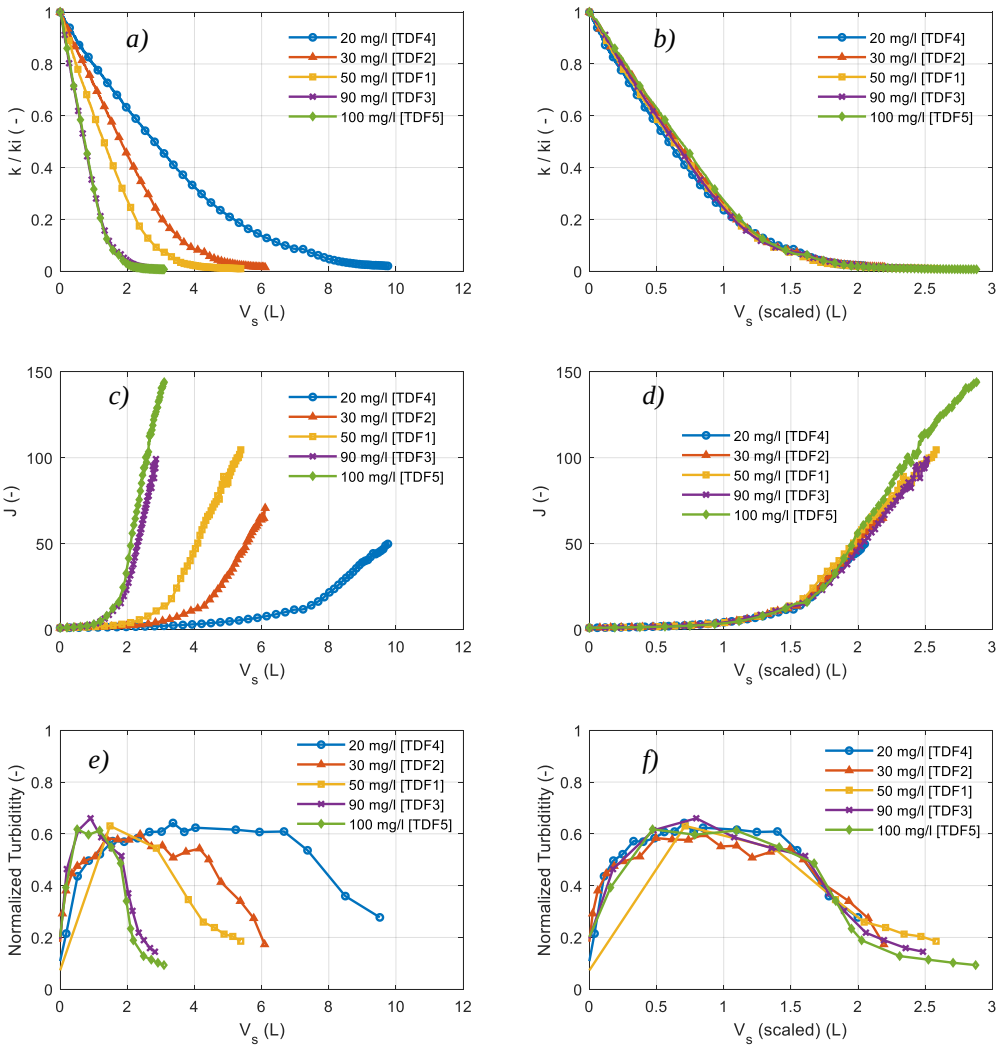


Figure 6.6: BH11 results for various suspension concentrations plotted against suspension volume (a, c and e) or scaled suspension volume (b, d and f). a) Normalized permeability, b) Scaled normalized permeability, c) Impedance, d) Scaled impedance results, e) Normalized turbidity and f) Scaled normalized turbidity.

#### 6.3.4.2 BH11 Master curve

As introduced in the previous section, *Figure 6.6* (*a*, *c*, and *e*), as well as the corresponding transformed curves (*b*, *d* and *f*), resulting in a curve collapse revealing a master curve. A significant part of the normalized permeability drop is in the CR part of the total trend. The normalized permeability for the various concentration experiments within the CR regime is presented in *Figure 6.7*. The slope from the normalized permeability is determined by performing linear regression for each suspension concentration varying experiment. The linear regression lines are indicated with dotted lines in *Figure 6.7.a*. The linear slopes are presented in *Table 6.2* The determined slopes are plotted against suspension concentration in *Figure 6.7.b*. From these results, it is seen that the slope of the permeability impairment increases linearly with suspension concentration. In other words, with a high concentration, the more damage occurs with at injected volume x, than seen with a low concentration at injected volume x. This can be explained by the following schematic drawing.

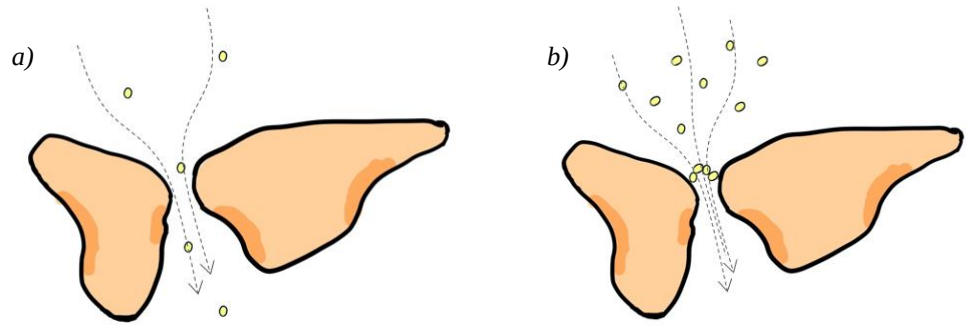


In case of a low suspension concentration (a), the particle spacing is greater than seen with the higher concentration (b). Consequently, with a high concentration probability of collapsing and plugging the porous medium is more evident.

While in the CR domain, the amount of volumes injected are identified for halving the normalized permeability, (i.e. $k/k_i$ = 50%). The results of $V_s$ at $k / k_i$ = 50% for the different suspension concentrations are presented in *Table 6.2*.

When focusing on the cake filtration part, i.e. CP part of the experiment, the MFI is determined by calculating the slope of the impedance versus volume for each concentration in the Ruth plot. The MFI for each concentration is presented in *Figure 6.8.b*. Here it is observed that a linear relationship could be distinguished between MFI and concentration. The linear regression line seems to intercept the x-axis at approximately 10 mg/l, which is expected considering the dissolution nature of the suspension and with zero suspension concentration, there is no specific cake resistance due to no particles in the fluid.

Table 6.2: CR parameters of BH11 at different WQ.

| Experiment ID | Porous media Type | *c* [mg/l] | $k/k_i$ slope | $V_s$ at $k/k_i$ (50%) [L] |
|---|---|---|---|---|
| TD-F4 | BH11 | 20 | -0.165 | 2.81 |
| TD-F2 | BH11 | 30 | -0.269 | 1.81 |
| TD-F1 | BH11 | 50 | -0.365 | 1.31 |
| TD-F3 | BH11 | 90 | -0.684 | 0.72 |
| TD-F5 | BH11 | 100 | -0.683 | 0.73 |

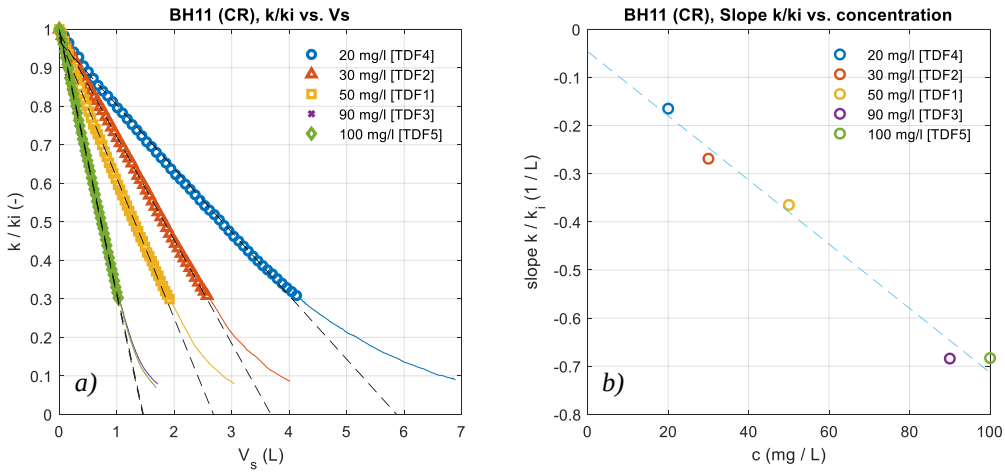


Figure 6.7: CR results for WQ experiments with BH11. a) Normalized permeability results versus suspension volume injected, with identification of linear regression lines. b) Normalized permeability slopes versus concentration.

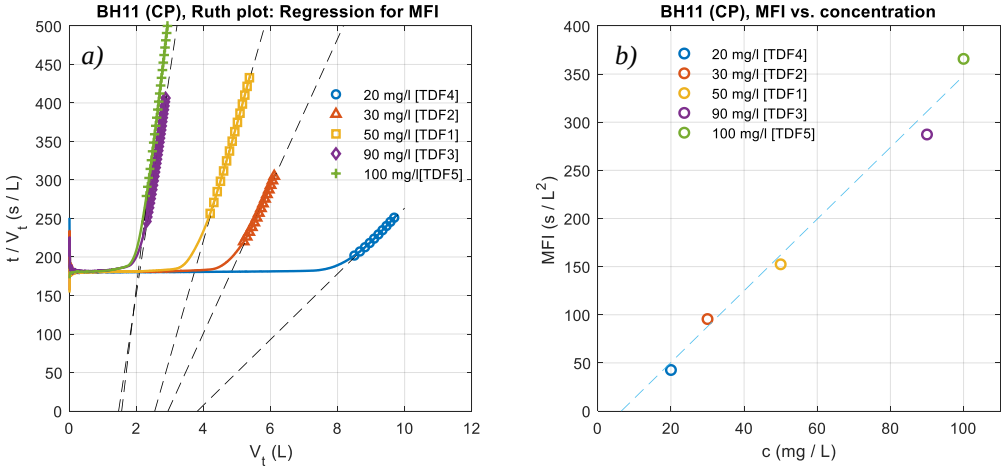


Figure 6.8: CP results for WQ experiments with BH11. a) Plotting the Ruth plot (t/V versus V) for MFI determination with various concentrations. b) Showing the linear relationship between MFI and concentration.

### 6.3.4.3 BER18 Master curve

*Figure 6.9* (*a*, *c* and *e*) with the corresponding transformed curves (*b*, *d* and *f*) using the factors of *Table 6.3*, again result in a curve collapse revealing a master curve. It must be noted that the flow rate in these experiments is half the rate of BH11. BER18 thin discs EFC requires only very limited suspension volume. As a result, the observed feature occurring during the switch from CR to CP as discussed in section *4.7* appears to be more significant as in the case of the BH11 experiments. Subsequently, it is observed that the scaling factors are highly resembling the suspension concentrations (*c*) in the same way as with the BH11 scaling factors. The scaling factors are plotted against concentration in *Figure 6.15* at the end of this chapter.

Table 6.3: WQ experiment where suspension concentration and scaling factor are given for BER18.

| Experiment ID | Porous media Type | *c* [mg/l] | Scaling factor [%] |
|---|---|---|---|
| TD-G5 | BER18 | 20 | 30 |
| TD-G4 | BER18 | 30 | 35 |
| TD-G2 | BER18 | 50 | 53 |
| TD-G3 | BER18 | 90 | 88 |

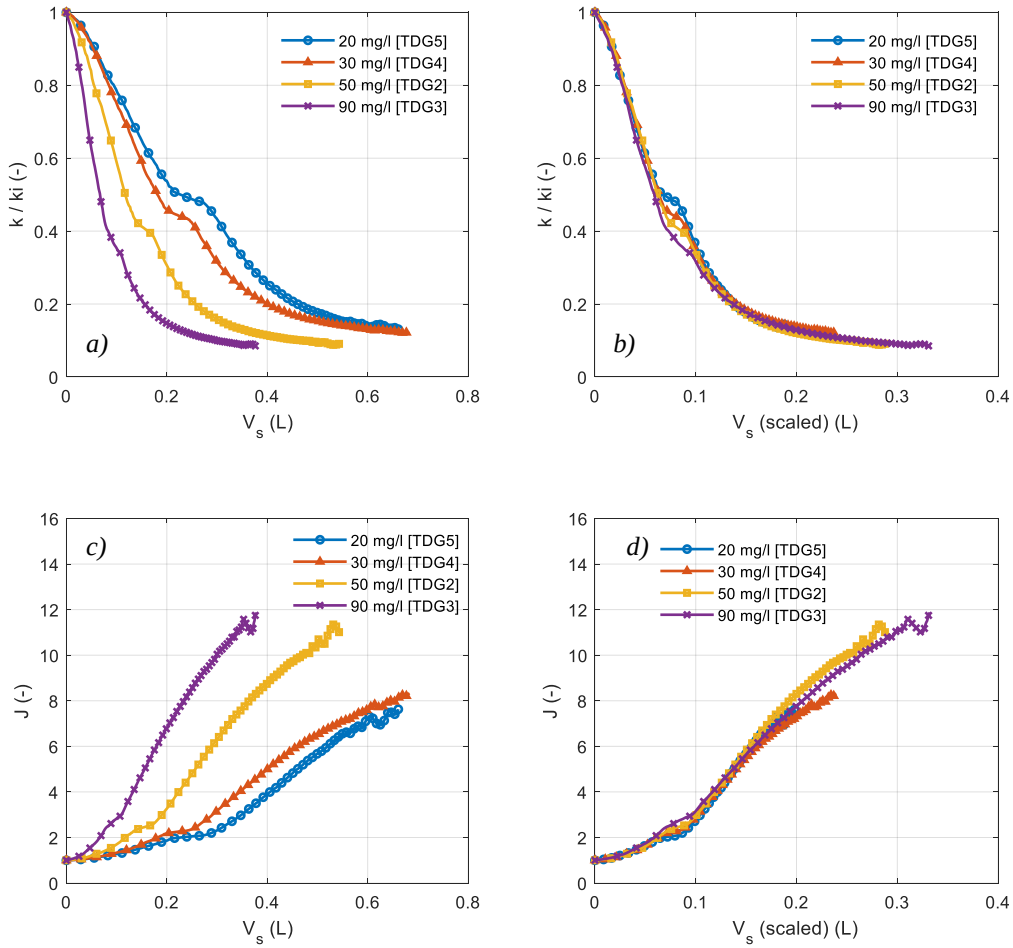


Figure 6.9: BER18 results for various suspension concentrations plotted against suspension volume (a and c) or scaled suspension volume (b and d). a) Normalized permeability, b) Scaled normalized permeability, c) Impedance and d) Scaled impedance results.

The normalized permeability drop presented in *Figure 6.10.a* is analyzed for the slope by performing linear regression of the first section within the CR regime. The results are given in *Table 6.4*, where it is seen that with increasing suspension concentration, the negative normalized permeability slope increases. As a result, the volume injected at $k/k_i$ = 50 %, decreases with increasing suspension concentration. Comparing the slopes of BH11 and BER18, one order of magnitude difference is demonstrated, which is in line with the permeability difference.

Within the CP part of the experiment, it is assumed that the cake properties are dominant during this part of the experiment. The impedance versus volume results is presented in *Figure 6.11*, which demonstrate a semi linear trend. Therefore, it is not sure if the cake is fully established, i.e. flow does not necessarily flow solitarily through the cake. As a result, linear regression is done for the last part of the trend in the CP regime. As discussed in the model section, plotting impedance versus volume injected provides information on the specific cake resistance. Specifically, the MFI can be determined by calculating the slope of the impedance versus volume for each concentration in the Ruth plot seen in *Figure 6.11.a*. The MFI is plotted against the corresponding concentration in *Figure 6.11.b*. Here it is seen that a linear relationship is found between MFI and concentration. Remarkably the linear lines intercept the y-axis (or minus x-axis). It is unclear why the MFI is too high and can't be explained along with the available data. As stated earlier, it is not sure if the cake is fully

established, so the MFI plot may give insufficient information. Comparing the MFI values from BH11 and BER18, there is a difference in one order of magnitude, similar as seen with the permeability.

Table 6.4: CR parameters of BER18 at different WQ.

| Experiment ID | Porous media Type | $c$ [mg/l] | $k/k_i$ slope [1/L] | $V_s$ at $k/k_i$ (50%) [L] |
|---|---|---|---|---|
| TD-G5 | BER18 | 20 | -2.4521 | 0.2282 |
| TD-G4 | BER18 | 30 | -2.9763 | 0.1829 |
| TD-G1 | BER18 | 50 | -4.4626 | 0.1190 |
| TD-G2 | BER18 | 90 | -7.9246 | 0.0690 |

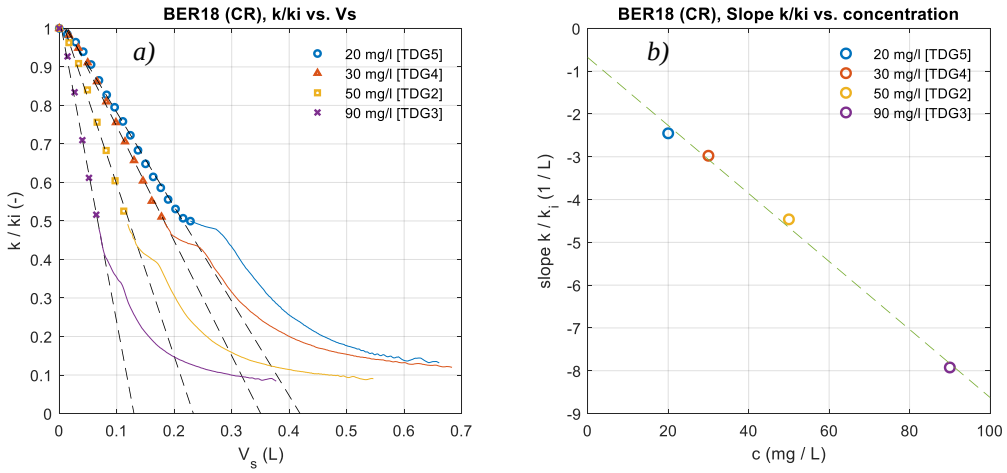


Figure 6.10: CR results for WQ experiments with BER18 thin discs. a) Normalized permeability results versus suspension volume injected, with identification of linear regression lines. b) Normalized permeability slopes versus concentration.

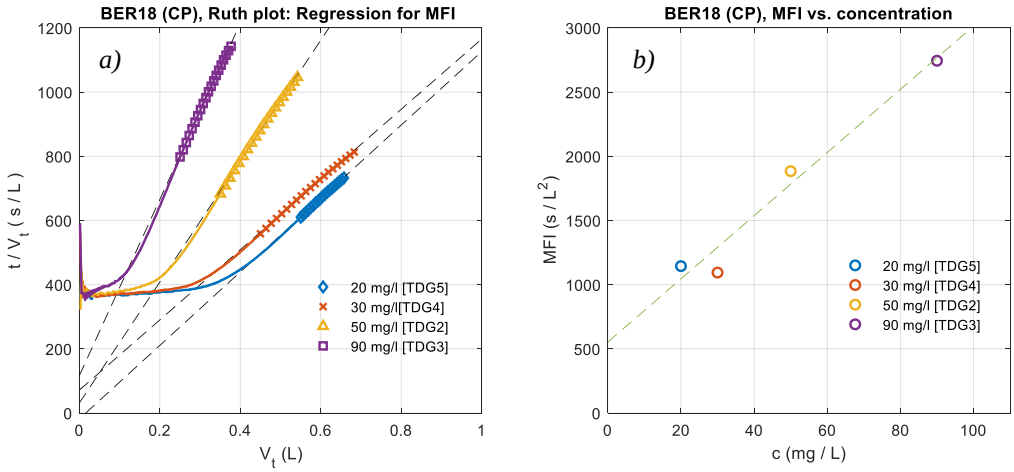


Figure 6.11: CP results for WQ experiments with BER18. a) Plotting the Ruth plot (t/V versus V) for MFI determination with various concentrations. b) Showing the linear relationship between MFI and concentration.

### 6.3.4.4 MF0.45 master curve

The same method of introducing a scaling factor is applied with the WQ varying MF0.45 experiments. Here the same observation is made: the scaling factors roughly resemble the suspension concentration, indicating that there is one master curve that scales with suspension concentration. The scaling factors are plotted against concentration in *Figure 6.15* at the end of this chapter alongside the scaling factors seen with the other porous media types.

Table 6.5: WQ experiment where suspension concentration and scaling factor are given for MF0.45.

| Experiment ID | Porous media Type | *c* [mg/l] | Scaling factor [%] |
|---|---|---|---|
| MF-G5 | MF0.45 | 20 | 26 |
| MF-F2 | MF0.45 | 30 | 43 |
| MF-F1 | MF0.45 | 50 | 50 |
| MF-F3 | MF0.45 | 90 | 85 |
| MF-F5 | MF0.45 | 100 | 91 |

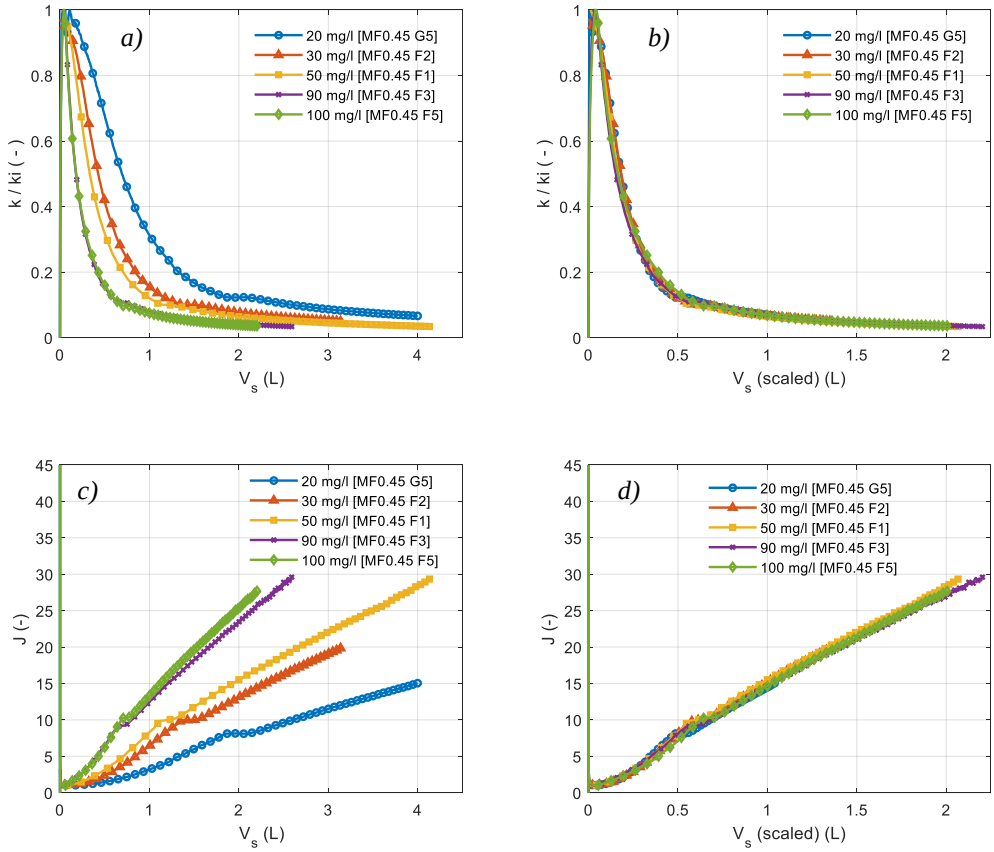


Figure 6.12: Results for various suspension concentrations plotted against suspension volume (a and c) or scaled suspension volume (b and d). a) Normalized permeability, b) Scaled normalized permeability, c) Impedance and d) Scaled impedance results.

Considering the CR part of the full trend, linear regression is done to obtain the slopes of the MF0.45 normalized permeability curves, which are plotted in *Figure 6.13.a*. The slopes and normalized permeability reduced to 50% are presented for each suspension concentration in *Table 6.6*. The slopes found from the linear regression are plotted against suspension concentration in *Figure 6.13.b*. From these results, it is seen that the slopes follow a linear relationship with suspension concentration.

Within the CP part of the experiment is visualized by plotting the Ruth plot (t/V versus V). Here a linear part is observed, and the MFI is determined via linear regression. The results are presented in *Figure 6.14.a*, where the MFI is plotted versus suspension concentration in *Figure 6.14.b*. Once more, it is seen that a linear relationship is found between MFI and concentration.

Table 6.6: CR parameters of MF0.45 at different WQ.

| Experiment ID | Porous media Type | $c$ [mg/l] | $k/k_i$ slope [1/L] | $V_s$ at $k/k_i$ (50%) [L] |
|---|---|---|---|---|
| MF-G5 | MF0.45 | 20 | -0.8230 | 0.694 |
| MF-F2 | MF0.45 | 30 | -1.0751 | 0.426 |
| MF-F1 | MF0.45 | 50 | -1.6074 | 0.334 |
| MF-F3 | MF0.45 | 90 | -2.4435 | 0.181 |
| MF-F5 | MF0.45 | 100 | -2.6090 | 0.179 |

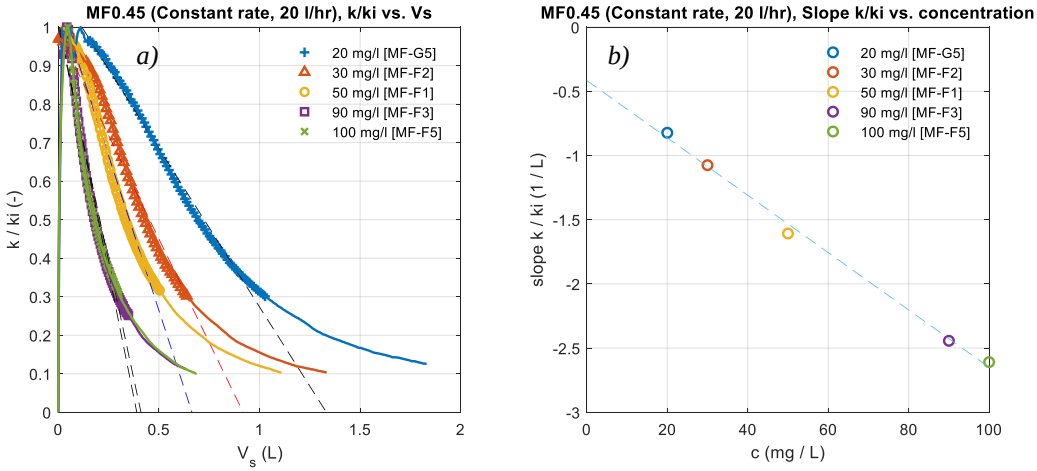


Figure 6.13: CR results for WQ experiments with MF0.45. a) Normalized permeability results versus suspension volume injected, with identification of linear regression lines. b) Normalized permeability slopes versus concentration.

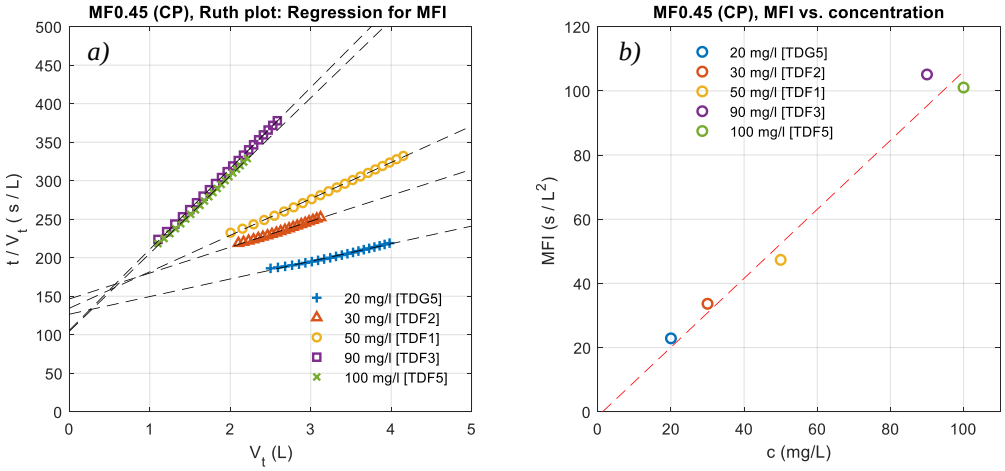


Figure 6.14: CP results for WQ experiments with MF0.45. a) Plotting the Ruth plot (t/V versus V) for MFI determination with various concentrations. b) Showing the linear relationship between MFI and concentration.

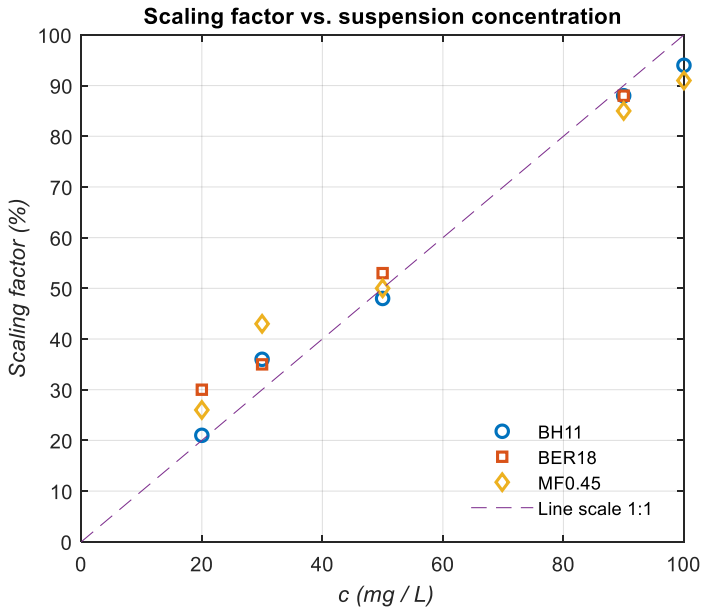


Figure 6.15: Scaling factors determined by the similarity curve collapse method plotted against corresponding suspension concentration for BH11, BER18 and MF0.45.

### 6.3.5 Comparing master curves for BH11, BER18 and MF0.45

From the similarity curve collapse method, it becomes evident that a single master curve is obtained from each porous medium, which scales roughly with concentration. However, there is some difference notable, e.g. volumes are different and therefore, the number of particles needed to plug the medium differs. In terms of a mass balance, a straightforward back on the envelope calculation is done, where for each porous medium the amount of volume is determined where the normalized permeability equals 10%, i.e. approaching the fully established EFC part. With the BH11, it is assumed that about 50% of the particles are allowed to pass through the medium. In the case of BER18 and MF0.45, full retaining is assumed. From the results presented in *Table 6.7*. On average, it is illustrated that these differences in retained mass.

Table 6.7: Back on the envelope calculation to determine the mass balance of retained particles.

| Porous medium | Concentration ($c$) (mg/l) | $V_s$ at $k/k_i$ = 10% (L) | Total Mass flowed (theoretically) [mg] | Mass retained [mg] |
|---|---|---|---|---|
| BH11 | 20 | 7.5 | 150 | 75 |
| | 30 | 4 | 120 | 60 |
| | 50 | 3 | 150 | 75 |
| | 90 | 1.8 | 162 | 81 |
| | 100 | 1.8 | 180 | 90 |
| BER18 | 20 | 0.6 | 12 | 12 |
| | 30 | 0.6 | 18 | 18 |
| | 50 | 0.4 | 20 | 20 |
| | 90 | 0.3 | 27 | 27 |
| MF0.45 | 20 | 2 | 40 | 40 |
| | 30 | 1.5 | 45 | 45 |
| | 50 | 1.1 | 55 | 55 |
| | 90 | 0.7 | 63 | 63 |
| | 100 | 0.7 | 70 | 70 |

## 6.4 Post Analysis

The SEM imaging results presents exciting insights on how the IFC and EFC are distributed through the thin discs. An apparent image is presented, illustrating the difference of particles size of Baracarb2 compared to the grain size and pore-throat size. From the SEM images, it is observed that the damage with the BH11 porous thin discs is mainly external, with same IFC patches within in the porous media, substantiating the damage sequence hypothesized in section *6.3.3*. The Mirco-CT scan results of BH11 demonstrate a distribution of the Baracarb2, highlighted throughout the thin disc. The results substantiate the same findings of the SEM images: damage is mainly in the form of EFC with some patches of IFC throughout the thin disc. Both methods of post analyzing the porous media give way for a better understanding of formation damage occurring in the reservoir rock.
The results of the post-treated thin discs show high recovery of the permeability up to 90% on average. There is potential in the application of ultrasonic waves and backflow on formation damage remediation.

## 6.5 Final reflection

As stated earlier, the data can be interpreted from two points of views: Reservoir Engineering point of view and Production Technologist / Chemist point of view. The permeability impairment (CR domain) or MFI determination (CP domain) can be successfully be determined using porous thin discs utilizing the Hydra. The usage of porous thin discs serves as an excellent bridging application between standard WQ tests with membrane filters and core flooding.

# 7 Conclusion

In this study, several flow experiments are carried out with Baracarb2 ($CaCO_3$) saline suspension to test the effect of Water Quality (TSS) on Formation Damage. This is carried out with porous thin discs and membrane filters. From the results and discussion, the following conclusions are drawn.

- Porous thin discs Bentheimer (BH11) and Berea (BER18) sandstone show homogenous results, with permeabilities of 2.00 and 0.170 Darcy, respectively.
- The particle size of Baracarb2 varies in between the 1 and 30 $\mu$m, with a mean (D50) particle size of 10 $\mu$m. PSD Baracarb2 show particle agglomeration over time and demonstrates an insoluble character of 5%, which consist of quartz, clinoptilolite and smectite.
- Particle suspension turbidity plotted against concentration show a linear trend, which illustrates that turbidity can be correlated to suspension concentration. The interception with x-axis substantiates the solubility of 10 mg/l of Baracarb2 in synthetic brine due to calcium undersaturation.
- Reproducibility of suspension filtration experiments utilising the hydra is high, meaning that similar results can be expected when adhering to the defined experimental procedure. The results are separated in a constant rate and a constant pressure regime. Comparing the porous media, a similar trend can be observed with a rapid linear decline in normalized permeability. Subsequently, a declining trend is observed towards a base value where it is assumed a full EFC is established.
- WQ variation tests are performed with each porous media, which demonstrates that (within the constant rate domain) the slope of permeability impairment increases with increasing concentration. More specifically, a linear trend is observed plotting normalized permeability slope versus suspension concentration. Considering the constant pressure domain, the MFI is obtained by plotting the Ruth plot. Here a linear relationship is found when plotting MFI against concentration.
- Via similarity curve collapse, it is demonstrated for one and the same set-up a master curve can be extracted for each porous medium which scales roughly with suspension concentration.
- Injectant and effluent turbidity measurements underpin the importance of measuring particle throughput concentration and damage mechanism identification.
- WQ tests porous thin disc compared to membrane filters show similar results. i.e. permeability impairment is linear in the first part of the CR regime, and impedance increases linear due to cake filtration in CP regime. Differences are present in terms of volumes and damage mechanism
- SEM and Micro-CT scan images facilitate in illustrating the damage within BH11 to be mainly EFC, with some small pockets of IFC throughout the porous thin disc. This substantiates the hypothesis of damage sequence from IFC to EFC.
- Post-treatment of porous thin discs utilising an ultrasonic bath and backflow demonstrate that the damage is 90% reversible under the given flow conditions.

Basically, the Con-vergence hydra results indicate that:

- From a Reservoir engineering point of view, the Hydra has great potential for on-site testing permeability impairment using porous thin discs, which gives fast, reliable results (half an hour test)

- From a Production technologist / Chemist testing point of view, experiments with porous thin discs utilising the Hydra demonstrate the applicability of MFI determination.

# 8 Recommendations

Due to the COVID-19 outbreak, the laboratory study became more constrained in time. Fortunately, most of the experiments were completed before the end of March. Below a few recommendations that can benefit future research and development.

Particle stability study of the Baracarb2 particles in synthetic brine could be further investigated. In both particle size tests, total replacement of the clean filtered synthetic brine with Baracarb2 suspension resulted in the ultrasonic probe malfunction. This could have a positive effect on particle agglomeration. Only one stirring speed was tested, namely 500 rpm, which was the standard stirring speed in the Malvern 2000G tank. Multiple stirring speeds could be investigated to test the potential occurrence of the orthokinetic agglomeration [35] of Baracarb2.

The non-calcium carbonate content could be further investigated to understand the behaviour and size of this contaminant. In terms of the calcium undersaturation, synthetic brine could be made with the addition of the salt bicarbonate to act upon the dissolution feature.
Other model contaminants (or a combination of) or different particle size mixtures could be considered for testing the effect of Water Quality on Formation Damage using porous thin discs.

Other sandstone types could be considered as porous thin discs to test heterogeneity between different reservoir rock. Different membrane filters of various sizes or type (e.g. Isopore, instead of Millipore) could be tests with suspension free FSB and Baracarb2 suspension injection tests.

Also, the role of wettability could be further investigated by conducting a WID test with porous discs having a residual oil saturation ($S_{or}$). A residual oil saturation is common in a sandstone reservoir.

The Hydra has limitations in terms of operational pressure and rate envelope as well as internal contamination. Con-vergence could be consulted for the optimal cleaning procedures and replacement of parts.

Constant pressure tests with porous thin discs as well as membrane filters at different *dP* could provide more information on the specific cake resistance and cake properties.

# Appendix A

## A.1. Cumulative and Differential PSD results diluted suspension Baracarb2 in FSB

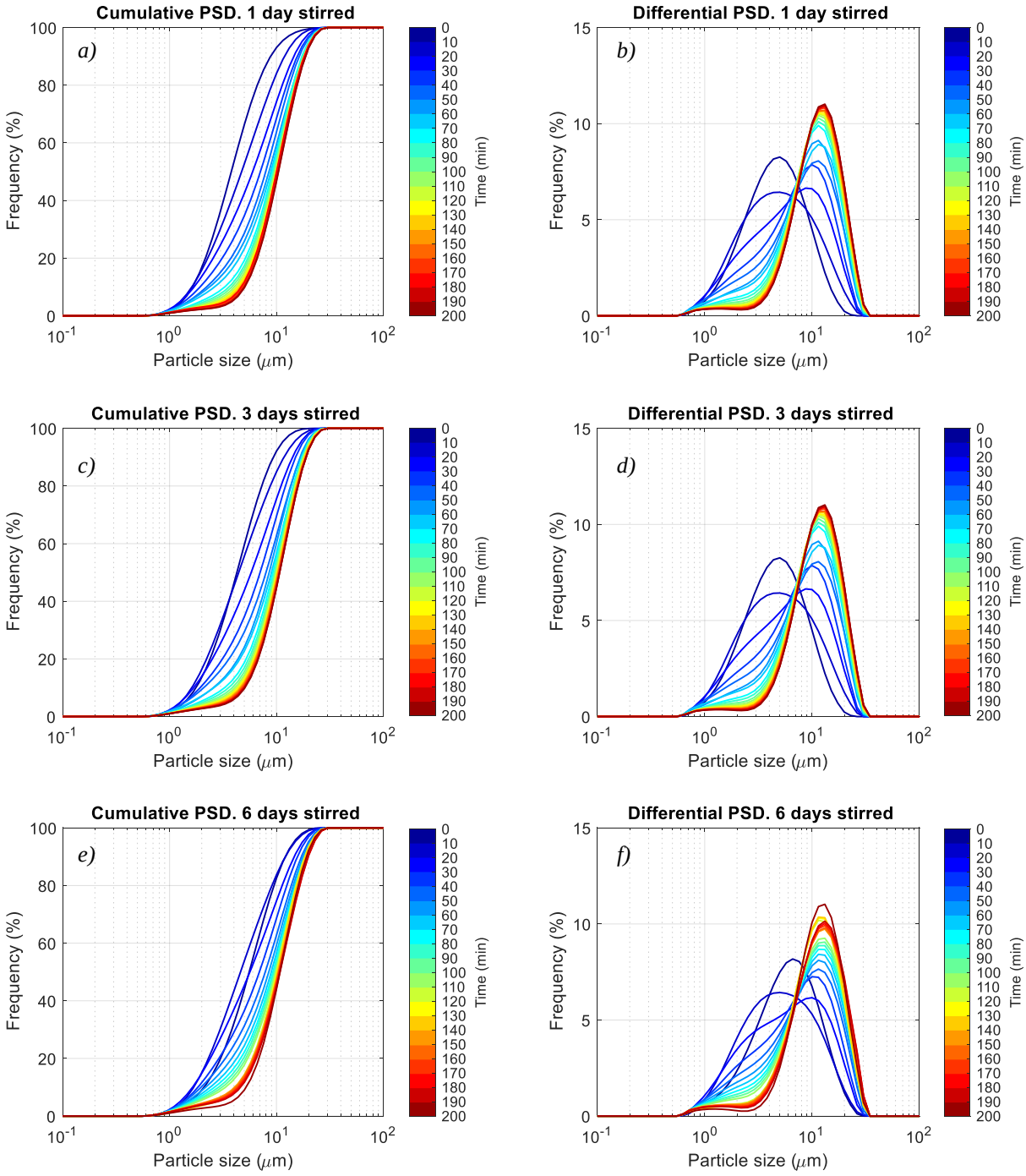


Figure A.1: Cumulative and Differential PSD results of the diluted suspensions of Baracarb2 in FSB. a) Cumulative PSD 1day stirred, b) Differential PSD 1day stirred c) Cumulative PSD 3day stirred, d) Differential PSD 3day stirred e) Cumulative PSD 6day stirred, f) Differential PSD 6day stirred.

# A.2. Obscuration results for diluted suspensions: Baracarb2 in FSB

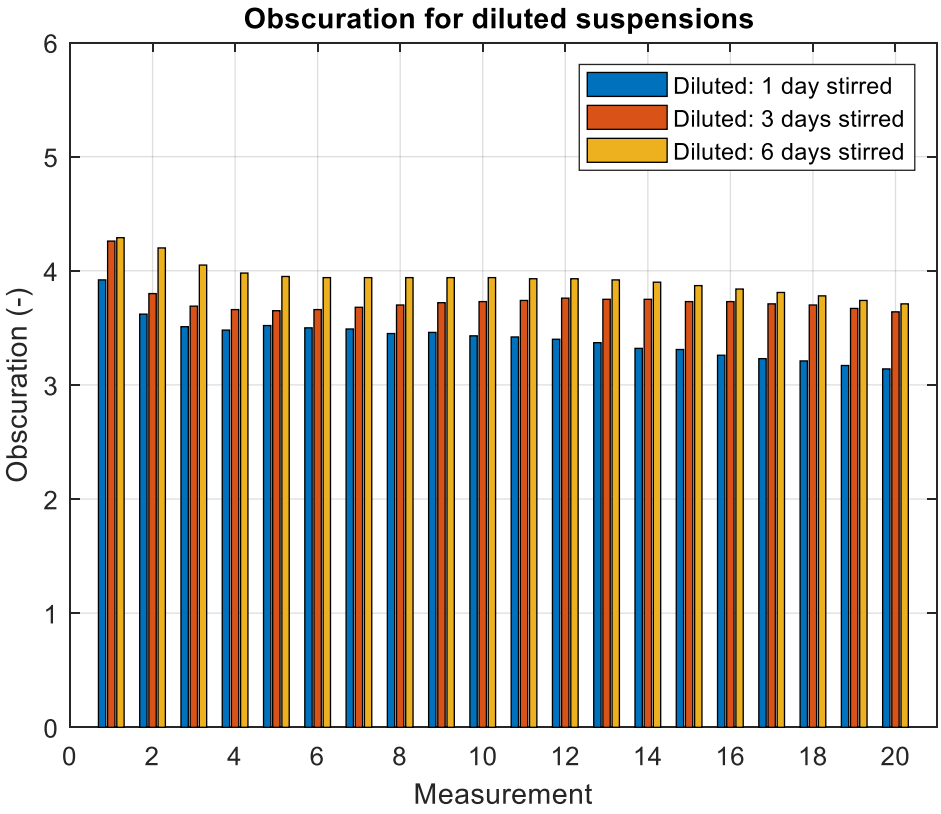


Figure A.2: Obscuration levels corresponding to the diluted Baracarb2 suspension samples tests.

# Appendix B

In *Figure B.1* a schematic cross-section is made from the membrane setup and thin disc setup. To create the thin disc setup, the membrane setup is modified by removing the screen and adding a silicon ring to mount the thin disc in place.

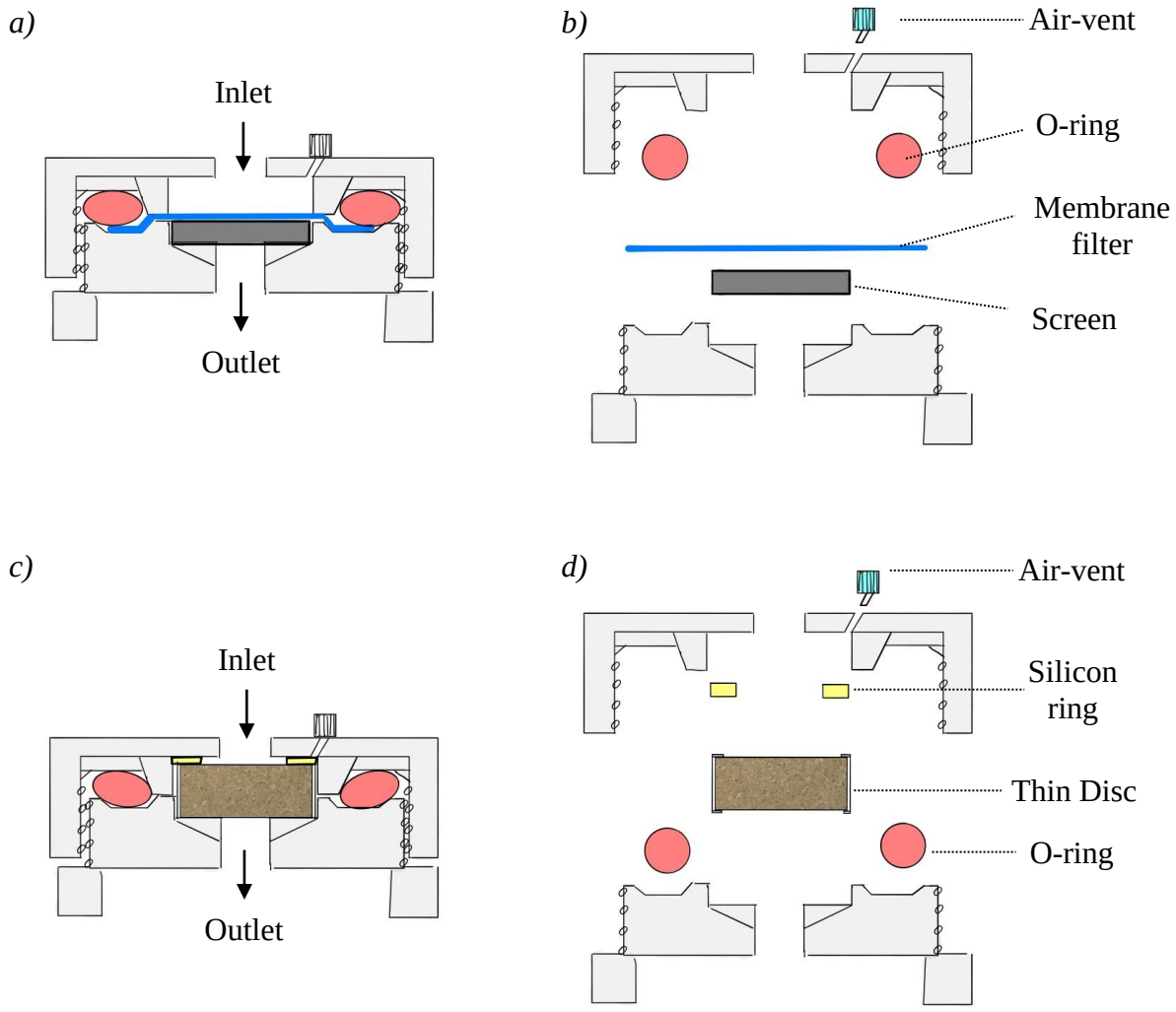


Figure B.1: a) Schematic drawing closed membrane setup b) Opened membrane setup c) Closed thin disc setup d) Opened membrane setup.

# Appendix C

## C.1. Hydra cleaning procedure

After a suspension flow experiment, particles get retained in the tubing and equipment within the Con-vergence Hydra. This was first observed by analyzing a membrane filtration test response with running clean demi water through the system with an MF0.45 filter installed. According to Darcy's law, flowing a clean fluid through a porous medium with a constant rate should equal a constant pressure gradient in return, considering steady laminar flow and incompressible media. However, an increasing pressure gradient over time is observed, which could be explained by the membrane collecting particles causing the permeability impairment, translating in a pressure increase. By visual analysis, some brown filtrate could be recognized on the membrane filter after the first clean fluid test, which is visible in *Figure C.1*.

To clean the Hydra, a protocol was created, which includes multiple steps. Straight after finishing an experiment, both inlet lines are flushed with at least five litres of demi water. Next, a non-ionic surfactant (Nonidet) solution is prepared, which is hooked up in a closed-loop system. Here the effluent is collected in the influent glass and is therefore re-used. Additionally, an MF0.45 filter is installed to capture the particulates remaining in the system. A programme is created which flows 100 litres at a constant rate of 50 l/hr. Three of these tests are run sequentially, including replacement of a membrane filter after each test. From the pressure gradient responses and pressure gradient slope visible in *Figure C.2*, it can be noted that the pressure gradient increase over time becomes smaller for each follow-up test. This indicates that the permeability impairment is less each test, or in other words, a cleaner system after each 100-litre flood. Test 1 is stopped in an earlier stage because of the maximum pressure of 4 bar is reached. This is usually the case for the first Nonidet solution membrane clean-up test. As a second measure for an indication of particle contamination, the turbidity is measured before each suspension injection test, and results are neglectable compared to the suspension turbidity.

Another explanation for an increasing pressure gradient with a constant rate is recognizing that the porous medium is not fully incompressible. As seen from *Figure C.1*, the pattern of the screen is visible in the membrane filter. This is due to the high flow rate of 50 l/hr, that pushes the membrane into the screen.


Figure C.1: Post analyses on MF0.45 membrane filters each test.

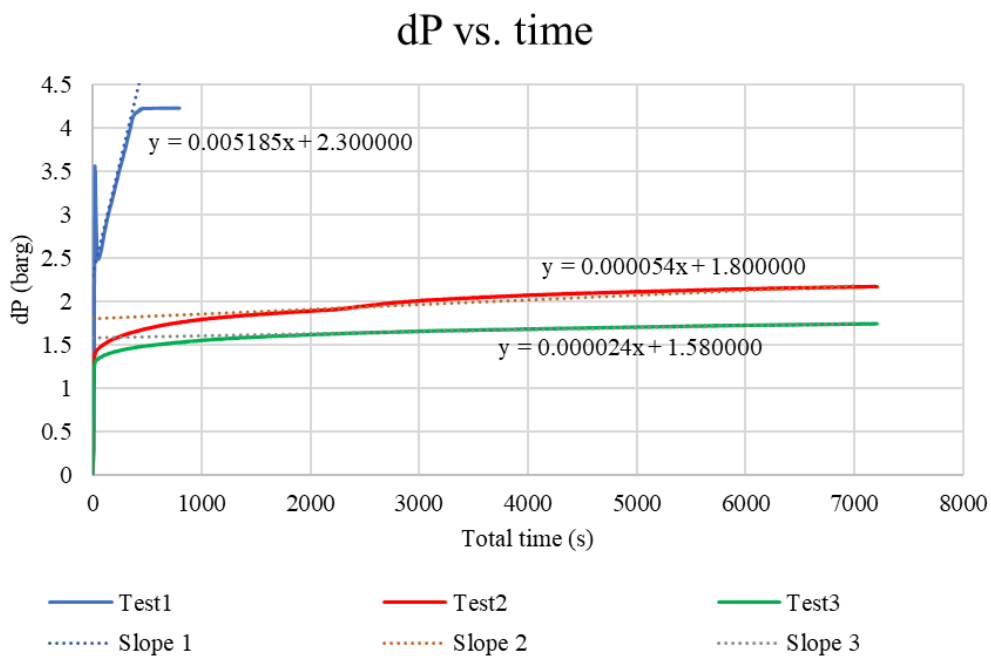


Figure C.2: Pressure gradient from three membrane filtration (MF0.45) tests using a Nonidet solution.

# Appendix D

## D.1. BH11 Characteristics and Permeability plot

Table D.1: Results on BH11 porous thin discs.

| Sample ID | $L_{TD}$ [mm] | $D$ [mm] | $\varphi$ [%] | $\rho_g$ [g/cm$^3$] | $\rho_b$ [g/cm$^3$] | $V_b$ [ml] | $V_g$ [ml] | $V_p$ [ml] | $k$ [Darcy] |
|---|---|---|---|---|---|---|---|---|---|
| TDF1 | 8.09 | 34.85 | 24.0 | 2.642 | 2.007 | 7.594 | 5.769 | 1.826 | 2.06 |
| TDF2 | 8.09 | 34.87 | 24.0 | 2.641 | 2.007 | 7.578 | 5.761 | 1.818 | 2.03 |
| TDF3 | 8.08 | 34.85 | 24.2 | 2.641 | 2.002 | 7.534 | 5.711 | 1.823 | 2.06 |
| TDF4 | 8.10 | 34.85 | 24.0 | 2.641 | 2.007 | 7.616 | 5.788 | 1.827 | 1.90 |
| TDF5 | 7.73 | 34.89 | 24.2 | 2.640 | 2.001 | 7.225 | 5.478 | 1.747 | 2.06 |
| TDF6 | 8.07 | 34.87 | 24.0 | 2.641 | 2.008 | 7.581 | 5.764 | 1.818 | 1.80 |

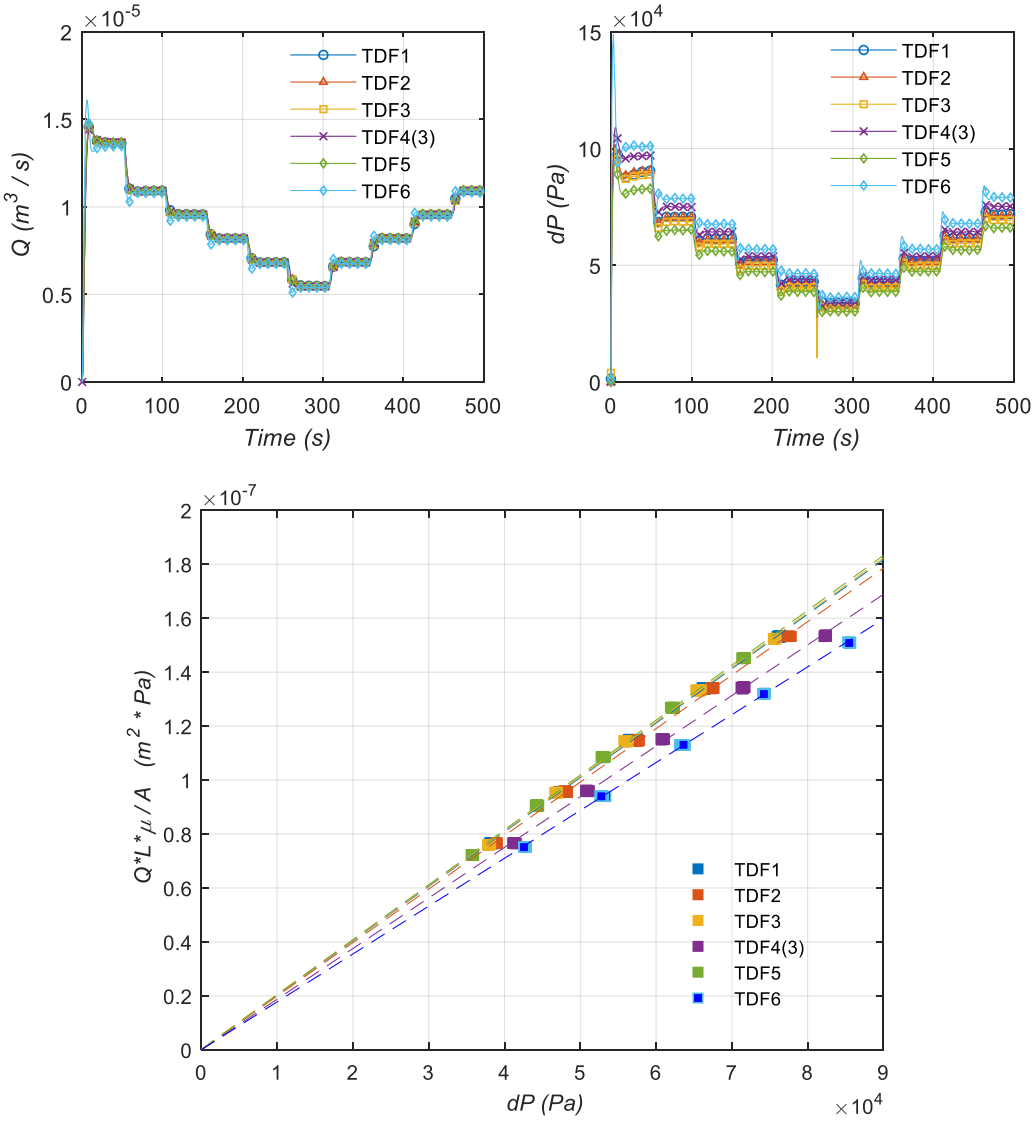


Figure D.1: BH11 rate step tests results where the flow rate is plotted against pressure drop to determine the slope, i.e. the permeability of the porous thin discs.

# D.2. BER18 Characteristics and Permeability plot

Table D.2: Results on BER18 porous thin discs.

| Sample ID | $L_{TD}$ [mm] | $D$ [mm] | $\varphi$ [%] | $\rho_g$ [g/cm$^3$] | $\rho_b$ [g/cm$^3$] | $V_b$ [ml] | $V_g$ [ml] | $V_p$ [ml] | $k$ [Darcy] |
|---|---|---|---|---|---|---|---|---|---|
| TDG1 | 8.09 | 34.56 | 20.7 | 2.650 | 2.102 | 7.474 | 5.929 | 1.545 | 0.169 |
| TDG2 | 8.10 | 34.56 | 20.7 | 2.650 | 2.101 | 7.495 | 5.942 | 1.553 | 0.170 |
| TDG3 | 8.09 | 34.59 | 20.7 | 2.651 | 2.103 | 7.486 | 5.938 | 1.547 | 0.175 |
| TDG4 | 8.10 | 34.74 | 20.6 | 2.651 | 2.103 | 7.519 | 5.967 | 1.552 | 0.161 |
| TDG5 | 8.07 | 34.61 | 20.5 | 2.650 | 2.108 | 7.486 | 5.954 | 1.532 | 0.154 |
| TDG6 | 8.10 | 34,55 | 20.7 | 2.650 | 2.102 | 7.498 | 5.948 | 1.550 | 0.152 |

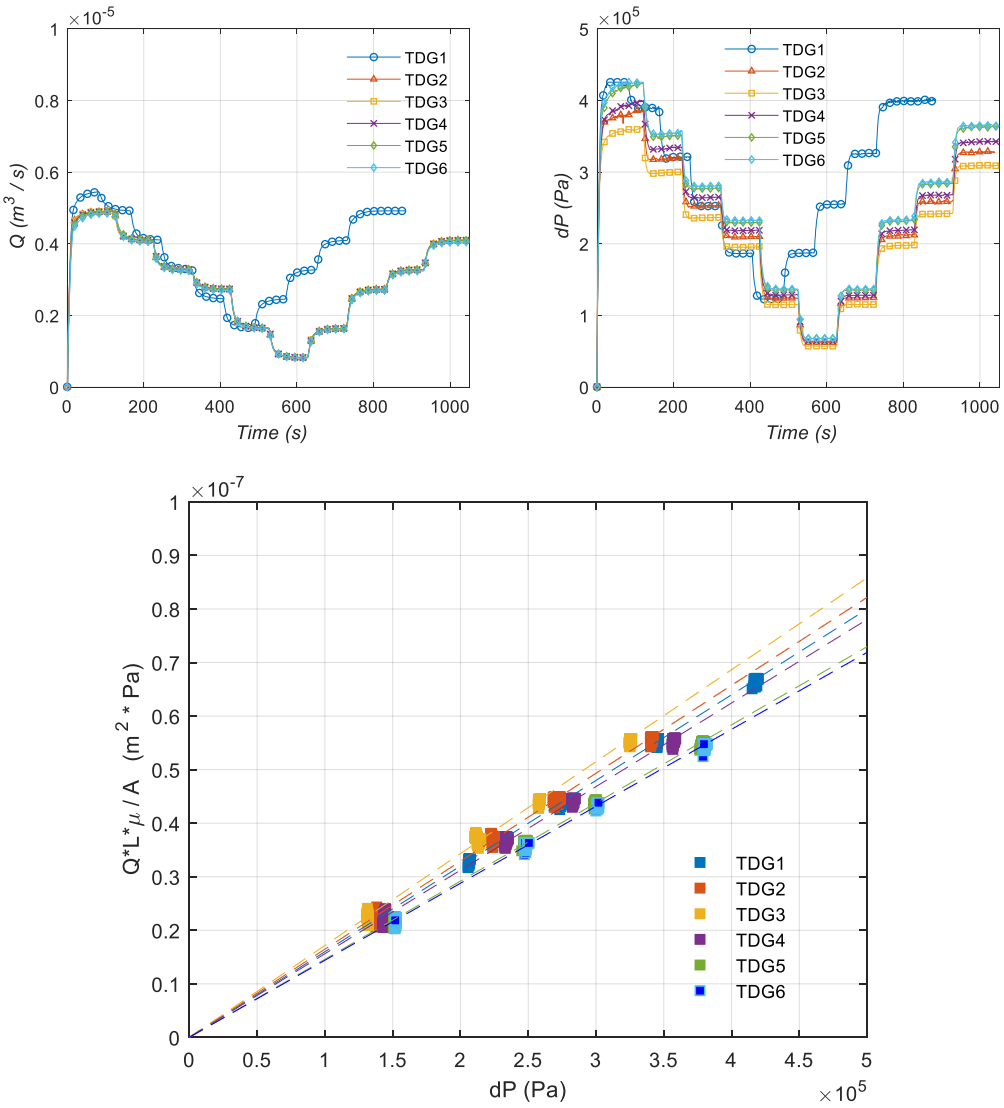


Figure D.2: BER18 rate step tests results where the flow rate is plotted against pressure drop to determine the slope, i.e. the permeability of the porous thin discs.

# Appendix E

## E1. TD-G2 and TD-G6: Salinity independence.

Table E.1: Porous thin disc, operational conditions and suspension specifications of the reproducibility experiments TD-G2 and TD-G6.

| Experiment ID | Porous media Type | $Q_0$ [l/hr] | Brine type | $c$ [mg/l] | Duration [min] | $V_{inj}$ [L] | $\varphi_{eff}$ [%] | $k_i$ [Darcy] |
|---|---|---|---|---|---|---|---|---|
| TD-G2 | BER18 | 10 | 2 | 50 | 11.7 | 0.88 | 20.7 | 0.177 |
| TD-G6 | BER18 | 10 | 1 | 50 | 8.1 | 0.76 | 20.7 | 0.155 |

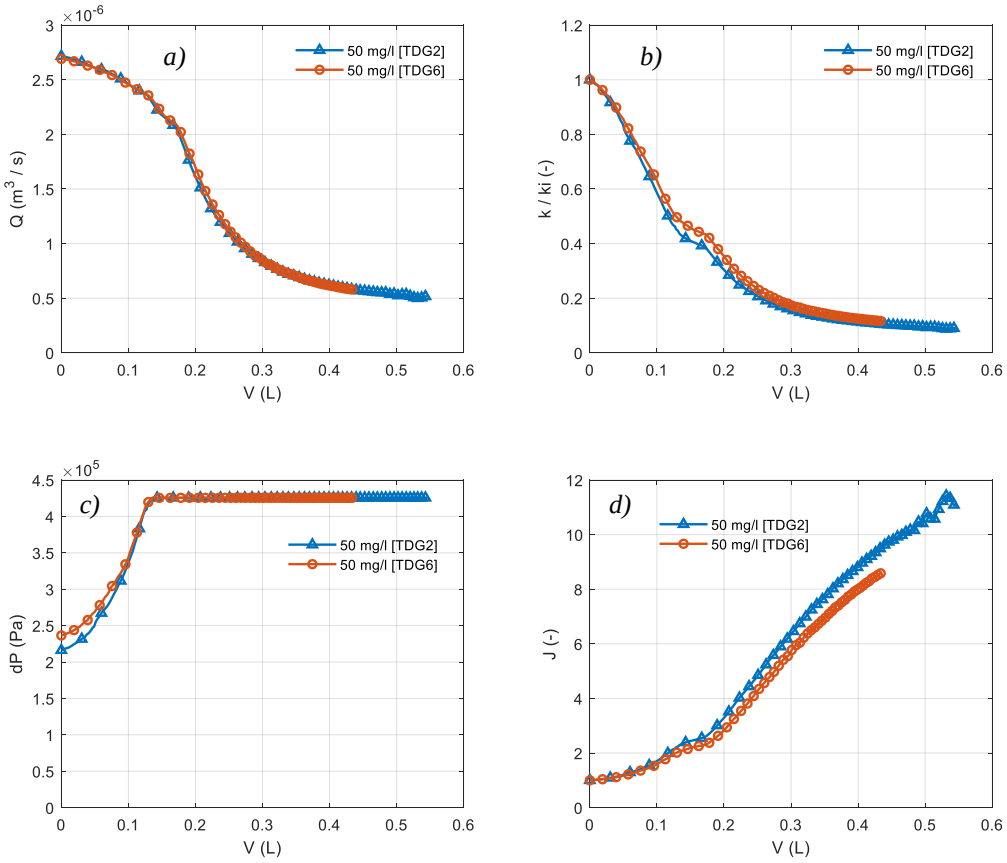


Figure E.1. Results of experiments TD-G2 and TD-G6 versus suspension volume injected: a) Flowrate, b) Normalized permeability, c) Pressure drop and, d) Impedance.

# Appendix F

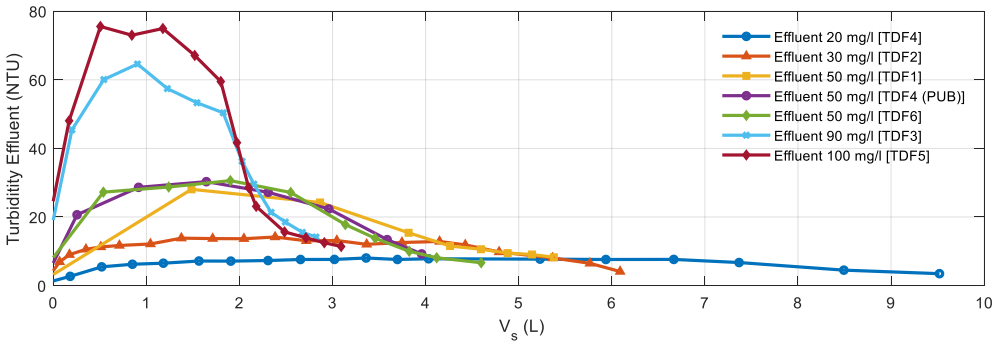


Figure F.1: BH11 Turbidity effluent results plotted against suspension volume injected for multiple suspension concentrations

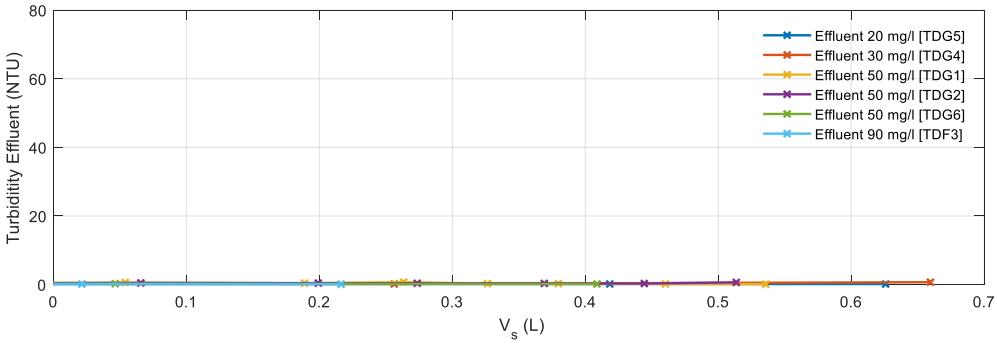


Figure F.2: BER18 Turbidity effluent results plotted against suspension volume injected for multiple suspension concentrations

# Appendix G

## G.1. SEM image of BH11 thin disc TD-F5

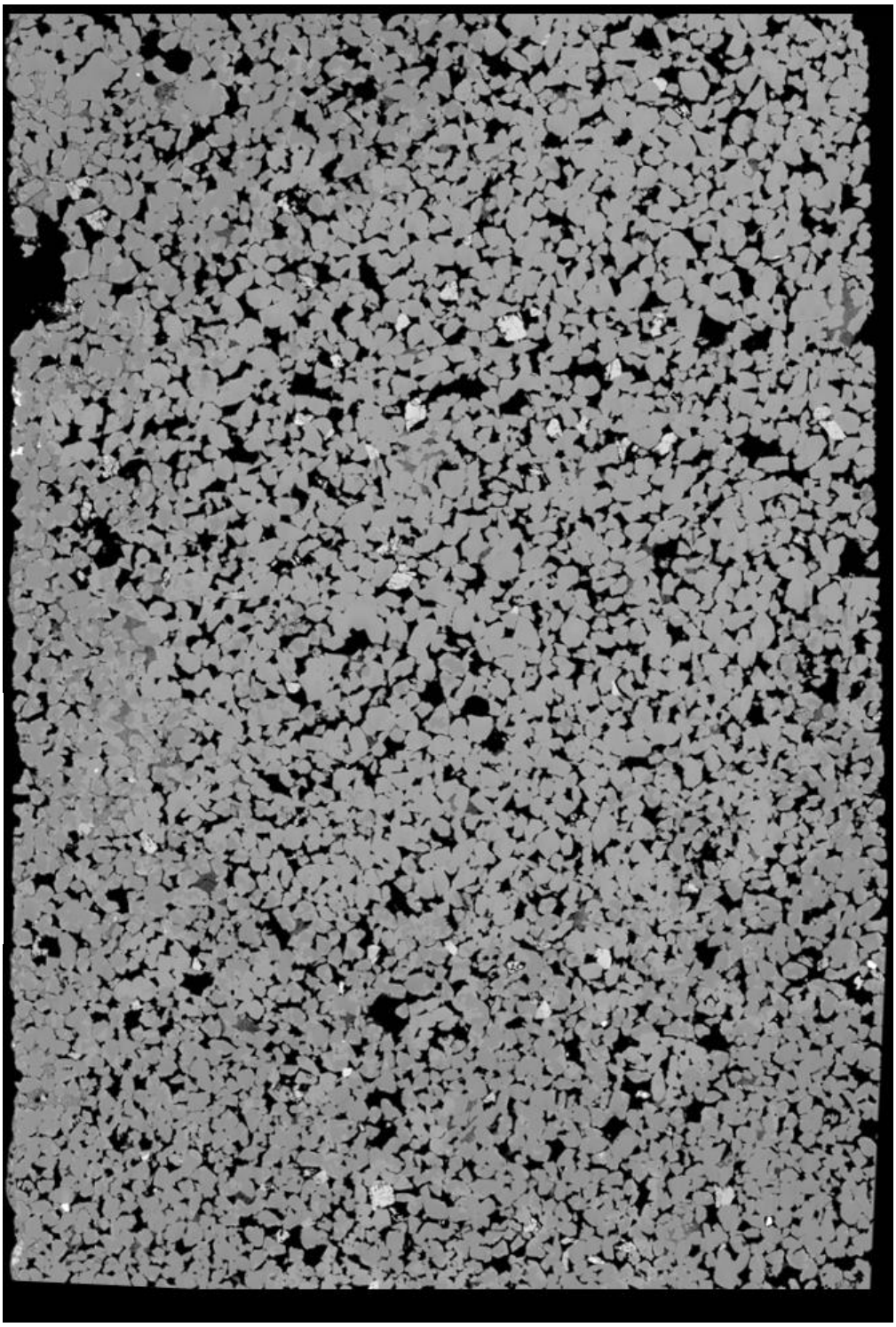


Figure G.1: Stitched SEM images of BH11 thin disc: TD-F5

# G.2. Micro-CT scan of BH11 thin disc TD-D1

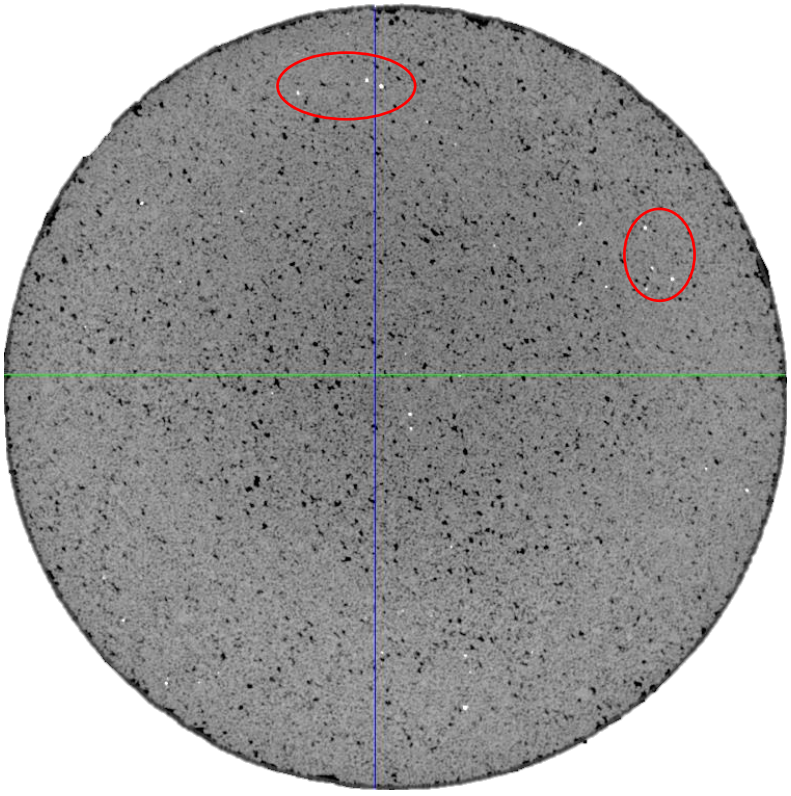

Figure G.2: Micro-CT scan of clean porous thin disc: TD-D1

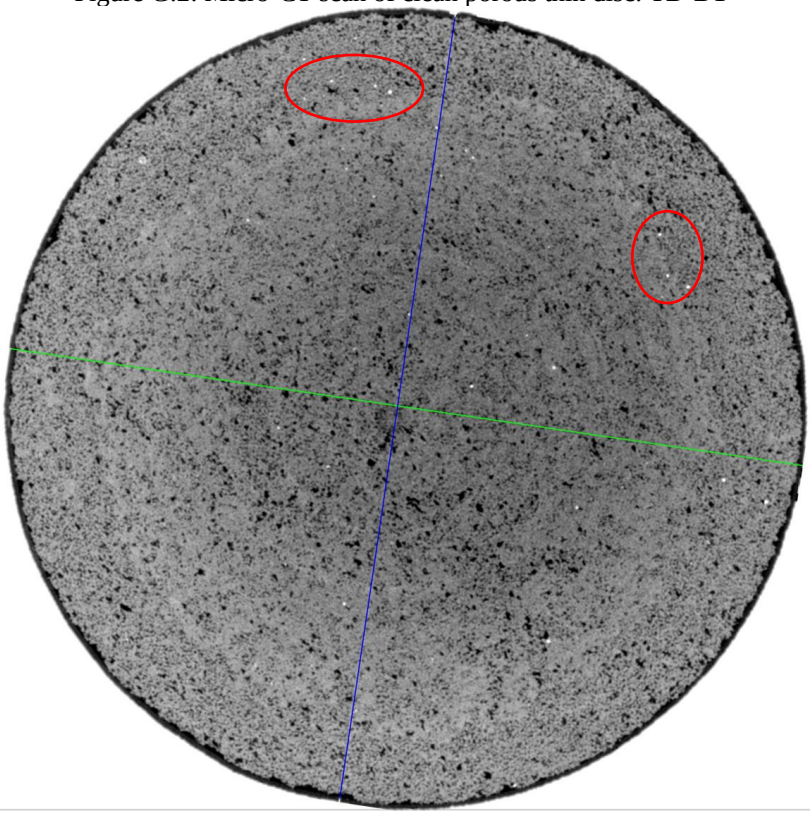

Figure G.3: Micro-CT scan of damaged porous thin disc: TD-D1

# Bibliography


[1] S. R. Chard and N. Saunders, “Produced water report: Regulations, current practices, and research needs,” *WEFTEC 2019 - 92nd Annu. Water Environ. Fed. Tech. Exhib. Conf.*, pp. 2483–2491, 2019.

[2] N. Jamous and K. Müller, *Environmental Performance Indicators*, no. January. Berlin, Heidelberg: Springer, 2018.

[3] J. W. Schoof, F., Van der Hout, M., Van Zanten, J., Van Hoogstraten, “Platform Geothermie. Master Plan Geothermal Energy in the Netherlands. Technical report, DAGO, EBN, Platform Geothermie, Stichting Warmtenetwerk,” 2018.

[4] T. J. Van Der Hulst, “Injectivity reduction in geothermal wells,” 2019.

[5] M. M. Sharma, S. Pang, K. E. Wennberg, and L. Morgenthaler, “Injectivity Decline in Water Injection Wells: An Offshore Gulf of Mexico Case Study,” *SPE Prod. Facil.*, vol. 15, no. 01, pp. 6–13, 2000.

[6] F. Civan, *Reservoir formation damage*. Houston, Texas: GULF Publishing Company, 2015.

[7] D. B. Bennion, F. B. Thomas, D. Imer, and T. Ma, “Water quality considerations resulting in the impaired injectivity of water injection and disposal wells,” *Can. Int. Pet. Conf.*, vol. Petroleum, 2000.

[8] C. C. Patton, “Injection-Water Quality,” *J. Pet. Technol.*, vol. 42, no. 10, pp. 1238–1240, 1990.

[9] O. Karazincir *et al.*, “Impact of Injection Water Quality on Injectivity – A Lab Study,” in *SPE Annual Technical Conference and Exhibition*, 2019.

[10] O. J. Vetter, V. Kandarpa, and A. Harouaka, “Report: FLOW OF PARTICLE SUSPENSIONS THROUGH POROUS MEDIA,” 1982.

[11] O. J. Vetter and V. Kandarpa, “Report: PARTICLE CHARACTERIZATION FOR GEOTHERMAL OPERATIONS,” 1981.

[12] J. H. Barkman and D. H. Davidson, “Measuring Water Quality and Predicting Well Impairment.,” *JPT, J. Pet. Technol.*, vol. 24, pp. 865–873, 1972.

[13] R. P. Kellogg and D. J. Mercier, “Empirical Evidence Demonstrating Injection Containment and Absence of Injection Fracturing, Wilmington Oil Field Case Study,” *SPE West. Reg. Meet.*, vol. Society of, 2019.

[14] L. Costier, P. J. Van Den Hoek, C. Davidson, M. Ding, J. T. M. Vanden Berg, and R. A. Hofland, “Establishing water injection dynamics by leading-edge coreflood testing,” *Soc. Pet. Eng. - Eur. Conf. Exhib. 2009*, 2009.

[15] W. F. Cerini, W. R. Battles, and P. H. Jones, “Some Factors Influencing the Plugging Characteristics of an Oil-well Injection Water,” *Trans. AIME*, vol. 165, no. 01, pp. 52–63, 1946.

[16] J. P. Herzig, D. M. Leclerc, and P. L. Le Goff, “Flow of Suspensions through Porous Media— Application to Deep Filtration,” *Ind. Eng. Chem.*, vol. 62, no. 5, pp. 8–35, 1970.

[17] A. Abrams, “Mud Design To Minimize Rock Impairment Due To Particle Invasion.,” *JPT, J. Pet. Technol.*, vol. 29, pp. 586–592, 1977.

[18] E. C. Donaldson, B. A. Baker, and H. B. Carroll, “Particle transport in sandstones,” *Proc. - SPE Annu. Tech. Conf. Exhib.*, 1977.

[19] O. J. Vetter, V. Kandarpa, M. Stratton, and E. Veith, “Particle Invasion Into Porous Medium and Related lnjectivity Problems,” *SPE Int. Symp. Oilf. Chem.*, vol. SPE intern, no. Society of Petroleum Engineers, 1987.

[20] A. Murtaza, “Injectivity decline in ultra-filtered water flooding of high permeability

sandstone reservoir," 2017.
[21] C. C. McCune, "on-Site Testing To Define Injection-Water Quality Requirements.," *JPT, J. Pet. Technol.*, vol. 29, pp. 17–24, 1977.
[22] J. Rochon, M. R. Creusot, P. Rivet, C. Roque, and M. Renard, "Water quality for water injection wells," *Proc. - SPE Int. Symp. Form. Damage Control*, pp. 489–503, 1996.
[23] M. M. Pang, S. Sharma, "A Model for Predicting Injectiity Decline in Water-Injection Wells."
[24] R. Farajzadeh, "Produced water re-Injection (PWRI): An experimental investigation into internal filtration and external cake build up," Delft University of Technology, 2004.
[25] Z. I. Khatib, "Prediction of formation damage due to suspended solids: Modeling approach of filter cake buildup in injectors," *Proc. - SPE Annu. Tech. Conf. Exhib.*, vol. Pi, no. pt 1, pp. 263–273, 1994.
[26] E. Aristov, S., van den Hoek, P., & Pun, "Integrated Approach to Managing Formation Damage in Waterflooding," in *SPE European Formation Damage Conference and Exhibition*.
[27] J. G. R. Eylander, "Suspended Solids Specifications for Water Injection From Coreflood Tests," *SPE Int. Symp. Oilf. Chem.*, 1987.
[28] R. C. Yerramilli, P. L. J. Zitha, S. S. Yerramilli, and P. Bedrikovetsky, "A novel water injectivity model and experimental validation using ct scanned core-floods," in *SPE - European Formation Damage Conference & Exhibition*, 2013.
[29] G. Foley, *Membrane filtration: a problem solving approach with MATLAB*. Cambridge University Press, 2013.
[30] A. Ruiz-García, N. Melián-Martel, and I. Nuez, "Short review on predicting fouling in RO desalination," *Membranes (Basel).*, vol. 7, no. 4, pp. 1–17, 2017.
[31] J. C. Schippers and J. Verdoum, "THE MODIFIED FOULING INDEX, A METHOD OF DETERMINING THE FOULING CHARACTERISTICS OF WATER," *Desalination*, vol. 32, pp. 137–148, 1980.
[32] A. E. Peksa, K. H. A. A. Wolf, and P. L. J. Zitha, "Bentheimer sandstone revisited for experimental purposes," *Mar. Pet. Geol.*, vol. 67, pp. 701–719, 2015.
[33] D. R. Maloney, M. M. Honarpour, and A. D. Brinkmeyer, "THE EFFECTS OF ROCK CHARACTERISTICS ON RELATIVE PERMEABILITY," vol. 441, 1990.
[34] H. Basal, "Experimental Study of External as well as Internal Core Formation Damage," Technical University of Delft, 2019.
[35] D. Dogon and M. Golombok, "Particle agglomeration in sheared fluids," *J. Pet. Explor. Prod. Technol.*, vol. 5, no. 1, pp. 91–98, 2015.
[36] Bariod (Halliburton), "Baracarb®-DF Product Data Sheet," 2010.
[37] H. Moes and R. Flash, "Advances in Particle Size Analysis by Laser Obscuration Time Combined technologies for particle size, shape and concentration measurement," vol. 31, no. 0, p. , 2006.
[38] K. E. Porter, "An Overview of Formation Damage," *J. Pet. Technol.*, vol. 41, no. no 08, pp. 780–786, 1989.
[39] F. A. H. Al-Abduwani, *Internal Filtration and External Filter Cake Build-up in Sandstones*. 2005.